Nuclear Heat Transfer and Passive Cooling

Volume 2: **Convection, Radiation and Conjugate Heat Transfer**

FRAZER-NASH CONSULTANCY

Introduction to the Technical Volumes and Case Studies

Convection, Radiation and Conjugate Heat Transfer

Natural Convection and Passive Cooling

Confidence and Uncertainty

Liquid Metal Thermal Hydraulics

Molten Salt Thermal Hydraulics

Liquid Metal CFD Modelling of the TALL-3D Test Facility

Fuel Assembly CFD and UQ for a Molten Salt Reactor

Reactor Scale CFD for Decay Heat Removal in a Lead-cooled Fast Reactor

System Code and CFD Analysis for a Light Water Small Modular Reactor

Authors:	Tim Houghton	Frazer-Nash Consultancy
	Richard Underhill	Frazer-Nash Consultancy
Contributors:	Andrew Beveridge	Frazer-Nash Consultancy
	Carolyn Howlett	Frazer-Nash Consultancy
	David Cuming	DBD International
	Edward Naylor	Frazer-Nash Consultancy
	Graham Macpherson	Frazer-Nash Consultancy
	Hector Iacovides	The University of Manchester
	Janne Wallenius	LeadCold
	Juan Uribe	EDF Energy R&D
	Ji Soo Ahn	Imperial College London
	Milorad Dzodzo	Westinghouse Electric Company
Technical Volumes Lead:	Tim Houghton	Frazer-Nash Consultancy
Approver:	Brian Gribben	Frazer-Nash Consultancy

Document Number: FNC 60148/49309R

Issue and Date: Issue 1, December 2021

Legal Statement

Preface

Nuclear thermal hydraulics is the application of thermofluid mechanics within the nuclear industry. Thermal hydraulic analysis is an important tool in addressing the global challenge to reduce the cost of advanced nuclear technologies. An improved predictive capability and understanding supports the development, optimisation and safety substantiation of nuclear power plants.

This document is part of *Nuclear Heat Transfer and Passive Cooling: Technical Volumes and Case Studies*, a set of six technical volumes and four case studies providing information and guidance on aspects of nuclear thermal hydraulic analysis. This document set has been delivered by Frazer-Nash Consultancy, with support from a number of academic and industrial partners, as part of the UK Government *Nuclear Innovation Programme: Advanced Reactor Design*, funded by the Department for Business, Energy and Industrial Strategy (BEIS).

Each technical volume outlines the technical challenges, latest analysis methods and future direction for a specific area of nuclear thermal hydraulics. The case studies illustrate the use of a subset of these methods in representative nuclear industry examples. The document set is designed for technical users with some prior knowledge of thermofluid mechanics, who wish to know more about nuclear thermal hydraulics.

The work promotes a consistent methodology for thermal hydraulic analysis of single-phase heat transfer and passive cooling, to inform the link between academic research and end-user needs, and to provide a high-quality, peer-reviewed document set suitable for use across the nuclear industry.

The document set is not intended to be exhaustive or provide a set of standard engineering ‘guidelines’ and it is strongly recommended that nuclear thermal hydraulic analyses are undertaken by Suitably Qualified and Experienced Personnel.

The first edition of this document set has been authored by Frazer-Nash Consultancy, with the support of the individuals and organisations noted in each. Please acknowledge these documents in any work where they are used:

> Frazer-Nash Consultancy (2021) Nuclear Heat Transfer and Passive Cooling, Volume 2: Convection, Radiation and Conjugate Heat Transfer.

Contents

1 Introduction

Conjugate Heat Transfer (CHT) is the coupling of heat conduction in solids with convective and radiative heat transfer in neighbouring fluids. The ability to predict the variation in temperature of solid components, such as pipework, vessels and structures, as a result of heating or cooling by a fluid is important for all Nuclear Power Plants (NPPs).

The objective of this technical volume is to describe how to model convection, thermal radiation and CHT, which are fundamental to the transfer of heat out of a reactor particularly under passive cooling scenarios. It is part of a set of documents that are intended to describe good practice and summarise the current state-of-the-art, and it is recommended that Volume 1 (Introduction to the Technical Volumes and Case Studies) is reviewed for context.

The benefit of CHT analysis and its impact on reactor design is discussed in this section before providing a detailed review of the modes of heat transfer and current analysis methods.

1.1 Conjugate Heat Transfer

CHT analysis is required when it is not sufficient to simply consider heat transport in the fluid, with an idealised thermal boundary condition applied at the fluid and wall interface. In these cases, the fully coupled problem, including heat conduction in the solid wall adjacent to the fluid, must be considered. Situations where this is necessary include:

- When the fluid temperature varies during a transient, the conduction behaviour and thermal mass[1] (stored energy) inside the vessel walls may have a significant impact on the heat transfer to the fluid and surroundings, and therefore the system performance as a whole.
- Conduction and the thermal diffusivity of the solids may have a significant impact on the flow behaviour if the temperature field inside a fluid and the surrounding vessel or pipework is complex, unsteady or three-dimensional.
- If the fluid temperature varies adjacent to a wall (for example due to unsteady poorly mixed flow or a moving free surface) the resulting temperature variations within the solid may cause fluctuating thermal stresses that can lead to thermal fatigue.

Therefore, in many circumstances it is necessary to properly account for the temperature variations within solids and fluids flowing around or through solid components, and the thermal coupling between the two. This can be achieved using a CHT approach, which predicts the temperatures within a fluid and the adjacent solids within the same analysis or coupled together.

[1] Thermal mass (or heat capacity) refers to the product of mass and specific heat capacity of a body (mc_p) and is a measure of a body's ability to absorb energy. This is sometimes referred to as 'thermal inertia', but this is a separate property ($\sqrt{k\rho c_p}$) used in geotechnical or planetary science but rarely in mechanical engineering. Thermal diffusivity ($\alpha = k/\rho c_p$) is a more relevant related quantity, which has significance in the transient conduction equation.

1.2 Impact on Reactor Design

The accurate prediction of fluid and solid temperatures is used to support performance assessments and structural integrity calculations as part of the design and safety of all NPPs.

1.2.1 Performance Assessments

Detailed predictions of the fluid and solid temperatures within the primary circuit are required under normal operation, start-up and shut-down transients, as well as during fault scenarios. These are used to determine the operating envelope and safety margins for the reactor design. This is particularly relevant to passive cooling systems, where the development of thermal gradients is essential to generate the buoyancy forces needed to drive the flow through the system. For example, CHT analysis is used to:

- Ensure that the maximum temperatures of key components remain within allowable limits (e.g. fuel cladding, fuel pellets, reactor pressure vessel and primary circuit components).
- Determine the rate of cooldown of the reactor under normal shut-down and fault scenarios and demonstrate the effectiveness of passive cooling systems, as a prolonged cooling period is required due to the large thermal mass and ongoing nuclear decay reactions.
- Predict the temperatures or heat flux where the conduction paths are complex/subtle, such as some decay heat removal systems or cross-core conduction under passive cooling.

1.2.2 Structural Integrity Calculations

CHT analysis is a key input into structural integrity calculations (Section 2.4) in order to demonstrate the integrity of Structures, Systems and Components (SSCs) and predict component life. Failures in components may be caused by situations such as large thermal shocks causing fracture (e.g. emergency cooling scenarios), temperature fluctuations over a long period causing fatigue or temperatures that lead to enhanced corrosion. Some examples relevant to NPP design include:

- Thermo-mechanical studies are required to calculate component temperatures, as internal stored energy, heat generation and conductivity induce stresses in components, welds and joints, especially if their state changes rapidly.
- Temperature fluctuations induced in solid materials through turbulent mixing processes may lead to thermal fatigue (cyclic thermal stresses and eventually to fatigue and cracking). For example, in 1998 a through-wall crack was discovered downstream of a T-junction (Kuhn *et al.*, 2010) at the Civaux-1 plant in France only five months after finishing construction, resulting in pipe rupture and release of radioactive steam into the reactor building. Therefore, predicting the impact, location, amplitude and frequency of those temperature fluctuations is crucial for the lifetime management of components used in NPPs.
- Excessive thermal stress caused by temperature differences in the fluid (e.g. thermal striping, stratification) can lead to thermal fatigue damage and cracks in feedwater nozzles, high pressure safety injection lines and residual heat removal lines (Jo *et al.*, 2003). For example, Pressurised Thermal Shock (PTS) is a key reactor safety issue that may impact the lifespan (and subsequent economics) of the plant due to stresses in the Reactor Pressure Vessel (RPV) downcomer caused by cold water injection (IAEA, 2010).

2 Technical Context

This section considers some of the key technical aspects of heat transfer with a focus on nuclear applications. The modes of heat transfer are introduced, followed by a discussion on surface modifications, material properties, thermal fatigue and key modelling challenges.

2.1 The Modes of Heat Transfer

Heat transfer is the movement of thermal energy due to a temperature difference. There are three modes of heat transfer, which are illustrated in Figure 2.1:

Conduction: In conduction, energy is transferred from more energetic particles to less energetic particles by interactions between them (e.g. direct interaction between atoms or molecules, movement of free electrons in metals). Conduction is generally the main mode of heat transfer within compact (non-porous) solids.

Convection: In convection, energy is transferred by the combination of bulk motion of a fluid (advection) and by diffusion (resulting from random molecular or turbulent motion). Convection is generally the most significant mode of heat transfer between solids and fluids at moderate temperature differences.

Thermal radiation: In thermal radiation, energy is transferred by the electromagnetic radiation emitted from matter, so no medium is required and heat transfer can occur in a vacuum. Solids, liquids and gases can all participate in thermal radiation heat transfer. Thermal radiation is often most significant at high temperatures.

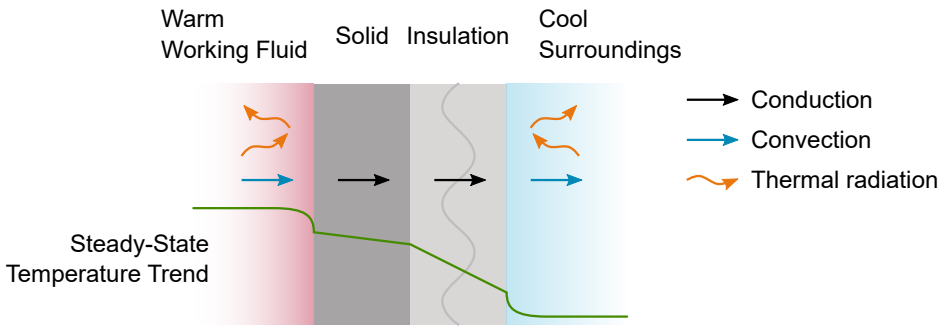

Figure 2.1: Example of three modes of heat transfer at an insulated wall.

One, two or all three of these modes may be important in a given situation. These modes are discussed further in the following sections. More general detail and explanation on heat transfer is available in Rogers and Mayhew (1992), Incropera *et al.* (2011) or Rohsenow *et al.* (1998)[1].

[1] In addition, Lienhard and Lienhard (2020) is free to download from web.mit.edu/lienhard/www/ahtt.html.

2.1.1 Conduction

The rate of heat transfer per unit area or heat flux (q) through a substance due to conduction is proportional to the gradient in temperature (T) according to Fourier's law:

$$q = -k\nabla T \quad \text{or in one dimension,} \quad q_x = -k_x \frac{dT(x)}{dx}$$

Where k is the thermal conductivity (assumed constant in this equation), a property of the material (Section 2.3). Although this is usually expressed as a scalar, it may be necessary to use a tensorial description for anisotropic materials, such as composites (Section 2.3) or 'effective' material properties in porous regions (Section 3.4.3.3).

2.1.1.1 Thermal Resistance

In heat transfer analysis it is often useful to separate the details of the geometry and material properties (which are often fixed in a given situation) from the temperatures (which may vary). This can be achieved for steady-state analysis using the concept of thermal resistances. In the simple plane wall in Figure 2.1, k is assumed to be a constant and the temperature gradient through the wall is therefore linear. Applying Fourier's law to such a wall, the rate of heat transfer through a given frontal area (A, normal to the heat flux) for wall thickness (L) is:

$$Q = kA\frac{\Delta T}{L} = \frac{1}{R_{th}}\Delta T \quad \text{where} \quad R_{th} = \frac{L}{kA}$$

Where ΔT is the temperature difference between the two surfaces of the wall and R_{th} is the thermal resistance due to conduction through the wall (which is large for a well insulating wall). Different basic geometries have different formulae for this thermal resistance (Section 2.1.2.4 presents an example for radial conduction in a cylindrical tube or pipe).

Thermal resistances are convenient because they can be used in a broadly similar manner to electrical resistances (i.e. by adding resistances in series and reciprocals of resistances in parallel). Section 2.1.2 and Section 2.1.3 develop thermal resistances further and include convection and thermal radiation. All of the thermal resistances occurring at the wall (for the three modes of heat transfer in Figure 2.1) can therefore be combined to form an overall thermal resistance $R_{th,oa}$.

This overall thermal resistance can be used to calculate the widely used 'overall heat transfer coefficient', 'overall thermal transmittance', 'U-value' or U (with units $\mathrm{W\,m^{-2}\,K^{-1}}$). However, it is important to note that approaches to defining R_{th} vary. In this volume R_{th} includes A (its units are $\mathrm{K\,W^{-1}}$) because for geometries where the frontal area changes along the direction of the heat flux (like radial conduction in a pipe) this is clearer. Therefore, $UA = 1/R_{th,oa}$, where A is some representative area, the basis of which should be clearly stated[2], see Section 2.1.2.4.

[2] In some references (particularly associated with the construction industry, which usually works with plane walls where the value of A is clear), R_{th} may not include A (i.e. have units $\mathrm{K\,m^2\,W^{-1}}$) and accordingly U would equal $1/R_{th}$.

Contact Thermal Resistance: Two solids that are touching are rarely in perfect thermal contact. Instead, the roughness of their surfaces and possibly small distortions in their geometry can cause narrow voids at the interface between the solids. These voids are likely to cause an additional thermal resistance. It may be appropriate to assess this contact thermal resistance by considering two resistances in parallel:

1. Conduction through the (probably small) patches where there is good thermal contact.
2. Conduction (and possibly also convection and thermal radiation) through the voids at the interface (which are likely to be filled with air or the surrounding fluid) based on a characteristic gap width.

The contact resistance may also be affected by forces acting over the interface, wear occurring in service, the cleanliness of the surfaces, and any other materials present at the interface. For more detailed assessments, experimentally measured contact resistances are available in wider literature (Rohsenow *et al.*, 1998).

2.1.1.2 Unsteady Conduction

Conduction through solids during transients is a key aspect of CHT, and this heat transfer is a function of temperature gradients in the solid that are likely to change over time. It is therefore useful to develop an understanding of the behaviour of these temperature gradients where a solid is in contact with a fluid, for which a key non-dimensional group is:

Biot number ($Bi = hL/k_s$), a ratio of convective and conductive heat transfer effectiveness

Where h is the convective Heat Transfer Coefficient (HTC) (Section 2.1.2), L is a characteristic length scale (e.g. half the thickness of a plate or the volume to surface area ratio for a more general geometry) and k_s is the solid thermal conductivity. Estimating Bi using a HTC correlation is often useful in the early stages of a CHT analysis:

- If $Bi < 0.1$, conduction within the solid is much more effective than convection to the fluid, so temperature gradients within the solid are likely to remain small. It may therefore be appropriate to ignore spatial temperature variations within the solid and use a single mass-average 'bulk' or 'mean' temperature to predict heat transfer through time. This is sometimes referred to as a 'lumped capacitance' approach.
- If the above criterion is not met, the surface of the solid is likely to respond to the fluid temperature more rapidly than the interior of the solid. As Bi increases, larger thermal gradients would be expected within the solid, so both spatial and temporal variations in temperature within the solid may be important for predicting heat transfer.

These two scenarios above are illustrated in Figure 2.2.

Another non-dimensional group that is often encountered in CHT analysis is the Fourier number ($Fo = \alpha_s t/L^2$), a non-dimensional timescale for conduction analysis (Rogers and Mayhew, 1992 and Incropera *et al.*, 2011). In the limiting case where the Biot number approaches zero, a 'lumped

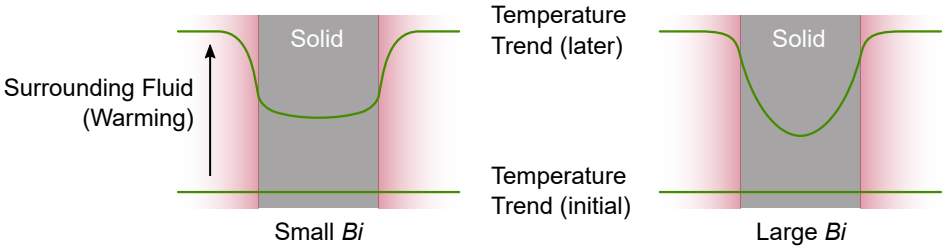

Figure 2.2: Illustration of temperature gradients in a solid surrounded by a warming fluid at two points in time, for small and large values of Bi.

capacitance' approach can be used to calculate the rate of heating or cooling of the solid:

$$\frac{\theta}{\theta_i} = \frac{T - T_\infty}{T_i - T_\infty} = e^{-BiFo} = e^{-\left(\frac{hA_s}{\rho V c_p}\right)t}, \quad \therefore t = -\frac{\rho V c_p}{hA_s} \ln\left(\frac{\theta}{\theta_i}\right)$$

Where T_i is the initial temperature of a solid surrounded by a fluid at temperature T_∞, and T is the temperature of the solid at time t.

2.1.2 Convection

Fluid motion is generally a key aspect of convective heat transfer, and a distinction is made between external and internal flows. Engineering judgement may be required to understand whether a flow is best considered as internal or external flow. For example, for a small cylinder crossing a large duct containing essentially uniform flow, the flow around the cylinder may closely resemble external flow, even though the flow down the duct as a whole is an internal flow.

External Flow: In this case, the flow as a whole is considered to be unconstrained (e.g. the flow over an aeroplane wing). There is therefore normally a clear 'free-stream flow' that is unaffected by surfaces, and a distinct boundary layer flow commonly develops adjacent to surfaces. The local heat flux per unit area (q) at a surface due to convection can be considered to be proportional to the difference between the temperature of the surface (T_w) and some representative free-stream fluid static temperature ($T_{s,\infty}$) for low speed flows[3], according to Newton's law of cooling:

$$q = h(T_w - T_{s,\infty})$$

Where h is the convective HTC, which depends on the details of the flow near the surface (Section 2.1.2.1).

Internal Flow: In this case, the flow as a whole is constrained by surfaces (e.g. the flow in a pipe). Significant gradients may therefore occur throughout the flow field, and there is often no clear free-stream flow. There is no clear $T_{s,\infty}$ that can be used for Newton's law of cooling, so it is therefore necessary to define a 'bulk' or 'mean' static temperature ($\overline{T_s}$ or T_b) that is characteristic of the flow and can be used instead of $T_{s,\infty}$. This bulk temperature is commonly based on a quasi-

[3] For high speed (high Ma) flows, the adiabatic wall or recovery temperature $T_{s,r}$ is typically used instead of $T_{s,\infty}$, to account for kinetic energy in the flow being dissipated as heat in the boundary layer.

mass-average across the flow[4]:

$$\overline{T_s} = \frac{\int_{A_{cs}} T_s dW}{\int_{A_{cs}} dW} = \frac{1}{W} \int_{A_{cs}} \rho U T_s dA_{cs}$$

The local heat flux per unit area (q) at a surface due to convection in internal flow can then be calculated using a HTC in a similar manner to low speed external flows:

$$q = h(T_w - \overline{T_s})$$

It is noted that while $T_{s,\infty}$ is generally constant in low speed external flows, in internal flows $\overline{T_s}$ varies as the flow is heated or cooled (e.g. along the flow in a pipe).

2.1.2.1 Near Wall Flows and Convection

Immediately next to a surface (or 'at the wall'), the velocity and temperature of the flow is normally considered to be the same as those at the wall itself, so heat transfer at the fluid-solid interface is entirely due to heat conduction. Further into the fluid, the wall-parallel fluid motion enhances the transfer of thermal energy, which makes the temperature profile in the fluid layers away from the wall flatter and the temperature gradient at the wall stronger. Comparing Fourier's law (Section 2.1.1) and Newton's law of cooling (above) indicates that the HTC depends on this temperature gradient at the wall. This section introduces some aspects of flows that can alter these gradients, and hence affect heat transfer.

As noted above, external flows often feature a free-stream flow with momentum and thermal boundary layers between this flow and the wall. Across these two boundary layers, velocity and temperature respectively, start to change from their wall values to asymptotically approach their free-stream values. In the case of the velocity boundary layer, the rate of growth depends on the balance of the rate at which the wall-parallel momentum is convected along the wall-parallel direction and the rate at which it is transported in the wall-normal direction through molecular and turbulent mixing. The rate of growth of the thermal boundary layer is determined by the corresponding balance in the transport of thermal energy (Figure 2.3).

The temperature and velocity gradients (and hence HTC) are well understood for simple boundary layers, such as flat plates or fully developed pipe flow, but are strongly affected by factors such as:

- The nature of the free-stream flow. Aspects such as local acceleration and deceleration, turbulence levels, vorticity and flow impingement on the surface.
- Whether the flow is laminar, turbulent or transitional. Turbulence enhances the mixing of momentum and heat (across velocity and temperature gradients respectively).
- The behaviour of the boundary layer itself. Aside from turbulence, features like separation have a significant impact.
- The properties of the fluid. These have a significant impact on the transport of momentum and heat.

[4] Strictly, only extensive properties (that define a property per unit mass) can be mass-averaged. In this case, the relevant extensive property is enthalpy, so strictly this equation is only valid for a perfect gas (Volume 3, Section 2.3.1) or incompressible liquid with a constant specific heat, since in these cases a change in enthalpy equals $c_p \Delta T_s$ and c_p can be cancelled from the equation. Further details on averaging non-uniform flows is available in Cumpsty and Horlock (2005).

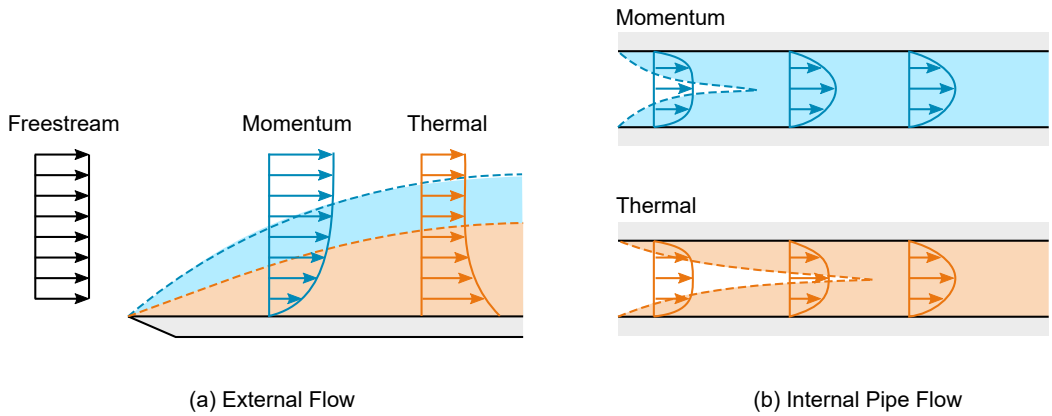

Figure 2.3: Illustration of momentum and thermal boundary layers.

- The detailed geometry of the surface. Roughness and surface features (Section 2.2) can have a significant impact on the local flow field near the surface.

The behaviour of boundary layers is a significant topic in its own right, and a detailed discussion is provided by Schlichting and Gersten (2017). Turbulence and transition both affect heat transfer and are particularly significant issues for passive cooling systems; further details are provided in Volume 3 (Section 2.2.3). In some flows the temperature and velocity gradients can be similar (the Reynolds analogy, Section 3.4.6), but this is not always the case as discussed further for liquid metals in Volume 5 (Section 2.1.2).

In summary, the convective heat transfer at walls is strongly influenced by the detailed near-wall flow field, and can therefore be affected by many factors.

2.1.2.2 Natural, Forced and Mixed Convection

These terms describe different mechanisms of convective heat transfer that might occur depending on the significance of local buoyancy effects. Heat transfer by natural, forced and mixed convection is discussed in Volume 3 (Section 2.2.1).

2.1.2.3 Heat Transfer Coefficients (HTCs)

Heat transfer coefficients, or 'film coefficients' are extremely convenient and widely used across industry. Among their many advantages, HTCs:

- Enable engineers to compare and discuss work on convective heat transfer, and are often easy to sense-check against values in textbooks or wider literature.
- Are invaluable as an input to system performance models (Section 3.2), which may be based on detailed Computational Fluid Dynamics (CFD) analysis (Section 3.4), and transferring information about convective heat transfer between different analyses (such as from a CFD assessment to a structural assessment, Section 2.4).

However, HTCs have some significant limitations, which include:

- Even in relatively simple situations that involve fully developed flow over a surface, there may

still be significant sources of uncertainty in the HTC due to surface roughness (Section 2.2.1) or non-idealised boundary conditions (i.e. not isothermal or constant heat flux).

- In practice, many real flows are complex and three-dimensional with non-idealised boundary conditions. This is a particular consideration and source of uncertainty/error where HTC correlations (Rohsenow *et al.*, 1998) are used in a system code (Section 3.2).
- Engineering flows often do not have a clearly identifiable local bulk temperature ($T_{s,\infty}$, $\overline{T_s}$), and so skilled engineering judgement is often needed to identify, and most importantly record, the most appropriate approach to calculate values of HTC. For example, applying a global reference temperature to get a local HTC in a system where the bulk fluid temperature changes significantly will lead to unrealistic values of HTC. This is particularly significant where CFD derived flow fields are being post-processed to provide inputs to other spatial models, and is considered further in Section 3.4.6.

In summary, HTCs are a useful tool. However, it is important to recognise that they are coefficients that attempt to represent the complex reality of heat transfer between fluids and solids. This heat transfer is driven by temperature gradients at walls, which are dependent on a wide range of factors, and are often a function of the dynamic conditions of the system and changing physical properties.

Local and Mean Coefficients: As noted above, the HTC (h) may vary continuously over a surface in response to changes in the flow field. For most engineering analysis, the heat transfer over a given area of surface is of interest, and an area-averaged HTC ($\overline{h}$) is therefore used. In situations where the flow changes significantly over the surface, different area-averaged HTCs may be used for different regions of the surface.

Correlations: A wide range of correlations have been developed to enable HTCs to be predicted in various situations. Many correlations are empirical, but some are developed analytically (particularly for laminar flow). These correlations are valid for the particular geometries, flow conditions and heat transfer conditions for which they were developed, and are often based on a correlation for the Nusselt number (Nu):

$$Nu = \frac{hL}{k_f}, \text{ a ratio of convective to conductive heat transfer in a fluid at a boundary}$$

Where h is the HTC, L is a characteristic length scale and k_f is the thermal conductivity of the fluid. Like h, Nu can vary continuously across a surface. Correlations may therefore be for the local value of Nu, or for an area-averaged value across a surface ($\overline{Nu}$).

Correlations for Nu or $\overline{Nu}$ are often parameterised by several key non-dimensional groups:

1. Reynolds number (Re), a ratio of momentum forces to viscous forces;
2. Grashof number (Gr), a ratio of buoyancy forces to viscous forces;
3. Prandtl number (Pr), a ratio of momentum diffusivity to thermal diffusivity.

Different correlations are appropriate for natural, forced or mixed convection, and for internal and external flow, since the temperature gradients in these flow fields vary significantly (Section 2.1.2.1), which is discussed further in Volume 3 (Section 2.2.1). In addition, correlations are often only valid for particular ranges of these dimensionless groups, so using correlations outside

of these acceptable ranges may result in errors. Checks are often included in system codes to generate warnings where correlations are being used outside of acceptable ranges, and these should be considered carefully (Section 3.2).

In laminar convection, the Nusselt number is also sensitive to the thermal boundary conditions and the constants that appear in the Nusselt number correlations have different values for uniform wall temperature (isothermal) and uniform wall heat flux thermal boundary conditions. However in turbulent heat convection, thermal wall boundary conditions have less influence on Nusselt number and in many cases the same Nusselt number correlation can be used for both types of thermal wall boundary conditions.

Many industrial applications feature complex geometries and three-dimensional or transient flow fields with forced, natural or mixed convection, making it difficult to identify appropriate correlations to use (CSNI, 2015a). These factors can motivate the use of CFD, which models the temperature gradients and heat fluxes directly, and does not therefore use HTCs (although HTCs are commonly used for external boundary conditions in CFD models, see Section 3.4).

A wide range of correlations are available in textbooks (such as Incropera *et al.*, 2011) for internal/external flow, laminar/turbulent flow, and natural, forced and mixed convection with more detail provided in Kakaç *et al.* (1987) and Rohsenow *et al.* (1998) for specific geometries. Further information on low Pr correlations suitable for liquid metals is provided in Volume 5 (Liquid Metal Thermal Hydraulics).

Correlation Inputs: Once a suitable correlation has been chosen, the variables on which it depends must be assessed. Sources of correlations often provide guidance on how to calculate values used in correlations, and this should be considered if provided. However, some challenges posed by this may include:

Characteristic Length Scales: In many situations determining these is straightforward (e.g. where the internal diameter of a pipe or stream-wise length of a plate is needed), but in some circumstances it may not be (e.g. where geometry deviates from the simple geometry on which the correlation is based). While guidance may be provided with the correlation, engineering judgement may be required to consider what values might be appropriate in the light of the expected flow field. For example, hydraulic diameter is often used for non-circular ducts.

Characteristic Flow Velocity: For external flow, engineering judgement may be required to identify a suitable free-stream velocity that can be used. For internal flow, it may be necessary to calculate either a 'superficial' velocity based on the mass flow rate or a mass-averaged velocity based on the flow in the region of interest.

Fluid Material Properties: These typically vary with pressure and temperature (Volume 3, Section 2.3). In many situations, the local pressure variations within the flow are small, so material properties can be assessed at a nominal pressure for the region of interest. However, this is not likely to be true for temperature where there is significant heat transfer, which is driven by temperature gradients:

- For external flow, where temperature differences cause modest differences in material properties a 'film temperature' is commonly used: $T_{film} = (T_w + T_{s,\infty})/2$. Iterations may therefore be needed to update the film temperature and associated properties based

on the evolving wall temperature (T_w).

- For internal flow, the bulk fluid temperature ($\overline{T_s}$ introduced above) is often used to evaluate properties for fully developed flow. In some cases a film temperature based on the mean of the wall temperature and bulk temperature may be used: $T_{film} = (T_w + \overline{T_s})/2$.
- Where large differences in material properties occur, a property ratio method may be more appropriate (Gebhart *et al.*, 1988). Due to the large viscosity ratio and high Pr in molten salts, this is covered in more detail in Volume 6 (Molten Salt Thermal Hydraulics).

The appropriate temperature to use is part of the definition of a correlation; the material properties are used to evaluate the non-dimensional numbers and k is used to convert Nu to h. Significant inaccuracies can therefore result from using the wrong definition.

Overall, when using a Nusselt number correlation, the length scales and velocity scales used to calculate the values of the relevant dimensionless numbers must be the same as defined in the correlation (i.e. consistency with the source is important and variation in definitions does exist).

2.1.2.4 Thermal Resistance

The concept of thermal resistance is introduced in Section 2.1.1.1. The thermal resistance for convective heat transfer at a surface (R_{th}) follows easily from Newton's law of cooling, using an average heat transfer coefficient ($\overline{h}$) over a given surface area (A):

$$Q = \overline{h}A(T_w - T_{s,\infty}) = \frac{1}{R_{th}}(T_w - T_{s,\infty}) \quad \text{where} \quad R_{th} = \frac{1}{\overline{h}A}$$

This is for external flow; for internal flow, $T_{s,\infty}$ is replaced by $\overline{T_s}$. This thermal resistance can be combined with other resistances to form an overall thermal resistance (as discussed in Section 2.1.1). For the simple wall shown in Figure 2.1, the overall thermal resistance would be the sum of the thermal resistances below (neglecting thermal radiation, Section 2.1.3):

1. A convective thermal resistance on the warm surface.
2. A conductive thermal resistance through the solid (Section 2.1.1).
3. A contact thermal resistance between the solid and the insulation, if appropriate (Section 2.1.1).
4. A conductive thermal resistance through the insulation (Section 2.1.1).
5. A convective thermal resistance on the cool surface.

In some situations resistances are used directly, such as for fouling resistances ('fouling factors' or 'dirt factors') on the tubes of shell and tube type heat exchangers (ζ, generally provided with units $\mathrm{K\,m^2\,W^{-1}}$). Considering a cylindrical tube with fouling on the inner (ζ_i) and outer (ζ_o) surfaces, a thermal resistance for radial conduction through a tube of $\ln(r_o/r_i)/2\pi Lk$ (where r_o and r_i are the outer and inner radii respectively and L is the length of the tube) and using the outer surface area of the tube ($A_o = 2\pi r_o L$) as the reference area:

$$Q = UA_o\Delta T \quad \text{where} \quad \frac{1}{UA_o} = R_{th,oa} = \frac{1}{\overline{h_i}A_i} + \frac{\zeta_i}{A_i} + \frac{\ln(r_o/r_i)}{2\pi Lk} + \frac{\zeta_o}{A_o} + \frac{1}{\overline{h_o}A_o}$$

$$\text{so that} \quad \frac{1}{U} = R_{th,oa}A_o = \frac{1}{\overline{h_i}}\frac{r_o}{r_i} + \zeta_i\frac{r_o}{r_i} + \frac{r_o\ln(r_o/r_i)}{k} + \zeta_o + \frac{1}{\overline{h_o}}$$

As noted in Section 2.1.1, the area (A) may be omitted from the thermal resistance (R_{th}) in some contexts, so care is needed in calculating the overall thermal transmittance (U) and the reference area used should be stated clearly. In multilayer systems, if there are orders of magnitude differences between the thermal resistance of the different layers (e.g. steel and insulation) then it can sometimes be appropriate to approximate it as a single layer system, controlled by the layer with the highest thermal resistance.

2.1.3 Thermal Radiation

All surfaces continuously emit, reflect and absorb electromagnetic radiation; the intensity and spectrum of wavelengths of the emitted photons depend on the temperature of the surface[5]. In general, thermal radiation exchange at surfaces depends on:

- The angle at which the radiation arrives or leaves.
- The wavelength of the radiation.
- The material of the surface and its condition.
- Fluid transparency and properties between surfaces.
- How directional or diffuse the incoming or reflected radiation is.

Any medium between surfaces, except a vacuum, can also 'participate' in thermal radiation exchange (i.e. absorb, emit and scatter radiation passing through it), although in many cases this is minimal (as in air). Dealing with thermal radiation in full detail is complex, and so simplifying assumptions are often used:

- Surfaces considered 'diffuse' (i.e. emission or absorption are independent of direction), 'gray' (i.e. properties are independent of radiation wavelength) and opaque (i.e. no transmission of thermal radiation occurs through the surface).
- Surfaces (or parts of surfaces) considered to be isothermal.
- The medium between surfaces considered to be non-participating.

These simplifications allow the heat transfer between surfaces to be calculated, based on the Stefan-Boltzmann law for the emitted heat flux due to thermal radiation from a surface (E):

$$E = \varepsilon \sigma T^4$$

Where T is the absolute temperature, σ is the Stefan-Boltzmann constant and ε is the surface emissivity (Section 2.1.3.2). The absorptivity of a surface (α) defines how much incident radiation is absorbed (with $1 - \alpha$ reflected). Kirchoff's law states that $\alpha = \varepsilon$ at each wavelength. This means that highly reflective surfaces also do not emit significantly. For gray surfaces, this is simplified to be the case across the entire spectrum, which is a sufficiently accurate approximation for most applications, notably excepting semi-transparent media and where insolation (e.g. heating caused by solar radiation) is important. For insolation, surfaces may well not be gray due to the high temperature of the sun (hence different radiation wavelengths), so that different values of absorptivity and emissivity are required.

[5] For the temperatures in most nuclear applications, emission is almost entirely in the Infrared (IR) range of the electromagnetic spectrum, with few very high temperature surfaces emitting in the visible range (or 'glowing').

Aspects of participating media and non-gray interactions are discussed for molten salt in Volume 6 (Section 2.5). A more complete description of the concepts and governing equations for thermal radiation and typical engineering approximations can be found in Incropera *et al.* (2011), and substantial details can be found in more specialist texts by Modest (2013) and Howell *et al.* (2016).

The non-linearity of thermal radiation with temperature usually requires numerical or iterative solution. Possibly for this reason, thermal radiation is often neglected from heat transfer calculations as a simplification. However, this may well introduce substantial inaccuracy (even at moderate temperatures) so omitting thermal radiation from heat transfer analysis should be considered carefully. This is particularly true in passive cooling situations where thermal radiation can suddenly become significant to a point where it can provide a fundamental part of a cooling duty.

2.1.3.1 Enclosures

For an enclosure of N gray surfaces, analysis is complicated by the fact that each surface absorbs part of the incident radiation and reflects part, and incident radiation contains components from multiple previous surface emissions and reflections. This leads to a set of N simultaneous equations for the net rate that energy leaves each surface (i) of the enclosure, that are framed in terms of the radiosity (J_i) which is the thermal radiation leaving a surface (the sum of the thermal radiation emitted and the reflected part of the incident irradiation). By solving for the set of radiosities, the heat fluxes or temperatures of surfaces can be determined (more detail is available in Incropera *et al.*, 2011).

$$Q_i = \sum_{j=1}^{N} Q_{ij} = \frac{E_{b,i} - J_i}{(1-\varepsilon_i)/\varepsilon_i A_i} = \sum_{j=1}^{N} \frac{J_i - J_j}{(A_i F_{ij})^{-1}}$$

Where F_{ij} is the view factor between the i, j pair of surfaces, which is the fraction of the thermal radiation leaving surface i that is intercepted by surface j. For an N-surface enclosure, there is an $N \times N$ view factor matrix. Values may well be non-zero for $i = j$, so that a surface intercepts some of its own thermal radiation (e.g. all concave surfaces will to some extent). View factors have the properties of reciprocity and summation (which are useful in determining their values) so that:

$$A_i F_{ij} = A_j F_{ji} \quad \text{and} \quad \sum_{j=1}^{N} F_{ij} = 1$$

It is common to use the special case of the two surface enclosure, which simplifies the radiosity equation to:

$$Q_{12} = Q_1 = -Q_2 = \frac{\sigma(T_1^4 - T_2^4)}{\frac{1-\varepsilon_1}{\varepsilon_1 A_1} + \frac{1}{A_1 F_{12}} + \frac{1-\varepsilon_2}{\varepsilon_2 A_2}}$$

There are a number of useful simplified cases where this can be applied, such as:

- A small convex object in a large enclosure like a big room or the environment. In this case $A_1/A_2 \approx 0$ and $F_{12} = 1$, so $Q = \sigma\varepsilon_1 A_1(T_1^4 - T_2^4)$ and the emissivity of the large surroundings does not need to be known. As noted previously, for incident *solar* radiation the absorptivity of surfaces (α) may differ significantly from the emissivity (ε).
- Facing surfaces like large parallel plates or long concentric cylinders. Figure 2.4 shows the heat transfer across a gap between two solids separating hot and cold regions, such as may

occur in a double-walled vessel, layers of multi-foil insulation, or a contact resistance (Section 2.1.1.1). In parallel with thermal radiation across the gap, there will either be conduction through a stationary fluid, or enhancement of heat transfer by buoyancy driven convection (the separation distance, orientation and temperature difference between the surfaces will determine which). In this case $A_1 = A_2 = A$ and $F_{12} = 1$, and the emissivity of both surfaces is needed:

$$Q = \frac{\sigma A(T_1^4 - T_2^4)}{\frac{1}{\varepsilon_1} + \frac{1}{\varepsilon_2} - 1}$$

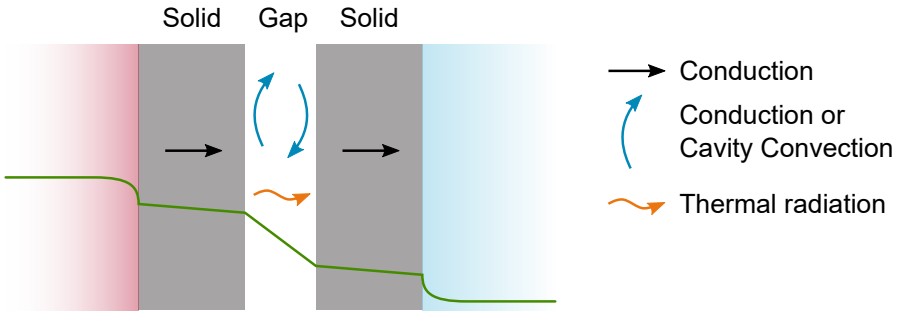

Figure 2.4: Thermal radiation in the gap between two solids.

2.1.3.2 Emissivities

The surface emissivity (ε) is the ratio of radiated energy compared to that which would be emitted from an ideal 'black body' at the same temperature ($E = \varepsilon E_b$). The emissivity of a surface is highly dependent on the material, its surface finish (roughness) or coating and the temperature. Highly polished metals can have values of $\varepsilon < 0.3$, or even $\varepsilon < 0.1$, whereas some of these materials when oxidised can have values of $\varepsilon > 0.8$. Painted surfaces, ceramics and natural materials like wood or paper often have $\varepsilon > 0.9$. Collections of data for a range of materials and surface conditions are provided in references like Modest (2013) and Howell *et al.* (2016).

The emissivity of surfaces on an as-installed component may be difficult to assess because the surface condition may vary through life on a plant, causing a significant source of uncertainty. This may need to be investigated using validation data, sensitivity studies and uncertainty quantification (Volume 4, Confidence and Uncertainty). Validation data also has uncertainty, however, because instruments like pyrometers, pyranometers and IR cameras require calibration. Surfaces can be painted with known emissivity paints or have small swatches of material with a known emissivity fixed to them, to help with taking measurements.

2.1.3.3 View Factors

Calculating view factors between two finite surfaces with an arbitrary orientation is a mathematically involved process. However, attempting this from first principles is not usually necessary. Since view factors are geometric parameters, either a dedicated tool with a numerical algorithm to evaluate them could be used, a CFD code with a Surface-to-Surface (S2S) model could be employed, or catalogues of pre-calculated configurations could be considered (such as Modest, 2013 or Howell *et al.*, 2016).

2.1.3.4 Thermal Resistance

The thermal resistance due to radiative heat transfer at a surface can be derived using the decomposition $(T_1^4 - T_2^4) = (T_1 - T_2)(T_1 + T_2)(T_1^2 + T_2^2)$ and the enclosure equations introduced in Section 2.1.3.1, for example (parallel plates):

$$Q = \frac{1}{R_{th}}(T_1 - T_2) \quad \text{where} \quad R_{th} = \left(\frac{\sigma A (T_1 + T_2)(T_1^2 + T_2^2)}{\frac{1}{\varepsilon_1} + \frac{1}{\varepsilon_2} - 1} \right)^{-1}$$

This illustrates that for thermal radiation R_{th} depends strongly on the surface temperatures (that are usually being calculated) and the complexities of multi-surface enclosures in a way that was not the case for conduction or convection. This makes thermal resistances less convenient to use when thermal radiation is involved.

2.2 Surface Modifications

The characteristics of the solid surface in contact with a fluid can have a significant impact on local heat transfer. It is possible to significantly increase or decrease the heat transfer by convection and/or thermal radiation by making deliberate modifications to the surface finish. It is also true, across industry, that surfaces rarely remain in their 'as manufactured' state once a component is in service. In order to predict the heat transfer between the solid and the fluid it is therefore important to consider the details and condition of the solid surface. This section discusses common surface characteristics and the implications for thermal hydraulic analysis.

2.2.1 Surface Roughness and Heat Transfer Enhancement

Surface roughness has the potential to significantly affect both the pressure loss and heat transfer through a component. A high surface roughness disrupts the viscous and thermal sublayers within the boundary layer. This promotes transition to turbulence and subsequent turbulence generation thereby increasing mixing and heat transfer. Surface roughness may be as an incidental consequence of manufacturing (e.g. machining, casting or welding) or may be deliberately controlled to achieve a specific heat transfer and hydraulic performance. It should also be noted that the roughness of a surface may change over time once a component is in service due to erosion or corrosion damage or the deposition of substances on the surface.

The extent to which roughness affects the flow depends on the height of the roughness compared to the thickness of the viscous sublayer in turbulent flow (Figure 2.5). For example, the thickness of the viscous sublayer decreases with increasing Reynolds number and therefore a smaller surface roughness will have an effect. For fully developed turbulent flow in circular ducts this is illustrated by the well-known 'Moody Diagram', which shows the friction factor as a function of roughness and Reynolds number (Section 3.4.2.5).

For internal flow in simple geometries, such as pipes, ducts or between plates, correlations for the Nusselt number under a range of conditions can be found in text books such as Rohsenow *et al.* (1998)[6]. Provision for random 'sand grain' rough surfaces is also made in most mainstream

[6] For fluids where $Pr \ll 1$, general correlations are often not applicable as discussed in Volume 5.

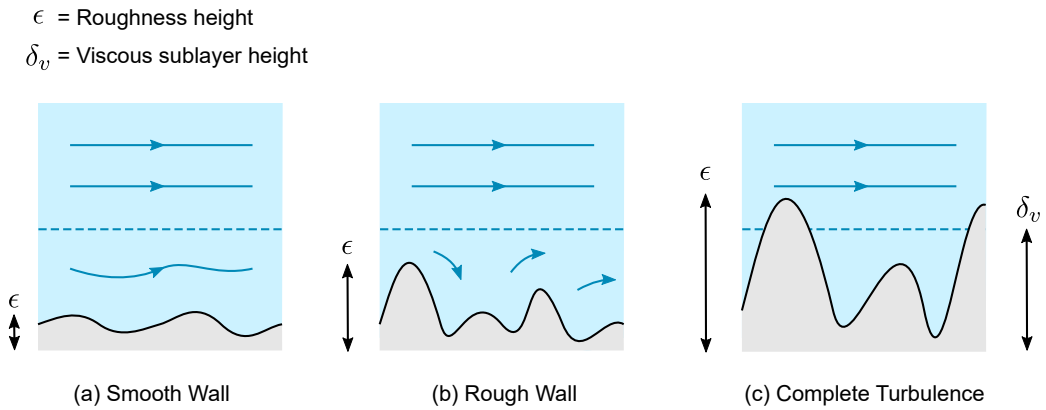

Figure 2.5: Illustration of impact of roughness on boundary layer.

CFD codes, but careful reference should be made to the code documentation, especially when predicting surface to fluid heat transfer in fluids where *Pr* is significantly different from 1.

The surface heat transfer from a rough surface can be several times that of a hydraulically smooth surface. For this reason designers sometimes deliberately roughen surfaces to increase heat transfer. Surfaces that are artificially roughened for the purpose of enhancing heat transfer often employ a regular pattern of protuberances or grooves (such as the ribs that may be used on fuel cladding). The heat transfer (and hydrodynamic) performance of these surfaces can be more complicated to predict. This is because the heat transfer enhancement achieved is often partially due to an increase in the surface area (the fin effect) as well as increased turbulent mixing in the near-wall flow. The performance of a specific surface design is often experimentally measured and can then be used as an input to predictive analysis.

Other design modifications that may be used to enhance single-phase heat transfer include extended surfaces (such as fins) and devices placed either on or close to the surface that change the flow to promote heat transfer. These are effective in both laminar and turbulent flow. Heat exchanger designers often make extensive use of a complex (and sometimes proprietary) combination of these modifications to achieve a high heat transfer in a compact design. Further details on a greater variety of surface heat transfer enhancement techniques can be found in Rohsenow *et al.* (1998, Chapter 11) or Saha *et al.* (2016).

Extended surfaces work by increasing the surface area available for heat transfer. Conjugate heat transfer is of vital importance in the prediction of heat transfer for a finned surface, as the temperature of the fin can vary significantly between the root and the tip. Helical fins act to both increase the surface area and modify the flow by introducing swirl. This increases the effective flow path and promotes mixing via secondary flows.

The spacer grids used to maintain the geometry of fuel assemblies are an example of flow modification to enhance heat transfer using a device remote from the surface of interest. These grids may be designed with vanes to increase flow mixing, in addition to their primary, structural support function. The corresponding increase in heat transfer between the fuel and the primary circuit fluid can be observed in the region downstream of each spacer grid.

2.2.2 Surface Deposition

The deposition of solids on surfaces within a nuclear reactor is almost always driven by a chemical reaction. The chemical composition of the exposed solid surface and the fluid determine the composition of the deposit and this therefore varies significantly between reactor technologies. Some surface deposits are beneficial, for example, stainless steel is designed to maintain a stable oxide layer giving it corrosion resistance. The rate of accumulation of the deposit and whether it adheres to the surface or breaks away are often highly dependent on local thermal hydraulic considerations, such as temperature and flow rate.

All reactor technologies have the potential to form deposits in the primary circuit. That most familiar to UK nuclear engineers is the deposition of carbon within the primary circuit of Advanced Gas-cooled Reactors (AGRs) (the chemistry of which is briefly described in ONR, 2019). The carbon deposition occurs throughout the circuit, but especially in the higher temperature regions, including on the fuel cladding (Figure 2.6). The deposit reduces the effectiveness of the heat transfer from the fuel to the coolant in two ways. Firstly, by reducing the effectiveness of the ribs on the surface of fuel (by accumulating between them) and, secondly, by introducing an additional thermal resistance as heat from the fuel must conduct through the deposit.

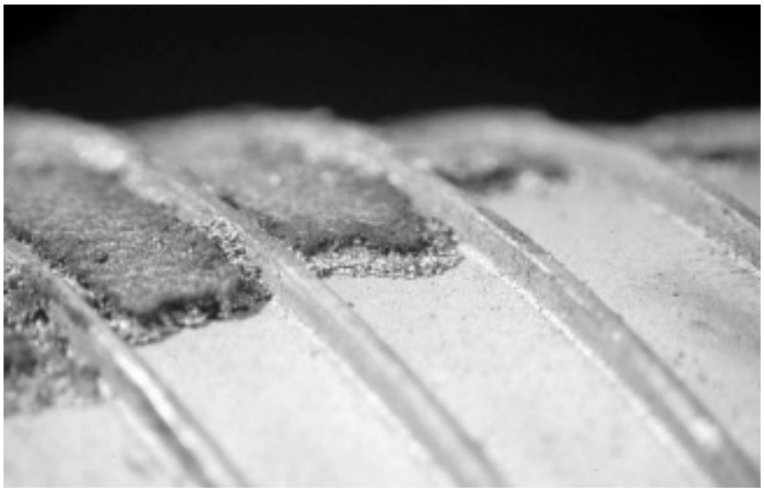

Figure 2.6: Picture of high levels of AGR fuel pin deposition (Mowforth *et al.*, 2015).

It is important for CHT modelling to consider if the presence of a deposit must be taken into account. This is often quite challenging as the thickness, location and thermal properties of the deposit may be subject to considerable uncertainty. Some deposits have complex, porous structures and some vary in thickness over the life of the reactor (e.g. after 40 years), building up and then breaking off into the flow or reducing in thickness due to a chemistry or temperature change.

In addition to the surface-to-fluid heat transfer, changes to the surface emissivity may also need to be considered. Predicting the occurrence of a deposit in a quantitative manner is even more complex and requires a multiphysics model coupling chemistry with thermal hydraulics. Even with modern modelling techniques, much still needs to be determined by inspection and experiment.

A complete study of deposits found in nuclear reactors is beyond the scope of this document.

However, considering the technologies most likely to comprise the next generation of NPP, the following sections consider relevant examples with references to enable further reading.

2.2.2.1 CRUD

The most important and highly studied deposit in a Pressurised Water Reactor (PWR) reactor is often referred to as Chalk River Unidentified Deposits (CRUD). It is used to describe the chemically and structurally complex scale that accumulates on the hottest regions of the reactor, including the fuel cladding, and is thought to be caused by sub-cooled boiling that precipitates solutes in the primary circuit fluids on the cladding surface. At typical PWR temperatures this process is aggravated by the inverse relationship between the solubility of key compounds and the water temperature. The CRUD accumulates as a porous layer, with boiling (and therefore further precipitation) occurring within its structure. The resulting CRUD is chemically complex, comprising a variety of compounds including both primary circuit constituents and corrosion products. A similar, although chemically slightly different deposit is also observed in Boiling Water Reactors (BWRs).

CRUD is of concern for several reasons including its effect on the core neutronics. Compounds of boron (intentionally present in the primary circuit water as boric acid used to control reactivity) can accumulate in the CRUD, locally suppressing the neutron flux. This can cause a phenomenon called CRUD Induced Power Shift (CIPS), also called the Axial Off-set Anomaly (AOA), where a downward axial shift in power distribution is observed. Control rods enter the core of a PWR from the top, so this could cause a delay in reactivity control. By the time the fuel is removed from the reactor, the CRUD itself can contain activated isotopes leading to increased radioactivity of the fuel. From a thermal hydraulic perspective, CRUD may impair the heat transfer from the fuel to the primary circuit fluid. The locally increased fuel cladding temperatures can lead to an increased rate of corrosion damage to the cladding. The presence of CRUD can also increases the fuel rod friction coefficient, increasing the pressure drop in affected areas of the core and potentially altering the core flow distribution.

Due to its importance to current generation reactor performance, CRUD has been extensively studied and significant guidance is captured in documents such as EPRI (2004), EPRI (2014) and EPRI (2020). Thermal hydraulics is of significance both to the prediction of the formation of CRUD and its impact on heat transfer. The prediction of CRUD formation requires the coupling of chemistry and thermal hydraulics (as described in Henshaw *et al.*, 2006). Multiphysics nuclear codes have been developed for this purpose, for example, the MAMBA code as described in Kendrick *et al.* (2013) was incorporated with a whole core model to predict CIPS using VERA, as part of the CASL programme (Collins *et al.*, 2018).

Prediction of heat transfer through a CRUD layer is complicated by the boiling that can occur within the porous structure and this is further complicated by the effect of the concentration of solutes on the saturation temperature of water. EPRI (2011) describes experimental work to determine the effective thermal conductivity of CRUD carried out using the Westinghouse Advanced Loop Tester (WALT) facility. The effective thermal conductivity is found to be highly dependent on the heat flux in addition to the thickness of the deposit. With increasing heat flux the fluid within the CRUD undergoes single-phase heat transfer, nucleate and 'wick' boiling, and dry-out. The study also found that under specific conditions of a small (around 15 µm) CRUD thickness and moderate heat flux, the CRUD acted to enhance heat transfer from the surface when compared to a clean rod,

by promoting the initiation of sub-cooled nucleate boiling. However, at higher CRUD thicknesses or higher (or lower) heat fluxes the CRUD is generally found to impair the heat transfer.

2.2.2.2 Oxide Layers in Heavy Metal Reactors

A protective layer on the surface of steel reactor components is required in a heavy liquid metal environment. Without it, the steel is attacked by dissolution of its components into the lead or Lead-Bismuth Eutectic (LBE) primary coolant. A popular solution to this problem is to introduce oxygen into the coolant to promote and maintain the formation of thin oxide layers on the steel surfaces. The level of oxygen needs to be carefully controlled: too little and the oxide layer will not be maintained; too high and the oxide layer may grow to a size where it spalls off the surface or oxides may form in the coolant itself (e.g. lead oxide). Excess oxide may then be transported by the coolant and deposit in the cooler regions of the reactor, potentially disrupting flow paths.

The nature of the oxide layer depends on the constituents of the steel. Oxides of iron and chromium are often present and a complex two or three layer structure can develop (further described in NSC, 2015). Due to the importance of corrosion resistance in heavy liquid metal reactors, an extensive range of relevant experiments have been published using a wide range of steels (for example Deloffre *et al.*, 2002). However, it is noted that work is still ongoing with no single best way forward identified to date.

The effect of the oxide layer on the conjugate heat transfer depends on its thickness and conductivity. The thermal conductivity of the oxide layer will depend on its composition and structure (e.g. the proportion of voids within the oxide). It is extremely likely to be lower than that of either the steel or the coolant and will therefore reduce the surface-to-fluid heat transfer, however, the effect may be negligible if the layer is thin. Despite the amount of work that has been undertaken, oxide layer studies focus on the formation, composition and structural characteristics of the layer (i.e. the factors that matter most to corrosion resistance) rather than the thermal properties. There is, therefore, likely to be considerable uncertainty in the thermal properties of the layer.

2.2.2.3 Metallic Deposits in Sodium and Molten Salt Cooled Reactors

The surface deposition within Sodium-cooled Fast Reactors (SFRs) or Molten Salt Reactors (MSRs) differs from other technologies. Of particular significance is that the oxide layer normally present on the surfaces of structural steels is not stable in these environments. The bare metal is therefore exposed to the coolant, potentially making it more vulnerable to corrosive attack.

Under these circumstances, alloying agents within the steel, such as chromium or nickel, are dissolved into the coolant in hotter regions of the reactor and these can then be deposited (or 'plate out') in cooler regions, such as heat exchangers. Any contaminants present in the coolant (inevitable in low concentrations) can also lead to the formation of oxide, carbide or nitride deposits. For MSR designs where the fuel and therefore the fission products are dissolved within the primary circuit fluid, deposition of some fission products has been found to occur on reactor surfaces.

Surface deposition is not an area of high concern for these reactor technologies. However, over time, the level of deposition may result in flow restrictions in narrow passages or heat transfer impairment (Pioro, 2016).

2.2.2.4 Graphite Dust in High Temperature Gas Reactors

Where graphite is used as a moderator, there is the potential for the generation, dispersion and deposition of this dust on surfaces within the reactor. This is of particular concern for pebble bed reactors where the movement of the pebbles generates dust by abrasion. This dust is then deposited on the fuel itself or may be transported by the primary circuit fluid and deposited on other reactor components (for example, the steam generator, as described in Peng *et al.*, 2016). The dust is radioactive so, as well as potentially impeding heat transfer, it complicates maintenance activities and could contribute to a radiological release in the event of a breach of the primary circuit.

2.2.3 Surface Corrosion and Erosion

The International Organization for Standardization (ISO) definition of corrosion is *'a physiochemical interaction leading to a significant deterioration of the functional properties of a material, or the environment with which it has interacted, or both of these'* (Féron, 2012). Corrosion damage can be found in a variety of engineering environments and applications, with one of the most widely encountered being the corrosion of metals in the presence of water.

Erosion is the degradation of a surface due to mechanical action. In fluid mechanics this can be by the impingement of a fluid on a surface or abrasion by solid particles, gas bubbles or liquid droplets suspended in the fluid. Corrosion and erosion can change the roughness of a surface and/or the local material properties of the surface material. Therefore, the possibility of corrosion and erosion damage to a surface needs to be taken into account when considering heat transfer.

Thermal hydraulics is also important in the occurrence of corrosion and erosion. For erosion, the momentum of the flow (and any particles suspended in it) is directly responsible for the damage. Important factors in the prediction of the rate of erosion include the flow velocity and the angle of impact with the surface. For corrosion, the fluid flow may transport the reactants involved to the surface and the rate of the chemical reactions associated with corrosion is often temperature dependent. Erosion and corrosion can also act together to cause more damage that either would alone. For example, in Flow-Accelerated Corrosion (FAC), fast flowing fluid is responsible for stripping away (or dissolving) corrosion products from the surface leaving it open to further attack (Figure 2.7).

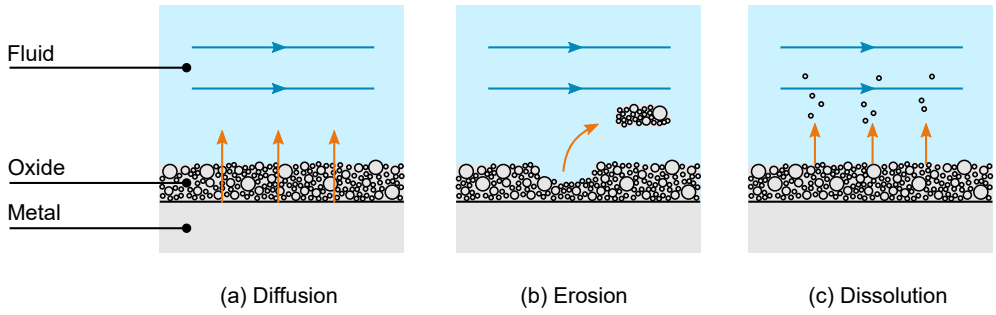

Figure 2.7: Illustration of processes occurring during Flow-Accelerated Corrosion.

In NPPs, the control of damage to reactor components is of key importance to both nuclear safety and the economic performance of the plant. Difficulties in the replacement of components in a

nuclear environment mean that the selection of materials with a long (>40 years) lifespan in the relevant (and industrially unique) environments are required. Additionally, irradiation can act to change the properties and structure of materials over their lifetime making them more vulnerable to damage.

Corrosion and erosion damage to NPP components is a large topic involving material science and chemistry as well as thermal hydraulics. Féron (2012) provides a useful overview of the subject of corrosion, including corrosion mechanisms commonly found in NPPs and in-service inspection an monitoring. The remainder of this section considers only aspects that potentially impact on CHT modelling rather than the wider topic.

2.2.3.1 Surface Geometry

An important consideration when attempting to model a corroded surface is that some corrosion products have a different physical structure and volume to the original metal material, as well as different material properties. The changes to the geometry of the corroded component may have a significant affect on the fluid to surface heat transfer if, for example, a geometrical heat transfer enhancement feature (see Section 2.2.1) has been destroyed or covered by oxide.

Aqueous corrosion is a commonly found example where the corrosion products (e.g. aqueous iron oxide) can have a significantly different structure and volume to the original steel. The majority of NPPs in current operation are Light Water Reactors (LWRs) that typically use water in both the primary and secondary circuits. These are a mature technology, so have had the advantage of learning from the reactors of the past with regard to material selection, but potentially higher risk areas are still present. The biggest corrosion issues are often found on the secondary (steam side) components (Féron, 2012), including the primary heat exchanger, and are often associated with FAC. This is likely to be a concern for all reactor technologies with a steam secondary system. Additionally, peripheral reactor systems often include pipes and tanks that are largely unprotected from the weather and so are vulnerable to damage by corrosion.

2.2.3.2 Surface Roughness

One of the easiest surface changes to envisage due to damage by erosion and corrosion is the surface roughness. For a smooth surface, damage can roughen it, enhancing heat transfer and increasing the friction factor (potentially resulting in higher pressure losses) as described in Section 2.2.1. It is also noted that surface roughness can have a very significant effect on initiation and progression of corrosion, with rougher surfaces often being more vulnerable that smoother ones. For example, Platt *et al.* (2015) illustrates the effect of surface roughness on oxidation of the fuel cladding material Zircaloy-4.

Corrosion and erosion can also act to reduce the surface roughness where ribs or other heat transfer enhancing features are present. This has significant overlap with the consequences of deposition as discussed in Section 2.2.2.

2.2.3.3 Surface Emissivity

Changes to a surface finish have the potential to significantly affect the radiative heat transfer by changing the surface emissivity. For example, polished stainless steel has an emissivity of around 0.3 whereas oxidised stainless steel has an emissivity of closer to 0.8 (Incropera *et al.*, 2011). As described in Section 2.1.3, the transfer of energy by thermal radiation is proportional to T^4, so changes to emissivity can significantly impact radiative heat transfer in nuclear reactors where the temperatures are high. This is important for passive cooling systems that rely on thermal radiation, as surface finish degradation could reduce the heat transfer effectiveness.

For commonly used materials, such as steel, values of emissivity are often readily available for a variety of surface conditions. However, a full range of information may be harder to find where specialist materials are used or where erosion or corrosion has degraded a surface coating, exposing the material underneath.

2.2.3.4 Surface Material Properties

Corrosion in particular can significantly alter the thermal and structural properties of the surface material. Generally, corrosion products (including oxide layers) are not considered to contribute to the structural properties of the component, so corrosion of a pipe (say) is effectively a thinning of its walls. Corrosion of alloys can alter the material properties of the surface without producing a deposit.

Fluids such as lead, LBE and molten salts can leach alloying agents such as nickel and chromium from steels, especially along the steel grain boundaries. This leaves a layer of material with a weakened, more porous structure close to the surface. Further information on steel corrosion in molten salt and heavy liquid metal environments is given in Zheng and Sridharan (2018) for salts and Zhang (2009) for lead/LBE.

For CHT, the specific material properties (especially conductivity) of any corrosion products present on the surface may be important. In a similar manner to surface deposition, the specific composition and material structure of any corrosion products may be hard to determine/predict with a high level of certainty, and so the information needed to determine thermal conduction through them may not be easy to acquire.

2.2.4 Surface Coatings

In engineering applications it is not unusual to deliberately apply coatings to the surface of components, paint being a very simple example. These coatings are often applied to increase the resistance of the surface to damage, but can be used for other reasons (e.g. to change the appearance of the surface).

A relevant recent example of coatings considered for a NPP application is in the development of accident tolerant fuels for LWRs as described in Terrani (2018). These are intended to reduce the rate of oxidation of the underlying Zr fuel cladding in the presence of high pressure steam under severe accident conditions. It is specifically noted in Terrani (2018) that, in this case, the coating is considered sufficiently thin to have no significant effect on the heat transfer.

An advantage of deliberately applied coatings (as opposed to surface deposits or corrosion) is that their effect on the thermal performance of a component can be considered (and potentially measured) at the outset. The information required to take account of these coatings in any CHT modelling is, therefore, more likely to be available.

2.3 Material Properties

Temperature gradients within a solid and how quickly the temperature changes over time is dependent on the thermophysical properties of the solid (density, specific heat capacity, thermal conductivity and emissivity). For transient simulations all of these properties are important in order to account for the thermal mass of the solid. In general, the properties of solids vary due to a range of factors that should be considered, including:

Nature of Solid: The properties of solids may be altered by a range of factors (such as contamination, addition of different species and ageing due to radioactivity). This means that the material properties may change through the life of the plant, particularly for those components in high radiation areas, such as the core. The key factors to consider and their impact are likely to be case specific.

Temperature: Temperature changes often cause large variations in solid properties. Therefore, the variations in properties with temperature are a key aspect to consider when performing thermal analyses with conjugate heat transfer. As for fluid properties, temperature varying properties can be implemented by linearly interpolating or fitting measured data (Volume 3, Section 2.3.2).

Surface Finish: As discussed in Section 2.1.3.2, the emissivity of a surface is highly dependent on the material, its surface finish and the temperature. Therefore, the emissivity of a solid can change through the life of the plant as the surface becomes oxidised or covered by a thin layer of deposit. As a result, the emissivity is a significant source of uncertainty in material property data that may need to be investigated.

Porosity: Some materials are porous (contain pores/voids that are filled with fluid), such as insulation or graphite. The impact of the fluid on the overall material properties needs to be considered and taken into account, if necessary. However, this is essential for porous zones (regions used to represent solid and fluid components, Section 3.3.4), such as perforated plates or tube banks, and effective material properties for the porous zone need to be carefully calculated (Section 3.4.3.3).

Anisotropy: Some materials, such as composites, reinforced concrete and porous media (Section 3.4.3.3), also have anisotropic properties, such as thermal conductivity, which may change over time. This can significantly impact the thermal gradients within the solid and so needs to be carefully considered. Anisotropic thermal conductivity is available in most CFD codes, but requires knowledge of the material specification or can be calculated using a detailed thermal model of the material.

The rest of this section identifies some sources of material property data and considers how these might be used. However, it is also important to understand the accuracy of the data itself, and so whether this needs to be considered as part of a sensitivity analysis or uncertainty quantification.

The properties of fluids are discussed in Volume 3 (Section 2.3).

2.3.1 Sources of Property Data

Possible sources of material property data for a number of common solids are presented below, although general values can be found in most text books, such as Incropera *et al.*, 2011. Whatever source is chosen, this is a key input to analysis work, so the accuracy of the data should be considered and the approach used documented.

Steel: Most SSCs are manufactured from different types (carbon, alloy or stainless) and grades (classification based on alloy content and manufacturing process) of steel. The type/grade of steel can significantly affect the thermophysical properties of the material, and so it is important to identify the actual steel used and determine its properties. It is worth noting that the thermal conductivity of stainless steel is significantly lower than carbon steel. Published sources of data for common steels include ASME (2019a), text books such as Davis (1998) or alternatively specification sheets may be obtained from the steel manufacturer, if known. In addition, IAEA (2006) and IAEA (2009) provide properties of some steels, as well as fuel material, cladding and moderator properties.

Insulation: Insulation is used inside and outside containment to reduce heat loss from hot surfaces. This is designed to have a low thermal conductivity and covers a wide range of different materials, such as Reflective Metallic Insulation (RMI), encapsulated fibreglass and calcium silicate. Published sources of data for common insulation materials include Incropera *et al.* (2011), alternatively specification sheets may be obtained from the manufacturer, if known. The uncertainty in insulation properties can be significant due to poor fitting, compression, ageing/damage over time, gaps between sheets or penetrations through the insulation, and so the effective thermal conductivity may be much higher than expected.

Concrete: Concrete is the most commonly used civil engineering construction material in the nuclear industry with different mixes used depending on the situation and application (density, strength and durability), and may be reinforced with steel rebar or internal cables (prestressed). The properties depend on the concrete mix used and can change over time due to ageing and thermal effects. Published sources of concrete material data include ORNL (2006) and The Concrete Centre's dynamic thermal properties calculator[7].

2.4 Structural Integrity

As discussed in Section 1.2.2, CHT analysis is often used to provide temperature fields in support of structural integrity assessments. As well as the direct impact of spatially varying temperature fields on stresses in materials, temperature fields are also critical in defining the material properties that are used in assessments. The properties of metals (such as Young's Modulus, yield stress and fracture toughness) change with temperature, and therefore a good resolution of the temperature field is key to a well-constructed and rigorous structural integrity assessment. This section introduces some key structural integrity concepts.

[7] www.concretecentre.com/Publications-Software/Design-tools-and-software/Dynamic-Thermal-Properties-Calculator-(1).aspx

2.4.1 Loading Categories

Before discussing how temperature fields are used in structural integrity assessments, it is necessary to introduce some concepts with respect to loading and consequently stress. Loading and the resulting stresses are categorised as either primary or secondary:

Primary loads are stresses that are required to equilibrate applied loads. They are known as 'sustained' or 'persistent'. As a structure deforms, primary loads do not relax (diminish) or reduce their effect on the structure, and may therefore cause unbounded deformation leading to failure. Examples of primary loading include loads arising from gravity or internal pressure.

Secondary loads are stresses that diminish as a structure deforms. An example of secondary loading is a load arising from constrained thermal expansion. The stresses are generated by the constrained expansion, so if the constraining structure were to displace, the stresses within the constrained structure would typically relax and not drive the structure to failure alone (although there may be complex interactions with other mechanisms).

While the above example categorises thermal stresses as secondary, in practice thermal stresses can be either secondary or 'long range' (primary in how they are assessed). A through-wall temperature gradient in a pipe and the resulting bending stress would typically be categorised as secondary. However, a long length of expanding pipework would be categorised as long range, when considering its effect on a connecting nozzle, anchor or vessel. This is because the deformation of the nozzle, anchor or vessel, will likely not lead to sufficient relaxation of this thermal expansion to avoid driving failure in the component.

2.4.2 Assessment Concepts

The purpose of a structural integrity assessment is to limit the possibility of failure to within recognised acceptable limits. The assessment procedures are numerously codified and these codes, although based on the same principles, are defined by national bodies and often have a basis in legislation. Examples of design codes used to design of piping and pressure vessels include ASME (2019b), BS EN (BSI, 2014, BSI, 2017) or AFCEN (AFCEN, 2018a, AFCEN, 2018b). These codes relate to new design, but the codified methods are used in assessing existing components as well.

Failure of an SSC would typically be defined as a breach of a pressure boundary or an inability to perform its intended function, both of which may have significant safety and economic impact. Protection against failure from the following broad concepts are assessed:

1. Plastic collapse: failure through gross plastic deformation.
2. Gross plastic strain: large stresses that result in plastic strains that are greater than the material ductility.
3. Cyclic loading: alternating loads that typically result in fatigue and/or alternating plasticity resulting in a 'ratchet' failure.
4. Buckling: instability in structures due to compressive loading effects.
5. Creep: this includes mechanisms like creep rupture, creep fatigue or creep crack growth resulting from high temperature service.

6. Defect tolerance: only routinely deployed for highly safety significant structures. This considers the tolerance of a structure to known or postulated defects (or cracks) and includes assessment of fatigue crack growth.

Assessment to these concepts is either conducted by rule and/or Finite Element Analysis (FEA) supported by assessment. The route is usually set by the assessment code, but where loading or geometry becomes complex (particularly with temperature fields) then the assessment is likely to be supported by FEA. An example FEA model is shown in Figure 2.8.

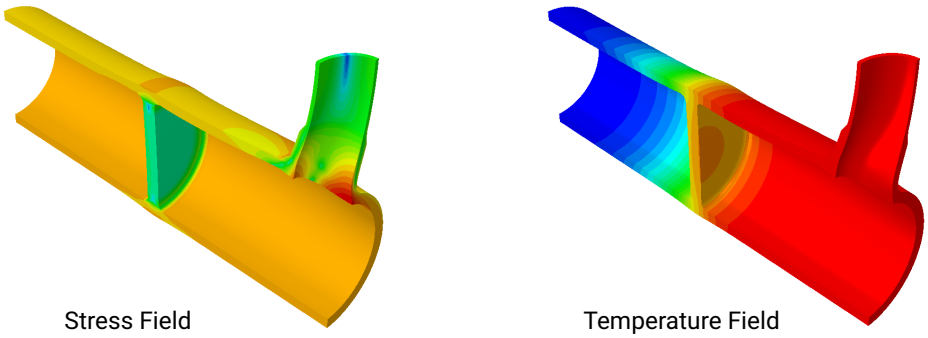

Figure 2.8: Example of stresses predicted by an FEA model.

Temperature fields are used extensively in these assessment concepts. Of particular interest are complex spatially varying fields (such as Figure 2.8) in a structure resulting in differential thermal expansion, through-wall temperature profiles (typically from thermal shocks) that result in bending stress profiles, or whole system temperature gradients or differentials resulting in long range thermal stresses. Temperature gradients are a key concern, as they set up differential expansions of the structure and this generates stresses. However, isothermal states are of equal concern, as creep in high temperature isothermal states and transients between two isothermal states are important (e.g. differential expansion between hot and cold plant states). An overview of how temperature fields might be used in each of the six failure concepts is discussed below.

Plastic Collapse: The load arising from temperature fields are only considered in plastic collapse assessments if they are judged to be long range. An example was given above of a long length of expanding pipework which could result in a primary load on any connected nozzle, anchor or vessel. The reason truly secondary loading is not assessed is that through yielding of the structure, the secondary load would relax and not lead to plastic collapse.

Gross Plastic Strain: The combined primary and secondary stresses are considered across any cycles that the component may see. The most severe of these tend to be between hot and cold plant states or thermal shock events. This will often see large reversing stresses that should be checked to ensure their total stress range does not exceed the ductility of the material of construction in one single cycle. The exhaustion of ductility leads to the rupture of the component.

Cyclic Loading: This considers loading that is applied to structures that could, through repeated alternating application, drive a failure of the structure. Codified methods often have amalgamated methods that deal with both fatigue and ratchet in one assessment but they are two different concepts. Both of these concepts are impacted by both primary and secondary loading:

- Fatigue is the initiation of crack-like defects in the structure through the repeated application of loads and is typically split into high and low cycle fatigue (Figure 2.9). The boundary between low cycle and high cycle fatigue is typically 10,000 cycles. Above this is high cycle fatigue, where small elastic alternating stresses initiate a crack like defect. Below a certain alternating stress level (that is material, geometrically and environmentally dependent) no defect will be initiated no matter how many cycles occur, and this is the endurance limit. Low cycle fatigue is typically below 10,000 cycles and is for larger stress ranges that see alternating plastic stresses. Low cycle fatigue is again concerned with initiating a defect, but through far fewer cycles compared to high cycle fatigue.
- Ratcheting is incremental increases in plasticity brought about by alternating loads that could ultimately lead to ductility exhaustion of the material. If the loading is shown to be within the ratchet boundary then the loading is said to have ‘adapted’ and any repeat application of the loading will not result in any further net accumulation of plastic strain. If the repeat loading is not within the ratchet boundary, the repeat application of load results in incremental accumulation of plastic strain that ultimately leads to ductility exhaustion.

Both of these concepts can be driven by thermal loads. Start up and shutdown of plants can be significant contributors, as can local thermal effects where rapid heating and cooling of the surface due to eddies in the adjacent fluid result in through-wall bending stresses.

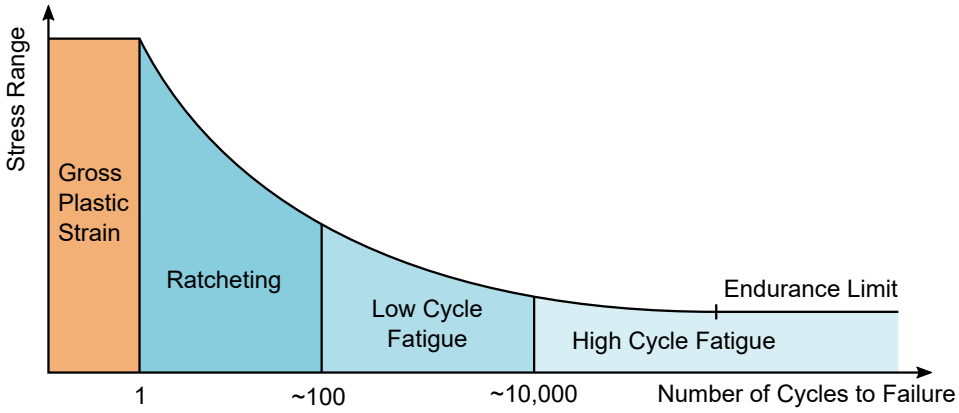

Figure 2.9: Cyclic loading of varying stress and failure mechanisms.

Buckling: The stability of vessel shells or piping networks is important, and buckling can be driven by constrained thermal expansion. The constrained thermal expansion can cause a compressive stress field that could result in buckling.

Creep: When metals operate for long periods of time at temperatures above approximately one third of their melting temperature, irrecoverable strains accumulate over time. These temperature and time dependent strains are referred to as creep strains. Two general types of failure can occur due to the accumulation of creep strain:

- Creep rupture results in the failure of a gross section of a component due to high accumulation of creep strain caused by the presence of primary loading.
- Creep ductility exhaustion can lead to localised cracking and is generally caused by creep strain accumulation from the relaxation of secondary stresses cause by thermal fields.

Where both creep strains and cyclic loading occur in a structure they can become synergistic, a phenomenon referred to as creep-fatigue. The presence of both simultaneously can lead to cracking of the component in unexpectedly short timescales than if fatigue and creep were assessed separately. Alternating thermal stresses, or creep strain from the relaxation of thermal stresses can have a significantly deleterious effect on creep-fatigue life.

If a structure operating in the creep temperature range is cracked, the crack will grow in the absence of any fatigue loading due to the accumulation of creep damage at the crack tip. If fatigue loading is also a contributor to crack growth, synergy between the fatigue and creep mechanisms can lead to accelerated crack growth rates. Alternating thermal stresses, or creep strain from the relaxation of thermal stresses can be a significant contributing factor in creep crack growth rates.

Defect Tolerance: In highly safety classified components there is likely to be an assessment of known or postulated defects. Any metallic structure can have a defect present at manufacture. Components are inspected using Non-Destructive Testing (NDT) techniques when they are built, but they typically have a threshold, below which defects cannot be detected. This threshold is driven by the physical constraints of the method deployed and the skill of the operator. In high safety duty components, these inspections are repeated at certain intervals through their life to identify defects that may have appeared through fatigue or environmental degradation, or even identify an original manufacturing defect that was missed.

Defect tolerance seeks to assess the tolerance of a structure to the presence of known or postulated defects. Defect tolerance assessments are based on fracture mechanics principles and determine the proximity of any defect to failure through either fracture or plastic collapse. A detailed appreciation of the stress field around these defects is key to these assessments and thermal fields are no less important. The loads will be classified as primary or secondary, but their impact can be significant in either case.

In situations with complex thermal fields and little margin, FEA can be deployed to model a crack sitting within a thermal field. Key crack parameters (J integrals) would then be evaluated and the impact of the thermal field assessed.

The growth of any defect can also be considered through an assessment of fatigue crack growth. This is again driven by a detailed understanding of alternating stresses within the structure and

thermal fields resulting from differential thermal expansion, through-wall effects and long range effects would be considered.

2.4.3 CHT Applications

This section introduces some examples of applications of using CHT analysis to support structural integrity assessments, while the impact of buoyancy on surface temperatures is discussed in Volume 3 (Section 2.1.3). Particular focus is given to understanding temperature fluctuations in solids that could lead to thermal fatigue.

Thermal fatigue: High-cycle thermal fatigue in T-junctions was initially investigated in the context of Liquid Metal-cooled Fast Reactors (LMFRs) in the 1980s, but received increased interest (Kuhn *et al.*, 2010, Selvam *et al.*, 2015 and Tunstall *et al.*, 2016) following the incident at the Civaux-1 plant in France. The Committee on the Safety of Nuclear Installations (CSNI) Vattenfall T-Junction benchmark (CSNI, 2011) investigated the ability of CFD to predict the amplitude and frequency of the thermal fluctuations, and demonstrated the improved performance of Large Eddy Simulation (LES) to simulate this phenomenon compared to Unsteady Reynolds-Averaged Navier-Stokes (URANS). CSNI (2015b) gives details on the frequencies of interest for high-frequency thermal fluctuation (or 'thermal striping'), where failures have been seen and general best practice guidance.

Pressurised Thermal Shock (PTS): Thermal loads on an RPV in a PWR may lead to very large stresses and growth of any flaws present. Cold water injection into the downcomer of the RPV can occur during Emergency Core Cooling System (ECCS) operation in response to a Loss-Of-Coolant Accident (LOCA). Therefore, PTS is a key reactor safety issue that may impact the lifespan (and subsequent economics) of the plant due to radiation embrittlement of materials over time (IAEA, 2010). This has been investigated extensively, and has been simulated in the most recent CSNI CFD benchmark on cold leg mixing[8]. The process of performing and validating CFD simulations relevant to PTS is also described in Study D: System Code and CFD Analysis for a Light Water Small Modular Reactor.

Thermo-mechanical loads: Thermo-mechanical studies of components are undertaken to calculate solid temperatures in order to determine the mechanical loads. One such example is a thermo-mechanical study of the bolts holding the PWR core shielding (Rupp *et al.*, 2009). The objective was the evaluation of the mechanical integrity of 1,000 bolts used to hold the peripheral thermal shielding part of the nuclear core, through a structural mechanics analysis of the thermal stresses. A coupled CFD/heat conduction simulation, using two separate codes, one for CFD (Code_Saturne) and one for heat conduction (SYRTHES) was carried out. The simulated temperature field of the bolts holding the peripheral shielding was transferred to a structural analysis code.

[8] The report for which has not been released at time of writing.

Fuel cladding temperature: The maximum allowable temperature of fuel cladding under steady-state, transient and accident conditions can limit reactor performance (IAEA, 2008). This is applicable to standard and wire-wrapped fuel assemblies, and is closely coupled to the core neutronics. This is a key output from subchannel code simulations of the core behaviour, but has more recently been investigated using CFD analysis including benchmark simulations of a 19-pin wire-wrapped rod bundle (Merzari *et al.*, 2016).

2.5 Modelling Challenges

This section introduces the typical challenges that may be encountered in modelling heat transfer in solids and fluids. Addressing these challenges is considered in Section 3.

Timescales: There is generally a large disparity between the timescales associated with detailed flow effects (less than a second), solid conduction (hours) and the whole system (multiple hours or days). Although a system or subchannel code can simulate long transient scenarios, they do not capture all complex flow features. By comparison, a CFD model can resolve the flow effects, but the large disparity between the characteristic timescales of the fluid flow (e.g. vortex shedding) and solid conduction (e.g. thermal mass) means that transient modelling of a CHT problem is impractical for large components or long transients, without a carefully designed modelling approach.

Heat Transfer Coefficients: HTCs, as discussed in Section 2.1.2.3, are widely used across industry as inputs for system codes, external boundary conditions for CFD models and to transfer information between models. However, empirical correlations are only applicable to simple flows with idealised boundary conditions, and it is often difficult to extract appropriate values of HTC from a CFD simulation. Therefore, there can be significant uncertainty in both empirical and CFD calculated values of HTC.

Contact Resistance: It is often assumed for analysis that two solid surfaces are in perfect contact with each other, but as discussed in Section 2.1.1.1 this is rarely the case. The imperfections and roughness on solid surfaces means that the amount of contact is unknown, varies between components and can change with time. Therefore, this represents uncertainty in the thermal resistance associated with the conductive heat transfer that should be considered.

Thermal Expansion: As solids heat up, the material expands based on the thermal expansion coefficient (1 m of stainless steel expands almost 10 mm between room temperature and 600 °C). This can potentially change the size of gaps between solids at different temperatures, e.g. the gap between the reactor and guard vessel for a Passive Decay Heat Removal System (PHRS). Since manufacturing drawings represent the cold geometry, it may be necessary but challenging to accurately predict the hot geometry and the impact/importance of thermal expansion needs to be carefully considered.

External Boundary Conditions: The heat lost to the environment (e.g. ambient air) can be sensitive to the applied external boundary conditions, as it often has a high thermal resistance. However, it is not possible to include an explicit representation of the external environment in most models, and so empirical correlations are used. This usually involves assuming natural or forced convection correlations based on the local component parameters. Therefore, it is often hard to take into account additional factors, such as varying wind conditions or buoyancy driven flow within an enclosure causing forced convection on a surface instead of locally calculated natural convection. This means that there can be significant uncertainty in empirically calculated external boundary conditions.

Cluttered/Complex Geometry: A real reactor geometry is large and complex with multiple bolts, flanges and cluttered geometry, such as heat exchangers. In most cases, it is not possible to model all of the geometry in detail, and so decisions need to be made on an appropriate level of simplification. This will depend on the objective of the simulation, and needs to be reviewed within the context of a graded approach. In some cases, small features, such as fillets, can have a large impact on the thermal mixing at a junction. Therefore, the level of simplification needs to reduce around the region of interest. Models can be simplified by reducing geometrical complexity or representing cluttered regions as a porous zone, although the effective material properties and pressure drop/turbulence are often hard to calculate with confidence (Section 3.3.4).

Heat Transfer in Turbulent Flows: Unlike in pure aerodynamics, which is dominated by the pressure-inertia balance, while turbulent effects are weaker, temperatures depend only on convection and turbulent heat flux balance and so the predictions are much more sensitive first to the kinematic turbulence model chosen and second to how it is extended to heat fluxes. Therefore, large differences can be observed in temperatures between simulations as a result of model choices. This means that predicting heat transfer with confidence in complex flows, such as separation and impingement flows, may be particularly challenging.

3 Methodology

This section discusses the methods used for predicting CHT, providing a concise overview to assist engineers performing analysis. Typical coupling methods are considered, before assessments using system and subchannel codes, CHT approaches, CFD analysis and experimental methods are discussed in more detail.

The overall approach to Nuclear Thermal Hydraulics (NTH) analysis is introduced and discussed in Volume 1 (Section 4.1). In general:

- System codes are often used to predict the performance of whole systems or groups of systems, while CFD is generally used to understand the detailed flow field in specific components.
- Application-specific codes (like subchannel or containment codes) are often used where some flow field modelling is needed, but a full CFD approach is too cumbersome or computationally expensive.
- Experiments are often used to understand overall behaviour using scaled systems, investigate detailed flow effects and provide comparative data to validate analysis methods.

The coupling together of different methods (i.e. multiscale and multiphysics analyses) are discussed in Section 3.1, while the different CHT approaches are considered in Section 3.3 as these are more relevant to CFD analysis.

3.1 Coupling Methods

Multiscale and multiphysics coupling is being increasingly used as part of the reactor design process, and offers significant advantages by combining the strengths and benefits of each analysis methodology. This is an active area of research across the nuclear industry to improve the integration and coupling between codes (Section 4).

It is important to note that Verification and Validation (V&V) should be undertaken for the coupled code as a whole, as well as the component models within the coupled code.

3.1.1 Multiscale

Multiscale modelling couples together multiple models at different scales and levels of resolution to simultaneously simulate a system. In NTH analysis, this means coupling together system (whole plant), subchannel (core behaviour) and CFD (detailed prediction of specific areas) codes. Zhang (2020) demonstrates that coupling has been achieved across most of the system/CFD codes described in Volume 1.

The most common multiscale modelling is the coupling together of system and CFD codes in order to simulate the behaviour of a plant/system under normal operation or fault scenarios with CFD models to resolve complex aspects of the flow in specific areas. This overcomes some of the limitations of system codes to model detailed mixing/stratification in pools, plena and complex geometry. In some cases, the increased computational expense associated with coupling is necessary, as otherwise it can lead to inaccurate system code results (Anderson *et al.*, 2008, Gerschenfeld, 2019 and Papukchiev *et al.*, 2019).

The simplest form of multiscale modelling is one-way coupling with a system code providing inputs for a CFD model or a CFD model providing a correlation, response surface or Reduced Order Model (ROM) for a system code. However, this is often not appropriate for reactor scenarios and so two-way coupling is required. The process of code coupling can be complicated and can significantly impact the accuracy of a coupled simulation. Various coupling methods have been developed, which are discussed and classified by Zhang (2020), as follows:

- Operation mode i.e. system and CFD codes run in serial or parallel. Parallel operation is more efficient and scalable, but is more complex to develop and maintain.
- Coupling architecture describes how the codes are coupled (internal or external). Internal coupling means that one code is compiled inside the other i.e. single executable, while external coupling means that the two codes are separate and communicate via input/output files, server-client (supervisor) or server-less (direct). Overall, the external server methods are considered the most efficient, flexible and maintainable.
- Domain coupling is one of the critical parts of the coupling process, as it specifies which code is in charge of which computational domains. In domain overlapping, the system code simulates the whole domain and overlaps the CFD model, while domain composition has separate models with data transfer at the interfaces (Figure 3.1). Domain overlapping is more robust and efficient and means that the stand-alone and coupled system code models are identical, but requires more intensive code modifications.

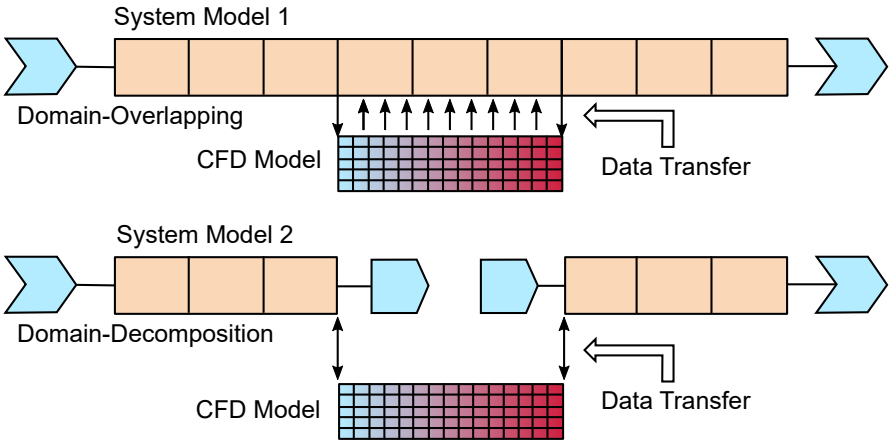

Figure 3.1: Domain overlapping and domain decomposition approaches (Zhang, 2020). This image is reproduced from an open access article under the terms of the Creative Commons Attribution License.

- Field mapping refers to the method used to transfer data between the different spatial reso-

lutions of the codes (CFD mesh is much finer than system code). This can be achieved using manual definition of mesh matching relations, user-developed toolkit for mesh matching or a third-party mesh-processing toolkit. A third-party toolkit is likely to be more accurate and flexible, but still requires significant code development to use.

- Temporal coupling is needed to ensure that the multiscale code coupling is synchronous in time. This can be implemented using explicit, semi-explicit or implicit coupling. Convergence is generally better using a semi-implicit or implicit method, which should improve the accuracy and robustness.

In general, it is important to ensure that the approaches are as consistent as possible between the two codes, especially if two-way coupling is being implemented, in areas such as material properties and boundary conditions.

3.1.2 Multiphysics

Multiphysics simulations involve coupling together multiple physical models or multiple simultaneous physical phenomena. From a NTH perspective, this is predominantly associated with coupling thermal hydraulics analysis with neutronics and structural analysis (CSNI, 2015a). Since this set of technical volumes is primarily focused on thermal hydraulics analysis, only a brief introduction to multiphysics simulations is provided.

Neutronics: The fuel cladding temperature and overall core behaviour depends on the balance between thermal hydraulics and neutronics. The thermal hydraulic behaviour depends on the heat release distribution due to radiation activity, while the neutronic behaviour is influenced by the fluid temperature, density and species concentration (e.g. boron). Most CFD software does not include any neutronics capability, while system/subchannel codes generally only include simple point kinetic neutronics models. Therefore, the coupling of CFD/system codes with more advanced (i.e. deterministic or stochastic transport) neutronics models will enable more accurate predictions of the fuel behaviour and fuel cladding temperature. An introduction to neutronics, and a discussion of thermal hydraulic/neutronic coupling, as well as guidance on more detailled references can be found in Voume 6.

Fluid-Structure Interaction (FSI): Although temperature predictions are a key input to structural integrity assessments (Section 2.4), coupling of CFD and structural codes is predominantly focused on Fluid-Structure Interaction (FSI), such as Flow Induced Vibration (FIV). This includes phenomena such as vortex-induced vibration, galloping/flutter, whirling, turbulence-induced vibration and acoustic vibration (Kaneko *et al.*, 2014). FIV is a key issue for NPPs because primary circuit flows can induce vibrations that cause damage or wear to fuel assemblies, heat exchangers or pipework. Depending on the feedback between the structural displacement and flow field, this can be simulated using one-way or two-way coupling. Coupling with structural codes is available in most CFD codes, but care needs to be taken to resolve the vibration response, particularly at high frequencies, and this is the focus of the current CSNI CFD benchmark at the time of writing.

3.2 System and Subchannel Analysis

System and subchannel codes are introduced in Volume 1 (Section 4.4.1) and their capability and limitations for modelling convection is discussed in Volume 3 (Section 3.1).

System codes are a key design tool, allowing the performance of a whole system (or a group of systems) to be assessed in a wide range of scenarios much more quickly than would be possible with other analysis methods. By contrast, subchannel codes are used to perform reduced-order spatial analysis of complex components within a system (particularly the reactor core) for which the use of more detailed CFD would be too expensive or cumbersome.

System and subchannel codes have the capability to model transient heat conduction within solid structures such as pipes and channel walls, albeit in a simplified manner compared to modelling the fluid flow. For many steady-state scenarios, or transient scenarios with largely isothermal mixing, these are generally reliable and robust. However, there are a number of scenarios involving CHT that are challenging to model using system and subchannel codes, some of which may present significant structural integrity issues. These physical scenarios include, but are not limited to:

- Reflooding the core following a (large-break) LOCA where the overheated fuel rods are quenched to avoid fuel damage.
- PTS may occur during overcooling events (e.g. ECCS water injection into cold legs and excessive heat removal by the secondary side). Natural circulation/flow stagnation is particularly important for PTS as cold water is delivered directly to the downcomer, if the loop flow stagnates.
- Temperature fluctuation may be observed due to turbulent mixing of two flow streams of different temperatures (e.g. in T-junctions). This phenomenon is often referred to as thermal striping, which can cause high cycle thermal stress and cracking.
- Thermal stratification is a phenomenon where two flow streams of different temperature come into contact. The temperature difference causes colder (therefore more dense) water to occupy the bottom portion of a pipe, while warmer water flows over the colder water. Thermal stratification typically occurs in pipes where low flow velocity is expected. The circumferential temperature gradient can cause thermal stress which can lead to fatigue damage (Kim *et al.*, 1993). Thermal stratification can occur in pressuriser surge lines, feed water lines and spray lines, particularly during start-up and shut-down processes.
- Flow reversal or counter-current flow can also occur in reactor components, such as steam generator tubes, upper plenum and core. This can lead to circumferential temperature gradients that can cause thermal stress and fatigue damage.

While system and subchannel codes may struggle to predict these scenarios, there are some special models implemented in these codes that can help improve the prediction of some of these phenomena. The following sections introduce system and subchannel codes, their application to CHT and highlight some of these particular aspects, but this should only be considered as a high level introduction; codes are typically accompanied by comprehensive user guides and validation information that should be consulted.

3.2.1 System Analysis

In system codes, solid components can be modelled using heat structures (or heat slabs) that are represented using simple geometry (e.g. rectangle, cylinder and sphere). Heat structures allow the calculation of heat conduction in solids and can model:

- Fuel pins/plates with nuclear or electrical heating.
- Heat exchangers.
- Heat transfer from pipe/vessel walls (e.g. environmental loss).

Heat structures may be classified into two groups: active structures (e.g. fuel rods and heat exchangers) and passive structures (e.g. pipe/vessel walls). While passive structures may not play an important role in a steady-state calculation, they may become significant heat sinks (or sources) during a transient scenario. Therefore, it is important to account for them in a simulation. Environmental heat loss may not be significant for full-scale NPPs and so may not be considered in a system code analysis. However, when modelling reduced-scale Integral Effect Test (IET) facilities, this heat loss can become significant, as the ratio of heat loss to core power becomes higher than that of a full-scale NPP.

In general, both one-dimensional (i.e. radial) and two-dimensional (i.e. radial and axial) forms of heat conduction are available in system codes. The two-dimensional form is typically used for fuel components when reflood is expected. The predicted temperatures of solid components should be used with caution depending on the complexity of the component and the scenario being analysed in the system code.

For components with a complex geometry and scenarios where the flow, pressure and coolant temperature conditions local to the component are changing rapidly, system codes may not accurately predict the true maximum or minimum temperature of the component. For components with a simple geometry in a scenario where the conditions local to the component are not changing rapidly (e.g. during steady-state operation or transient scenarios with largely isothermal mixing) system codes are more able to accurately predict solid temperatures.

3.2.1.1 Nodalisation

Users must normally specify the number of nodes in the radial direction of heat structures. As the computational cost can increase with increasing number of nodes, there is a trade-off between the solution accuracy and the number of nodes. In practice, a nodalisation sensitivity study may be necessary. The number of radial nodes typically varies between 2 and 20. If a solid structure (e.g. nuclear fuel rods) consists of different materials, a node should be placed at the interface between two materials. The mesh strategy can depend on the Biot number, Bi (Section 2.1.1.2). For example, the following recommendations are given for RELAP5-3D (Aumiller and Bettis, 2000):

- For higher Bi (i.e. > 15), a graded nodalisation with smaller node intervals near the surface may be appropriate.
- The recommended maximum surface node size can be expressed in terms of Bi as:

$$\beta_{max} = 1/(0.338Bi + 5.2)$$

where $\beta = 0.5\delta_1/L$, and δ_1 is the distance from the surface node to the first internal solid node and L is the wall thickness.

- It should be noted that too small a nodalisation ($\lesssim 10^{-4}$ m) may lead to numerical oscillations in the solution.

In the case of modelling reflood processes, the two-dimensional form of heat conduction should be considered. However, as the axial nodalisation is taken from the adjacent hydrodynamic volume, this can be too coarse to resolve the axial temperature gradient in the solid. In most system codes, an axial re-noding scheme is available to impose a finer nodalisation according to a set of criteria based on the local flow conditions.

3.2.1.2 Models

There are several special models available in most system codes, which are designed to deal with the scenarios described in Section 3.2 that can improve temperature predictions. These include:

- A reflood model that allows axial conduction, because this can play a significant role during the reflood process (Osakabe and Sudo, 1983). In addition, axial re-zoning or re-noding schemes may be available to resolve large axial gradients in temperature and/or heat flux.
- A Counter-Current Flow Limitation (CCFL) model may be considered when simulating reflood and/or PTS at tie plates, steam generator U-tubes or hot legs. Without a CCFL model, the code may incorrectly predict the thermal hydraulic behaviour (e.g. zero liquid delivery). However, it should be noted that counter-current flow of a single phase in a horizontal pipe (e.g. pressuriser surge line) cannot be modelled in system codes due to its inherent volume averaging technique. This therefore prevents the application of system codes to model thermal striping and thermal stratification in horizontal pipes.
- Some system codes may have a special model for thermal stratification in vertically oriented components (e.g. passive cooling pools) to limit the effect of numerical diffusion and improve the axial temperature profile prediction.
- Component specific models for nuclear fuel rods such as fuel deformation, gap conductance or metal-water reactions are available, however these models will contain approximations and so the user should review the impact of any simplification on the analysis.

3.2.1.3 Limitations

Other limitations of system codes to consider may include:

- System codes rely on a number of empirical correlations and a simplified set of governing equations which will have an impact on the accuracy of the temperature predictions, especially during scenarios where the plant conditions are changing rapidly.
- System codes do not necessarily reach a nodalisation independent solution (by increasing the spatial resolution).
- An explicit representation of some details of a complex reactor geometry and structures may not be possible.
- Due to the simplified treatment of turbulence in system codes, prediction of turbulent thermal mixing is limited in system codes which will impact heat transfer predictions.

- While system codes have multi-dimensional flow modelling capability for components such as the reactor vessel, these are typically limited in their fidelity and accuracy.
- Some system codes may have a tendency to predict lower Peak Cladding Temperatures (PCTs) and earlier quenching compared with experimental data (Choi and No, 2010, Li *et al.*, 2016). This is often attributed to code deficiencies in the film boiling and interfacial drag models.

These limitations should be considered carefully when undertaking system code analysis, and more detailed modelling should be considered if appropriate. For example, system codes could be used to provide initial and boundary conditions for higher fidelity analysis such as CFD or coupled with CFD codes to resolve complex local flow features (Section 3.1).

3.2.2 Subchannel Analysis

In subchannel codes, solid conductor models are available. In general, there are two types of models: rods and generic conductors (e.g. vessel internal and external structures). Similar to system codes, solid conductors are represented as cylinders (solid or hollow) or plates (Moorthi *et al.*, 2018). These allow subchannel codes to model vessel structures including:

- Nuclear or electrically heated fuel pins.
- Control rod guide tubes.
- Support columns.

In subchannel codes, an option to choose between one-dimensional (radial) and two-dimensional (radial and axial) forms of the heat conduction equation is available. Some codes such as CTF (Avramova and Cuervo, 2013) allow a three-dimensional (i.e. radial, axial and azimuthal) form of heat conduction. Multi-dimensional forms of heat conduction are recommended for cases with large temperature gradients in axial and/or azimuthal directions (e.g. reflood and quenching).

3.2.2.1 Mesh Generation

For cases with gradual heating/cooling, heat conduction in only the radial direction may be sufficient and the user needs to specify the number of radial points. While the number of radial mesh points must be sufficiently large to resolve the radial temperature profile, it can also increase the computational cost and so sensitivity studies may be required.

In the case of nuclear fuel rods, a typical radial mesh size used in the fuel region is approximately 10^{-3} m (Avramova and Cuervo, 2013). The multi-dimensional models may improve the code accuracy for scenarios involving large temperature gradients in the axial and/or azimuthal directions (e.g. during reflood). When axial conduction is selected, the axial mesh is typically taken from the adjacent fluid channel.

The assumption of negligible azimuthal temperature gradients may be sufficient for many analyses, but it can be important in some cases. The azimuthal mesh depends on how a rod is connected to the subchannel region and tends to be divided into four azimuthal sections, following the channel centred approach. Similar to system codes, subchannel codes can provide axial re-noding schemes for reflood calculation to impose a refined mesh according to a set of criteria based on local flow conditions.

3.2.2.2 Models

There are several special models available in most subchannel codes, which are designed to deal with the scenarios described in Section 3.2 that will improve the temperature predictions. These include:

- The presence of spacer grids can influence flow conditions, such as cross-flow and flow blockage, and may improve heat transfer by introducing turbulence (Sugimoto and Muraov, 1984). In most subchannel analyses, the effects of spacer grids are modelled using an effective loss coefficient, although some subchannel codes also have additional models specifically for spacer grids including heat transfer enhancement. However, as the geometry of spacer grids is simplified in subchannel codes, the results of CFD simulations could be used to better capture the effect of spacer grids in subchannel codes (Salko *et al.*, 2019).
- A turbulent mixing model is often available in subchannel codes to account for lateral turbulent exchange (Moorthi *et al.*, 2018). While this model is not specific to any phenomenon or scenario, it can impact the hydrodynamic volume solution which in turn can affect the solution of heat conductors. Users may be required to provide a mixing coefficient for single-phase and/or two-phase conditions and model sensitivity analysis may be required. However, the turbulent mixing model in most subchannel codes is simplified and applies the same turbulent diffusion coefficient to all mass, momentum and energy exchanges.
- As for system codes, special models for nuclear fuel rods (fuel deformation, gap conductance or metal-water reactions) may also be available in subchannel codes, and the impact of any simplification on the analysis should likewise be assessed.

3.2.2.3 Limitations

Other limitations of subchannel codes to consider may include:

- Subchannel codes depend on a number of empirical correlations and a simplified set of governing equations, so their suitability and validity needs to be understood for a particular application and software-specific guidance should be consulted.
- Subchannel codes are designed to model vertically-oriented components (e.g. reactor pressure vessel and core). Phenomena associated with horizontally-oriented components (e.g. thermal striping and thermal stratification) cannot be predicted.
- Only simplified heat conductor geometry is available.
- The fidelity of subchannel codes is lower than that of CFD and so may not be able to predict detailed local phenomena in channels.

Despite these limitations, subchannel codes are useful as they allow for multi-dimensional modelling with reasonable computational time. The accuracy of subchannel codes may be improved by using CFD results to provide additional information (or coupling with CFD) to account for complex geometry effects.

3.3 CHT Approaches

Common approaches to CHT analysis include uncoupled and coupled methods using a resolved solid, shell conduction or porous media zones. These are illustrated in Figure 3.2 and discussed in more detail in the following sections. A key reason for performing CHT analysis is to support structural integrity assessments (Section 2.4). Therefore, CHT analysis is often used to generate inputs for FEA models, enabling solid deformations, internal stresses and thermal fatigue to be predicted by structural engineers using tools that are familiar to them and well suited to these purposes.

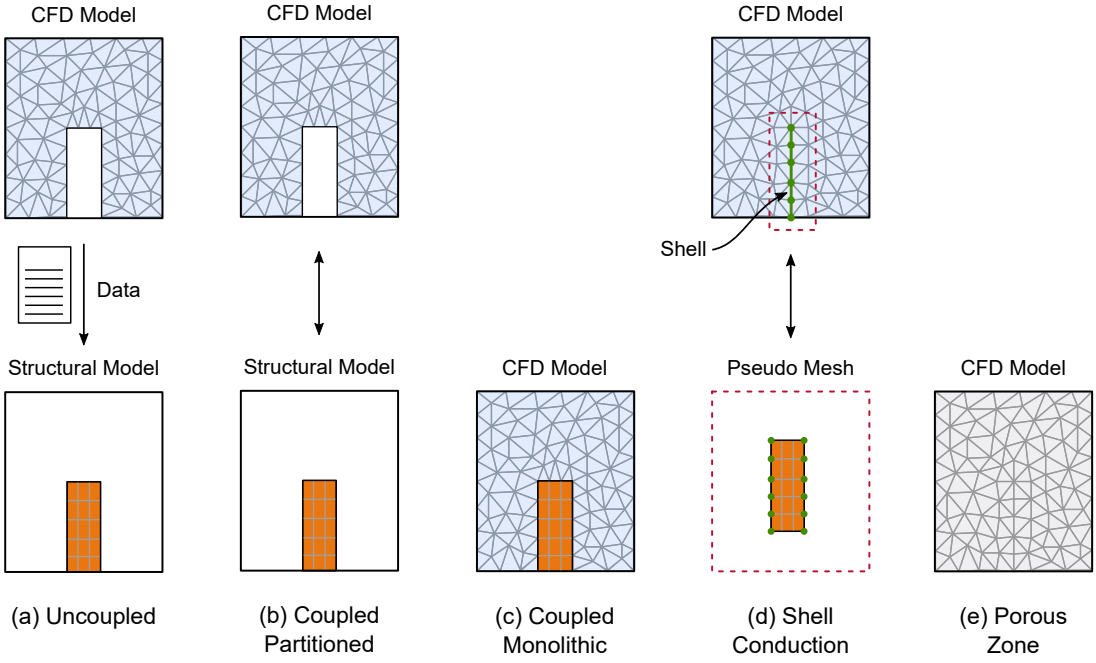

Figure 3.2: The main conjugate heat transfer modelling approaches.

3.3.1 Uncoupled

In this approach, the flow and fluid temperatures are predicted in a CFD model and the temperatures within solids are predicted in a separate thermal-structural FEA model. Information is passed one-way (from the CFD model to the FEA model) using data extracted from the flow solution. From a CFD perspective, the flow is predicted in the normal manner, but the following aspects are particularly significant:

- Setting appropriate boundary conditions for the CFD model, given that the solids are not modelled (discussed further in Section 3.4.3).
- Appropriate data will need to be extracted from the CFD solution in a form that can be used in the FEA model, often this is predicted HTCs and fluid temperatures or heat fluxes (discussed in Section 3.4.6).

In view of the one-way information exchange (from fluid to solid), this method is generally only appropriate for situations where the thermal environment is changing so slowly that the fluids and solids can be considered to be in a quasi-steady-state, or the heat transfer coefficient is effectively

independent of the solid temperatures (which may occur in forced convection flow).

An uncoupled approach may be the simplest and computationally cheapest method for calculating the temperatures and stresses within components over long fault scenarios (hours or days). For example, the temperature variation in a weld in a pipe network or tube plate during start-up, shut-down or fault scenario. In this example, the inlet flow rate and temperature (calculated using a system level method) varies with time during the fault. The transient temperatures within the solid may be calculated by:

- Calculating initial steady-state flow and temperatures within the component e.g. normal operation.
- Identifying and calculating a number of quasi-steady-state flow conditions over the transient (e.g. when the inlet flow rate and/or fluid temperature changes).
- For each condition, the fluid temperature and HTC is extracted using one of the methods described in Section 3.4.6. This could be a single value for a pipe or spatially varying value output at each face of the CFD model.
- The fluid temperatures and HTCs are then imported into the thermal-structural model as a time-varying boundary condition, so that the solid temperatures can be calculated over the whole fault scenario.

3.3.2 Coupled using Resolved Solid

In a fully coupled CHT approach, the energy equation for temperature needs to be solved in both the fluid and solid domains. The solid temperatures from the CFD solution can then be directly mapped onto an FEA model to calculate the thermal stresses. The physical processes and solutions of the governing equations can be either solved in a single model (monolithic approach) or in separate fluid and solid models (partitioned approach).

Monolithic or direct approach: The governing equations for both domains are conjugated by simultaneously solving a single large set of equations (Patankar, 1980). A single generalised conservation expression is implemented for the fluid and solid domains. This ensures spatial and temporal energy conservation across the fluid and solid regions, and is simple to use within a single CFD code. However, if the temperatures are required as part of a structural analysis, then the spatial and temporal thermal field will need to be extracted at appropriate time steps and imported into the structural model.

Although it is possible to separate the fluid and solid time steps, this approach often relies on explicit time integration for simplicity and is therefore penalised by small time stepping due to the most stringent phenomenon (Koren *et al.*, 2017). It is also beneficial to consider whether a partitioned mesh for parallelised solution is balanced appropriately, because the solid cells in a partition will have significantly lower computational requirements than the fluid ones.

Partitioned or iterative approach: This approach, described by Giles (1997), is based on a separate solution of each set of equations for the fluid and solid, respectively. Each solution of the solid or fluid domains produces the necessary outputs along the fluid-solid interface which is then used as the boundary condition for the other. This iterative approach is widely used in finite difference, element and volume methods. By splitting the problem, an additional common interface is created between the physical domains, through which energy is

exchanged, to allow the sub-domains to interact and yield a coupled solution. The use of a dedicated solver for the fluid and solid means that each can be optimised in terms of time step, algorithms or data structure.

Most procedures in the literature impose a temperature boundary condition (Dirichlet type) on the fluid side of the interface and a pure (Neumann) or mixed (Robin) heat flux condition on the solid side. The Dirichlet-Robin coupling schemes are shown to offer many attractive features over the Dirichlet-Neumann schemes (El Khoury *et al.*, 2017, Errera *et al.*, 2019), but requires selection of a suitable relaxation parameter which satisfies the stability and the fast convergence rate of the coupled problem (El Khoury *et al.*, 2017). The coupling is carried out so that both solvers compute temporal iterations separately until a given physical time that corresponds to the prescribed coupling time step (or 'coupling period'). At these instants, data from both solvers are exchanged with each other in order to update their boundary conditions. With synchronized solvers, the fluid and solid solver time steps must fulfil the following constraint:

$$\Delta t_{cpl} = N_s \Delta t_s = N_f \Delta t_f$$

where N_s and N_f are the number of iterations before exchanging data at the shared interface. Although partitioned approaches are flexible and enable direct coupling between the fluid and thermal-structural models, it is important to ensure that the interface is set up appropriately and that energy is conserved. This increases the user involvement and requires efficient dynamic coupling between the models.

Koren *et al.* (2017) note that the burden of solving heat transfer in the solid after each LES time step is impractical in large-scale simulations with an order of magnitude increase in computational time compared to every 50 iterations giving a moderate 18% additional cost for the coupled simulation. However, since the varying wall heat flux and temperature depends on the size of the coupling time step, a large value might impact the accuracy of a LES prediction as the unsteady phenomena may be under-resolved at the fluid-solid interface. Therefore, it is important to check the impact of the coupling time step on the LES results.

In both of these CHT approaches, the solid domain needs to be properly modelled and meshed. The parts of the computational domain containing fluids and solids are therefore both included in the computational mesh (Section 3.4.2). This can significantly add to the complexity and time required to build the model, especially if conformal meshes are used at the fluid-solid interface.

A fully coupled approach is suitable for any combination of fluid and solid regions, including complex conduction paths and inter-connected fluid-solid regions. It also enables time-varying temperatures to be calculated when the fluid and solid temperatures are strongly dependent on each other (e.g. mixed and natural convection, complex conduction paths and large Biot number). The main limitation of this approach is the need to properly resolve the timescales associated with the fluid phenomena, which often requires a small time step within the fluid domain. This means that long fault scenarios (spanning hours or days) are often unachievable within realistic analysis timescales even for Reynolds-Averaged Navier-Stokes (RANS) modelling methods. The reduced timescales and larger meshes associated with LES models currently make this approach impractical for all but the simplest cases.

3.3.3 Coupled using Shell Conduction

Creating full meshes for solids in order to resolve the temperature gradients within them can be onerous, yet for many geometries (such as pipes or ducting) the conduction behaviour is often quite straightforward. Therefore, some CFD software enables thin-wall or shell conduction to be modelled in the solver, by predicting the temperature variation within solids using a virtual (pseudo-mesh) that is generated by the CFD solver with a prescribed wall thickness. Although the implementation and terminology will likely be code dependent, these terms are commonly described as:

- Thin-wall conduction only accounts for heat transfer normal to the wall.
- Shell conduction also includes planar conduction through the (virtual) solid.

A wall/solid is typically represented by one or more layers which are added virtually by the computational solver. Thus, there is no need to create the wall geometry or generate a solid mesh. The thermal resistance of the wall is accounted for by assigning appropriate material properties. This approach enables a number of solid layers to be accounted for at the same time (e.g. metal pipe and surrounding insulation). Within the same model, complex three-dimensional areas of geometry might be resolved using coupled methods with a mesh, and more straightforward areas modelled using shell conduction.

External walls (fluid on one side): Shell conduction is ideally suited to applications with simple, uniform solid geometry (e.g. pipe walls, thin plates). This enables the thermal mass and conduction through the solid to be incorporated into the CFD solution. The main limitation is that the spatial temperature variation within the solid is not recorded as part of the solution, so this method is not appropriate if the solid temperatures are required for input into a thermal-structural calculation.

Internal walls (fluid on both sides): Shell conduction can be used to simplify the model geometry by eliminating the need to mesh the solid and allow prism layers to be generated in the fluid on both sides more easily. As with external walls, this means that the thermal mass and conduction through the solid is accounted for, although it will also increase the flow area and volume of the fluid region to some extent. Therefore, the reduced mesh complexity needs to be balanced against the impact on flow accuracy depending on the purpose and requirements of the CFD analysis. For thin walls surrounded by large fluid domains, this may well be acceptable.

3.3.4 Coupled using Porous Zones

Most commercial CFD solvers offer the ability to specify porous zones. These can be applied to a wide variety of problems, including perforated plates, tube banks and pebble beds. This applies an additional pressure loss to the flow that is usually based on a user specified anisotropic loss coefficient. In laminar flows, the pressure drop is typically proportional to velocity (Darcy's law), while in turbulent flows it is proportional to dynamic head (kinetic energy per unit volume of the flow).

In most cases, the superficial velocity, based on the volumetric flow rate, is solved within the CFD software to ensure continuity of momentum and mass flow. Therefore, care is needed to ensure that the loss coefficient is appropriately derived, and the treatment of turbulence within the porous

zone is understood (by default, the turbulence generation and dissipation rate is often assumed to be unaffected by the solid component). The thermal equations can be solved using an equilibrium or non-equilibrium model:

- Equilibrium model: The solid and fluid are locally assumed to be at the same temperature and are represented using effective material properties combining solid and fluid contributions, based on the porosity of the medium (percentage of fluid by volume). The thermal mass and conductivity of the solid components within the porous zone are taken into account using the zone porosity (Section 3.4.3.3). This enables an effective thermal conductivity of the porous zone to be calculated, and the thermal mass of the solid to be represented in the model.
- Non-equilibrium model: Separate temperatures are modelled for the solid and fluid zones with heat transfer between them. This approach is more appropriate for transient calculations because it enables changes in the solid temperature to 'lag' changes in the fluid temperature, because of its representation of thermal mass and the finite rate of heat transfer. In addition, the effect of porosity on the transport velocity for energy and species in the flow can be included, even if the superficial velocity is solved for (although this might vary between codes).

Porous zones provide a useful method of achieving the appropriate pressure drop and temperature change in regions that are too complex to mesh explicitly. However, care must be taken to ensure that the impact associated with this approximation on outputs required from the analysis is understood. In some cases, a detailed CFD model of a complex component (e.g. tube bundle) could be generated and solved at a number of representative conditions. This could be used to develop pressure drop, turbulence and thermal correlations for an equivalent porous zone model. This would provide more confidence in the porous zone model for this application and enable the impact of the approximation to be quantified.

3.4 CFD Analysis

This section considers CHT analysis using CFD. It builds on the more general discussion in Volume 1 (Section 4.5.3) and complements a number of more general topics given in Volume 3 (Section 3.2.2). General CHT approaches are considered in Section 3.3. As such, only areas particularly significant to modelling CHT using CFD are considered, such as approach, mesh generation, aspects of case definition and coupling.

Guidance on industrial CFD computations (e.g. industrial guidelines such as ERCOFTAC, 2000, NAFEMS, 2019, and CSNI, 2015b, and books such as Versteeg and Malalasekera, 2007) are good general references, but their focus is not on providing detailed guidance for CHT analysis.

3.4.1 CFD Approaches

A number of CFD approaches are available, primarily resulting from different ways of predicting turbulence, and these are introduced in Volume 1 (Section 4.5.3). The application of these approaches to CHT is introduced briefly below and discussed in more detail in the following sections. There are a range of approaches and numerous variations within each; for NTH, engineers must make informed judgements about the complexity and fidelity needed for their modelling work within

the context of a graded approach (Volume 1, Section 2.2.5) informed by their safety and economic case. More general NTH guidance is provided in D'Auria (2017) and CSNI (2015b).

DNS: Direct Numerical Simulation (DNS) can resolve all length and time scales within a flow field. As discussed in Volume 1, it is considered highly accurate, but is very computationally expensive, so is predominantly used to study low *Re* or *Gr* flows in simple configurations. For CHT, DNS has been used to study basic scenarios such as fully-developed channel flows with steel walls, backward facing steps and T-junctions (Tiselj *et al.*, 2020) and jets in cross-flow (Wu *et al.*, 2017). The extremely detailed data that DNS can provide has been used to develop fundamental understanding and refine the models used in other CFD approaches. However, in view of its limited industrial use, DNS is not considered further.

LES: In LES, the Navier-Stokes equations are 'filtered', so that a proportion of the turbulence is resolved using the mesh and the remainder is modelled using a Sub-Grid-Scale (SGS) model. As discussed in Volume 1, LES is much less computationally expensive than DNS and potentially more accurate than RANS, but the computational costs (which scale with *Re* and *Gr*) are still high. Within the context of a graded approach for NTH, LES is most likely to be used in areas of high safety significance or commercial impact. For CHT, LES may be able to predict the fluctuating metal temperatures resulting from the turbulence within the flow field that can cause thermal fatigue (i.e. unsteady temperature fluctuations under steady flow conditions). Therefore LES has been used for assessments of primary circuit components, such as T-junctions (CSNI, 2011), where hot and cold streams mix.

RANS: In RANS, the instantaneous flow variables in the Navier-Stokes equations are decomposed into mean and fluctuating parts, so that the mean flow is resolved and the effects of turbulence are represented by a model (unsteadiness in the mean flow can be captured using URANS). As discussed in Volume 1, RANS approaches are used for the vast majority of industrial CFD (including for CHT analysis) and are often used to support more detailed analysis methods like LES or hybrid approaches. Within the context of a graded approach for NTH, RANS is therefore likely to be used in most situations where CFD is needed, with the complexity of the modelling work reflecting the complexity of the case and the safety significance and commercial impact associated with the work. Despite their well-known shortcomings (which are discussed in Volume 3, Section 2.2.4), RANS models can provide useful CHT results, such as steady and transient temperature fields within solid components. For analysis of solid temperatures over long plant transients, URANS is likely to be the most detailed CFD method that can be used with practical computational expense.

Hybrid Methods: Hybrid methods combine RANS with aspects of LES within the same model, to take advantages of both. As discussed in Volume 1, there are a number of significantly different approaches available (and variants within these approaches). For CHT, hybrid methods may well be useful for modelling flows that feature unsteady thermal mixing, unsteady free-shear or highly separated flows away from walls. Resolving turbulent length scales in some areas of the domain is likely to increase the computational expense compared to RANS, but reduce it compared to LES. Like LES, the use of hybrid approaches is increasing in industry, and their use within a graded approach for NTH sits between the points made above for RANS and LES.

3.4.2 Mesh Generation

The majority of industrial CFD calculations use a computational mesh on which the flow is solved. The mesh is within the computational domain and is fitted to the geometry of interest. Its purpose is to enable gradients in the flow variables to be resolved by the solver, and its quality can affect the results of a CHT calculation significantly.

3.4.2.1 Computational Domain and Geometry

These key aspects of CFD analysis are considered in Volume 1 (Section 4.5.2). Additional aspects that may be significant for CHT analysis include:

- The chosen approach to modelling the solids (Section 3.3) is likely to affect what is included in the computational domain. Using a shell conduction approach is likely to reduce the size of the computational domain compared to what might be needed for a fully resolved solid approach.
- Where solids are being meshed, separate fluid and solid volumes are needed. These volumes should be coincident (so there are no gaps between them) and their features and curvature well aligned (errors may be created if the geometry is offset too much). Solid volumes arising from CAD models are likely to need a similar level of geometry 'clean-up' as the fluid volumes.
- The approach to defining boundary conditions within solids at the edge of the domain should be considered in the same way as fluids. It may be necessary to extend the domain (and hence add more mesh) to ensure the thermal boundary conditions do not have a distorting effect on the results of the analysis.

3.4.2.2 Meshing Background

General background on mesh types and quality is provided in Volume 1 (Section 4.5.2). The following sections consider meshing solid and fluid volumes in more detail; different meshes are required for LES and RANS work, so these are discussed separately (DNS is not included as it is little used in industry). Software specific guidance should also be considered to ensure the mesh is consistent with the CFD solver being used. Meshing often involves compromises, and the impact of these on the key results or figures of merit can be investigated using validation data, sensitivity studies and uncertainty quantification (Volume 1, Section 4.3).

As noted in Volume 1, when a flow solution is available, the predicted flow should be visualised on top of the fluid mesh and reviewed by an experienced CFD user who can consider whether the mesh is capable of appropriately resolving gradients that may (or perhaps should) exist in the flow. The predicted temperatures should be visualised on top of the solid mesh in the same way.

Software-specific guidance should also be consulted for guidance on mesh connections for CHT analysis. In general, meshes are preferably conformal for fluid to fluid mesh interfaces (i.e. every surface face in one volume has an equivalent surface face in the adjacent volume that it connects to, Volume 1, Section 4.5.2). For fluid to solid interfaces, meshes do not generally need to be conformal. However, the temperatures and heat fluxes in both the fluids and solids should be visualised together around the interfaces, to check for gaps, offsets and interpolation errors (particularly around any large differences in mesh sizing at an interface between fluid and solid volumes).

Additional checks such as reporting areas of interfaces and 'unmapped nodes' may be helpful to avoid errors.

3.4.2.3 Meshing Solid Volumes

Meshing solid volumes is often more straightforward than meshing fluid volumes (since gradients in flow fields do not need to be considered). However, it is still important that the mesh can capture the temperature gradients within the solid, and assessing *Bi* may help to improve understanding of these (Section 2.1.1).

If large temperature gradients are expected in the solid or there are small geometrical features containing large temperature gradients the mesh should generally be sufficiently refined to capture these. For thin solid components (e.g. pipe walls) structured hexahedral or prism cells (rather than unstructured mesh) are recommended through the thickness to capture the thermal gradient. This may be particularly important if the temperatures of the solid are used to perform structural integrity assessments. If this is the case, it is good practice to discuss the work with the structural engineer at the outset, so that the mesh and data exchange process can be designed correctly from the start.

For unsteady CHT analysis, a prismatic layer is recommended in the solid with a fine mesh at the fluid-solid interface to resolve the transient temperature profile in the solid. To demonstrate this, consider a constant surface heat flux into a solid at a uniform starting temperature; the initial temperature gradient at the wall boundary condition is fixed by the heat flux and the solid surface (wall) temperature, T_w, depends on the size of the first cell (T_s is the cell centre temperature of the first cell in the solid).

$$q = \frac{k}{\Delta x}(T_w - T_s), \ \therefore T_w = \frac{q\Delta x}{k} + T_s$$

This means that if the first cell is too large, the wall surface temperature is over-predicted. In practice, fixed heat flux conditions arising from an adjacent fluid do not occur, but the wall resolution does affect the predicted heat flux and interface temperature between the fluid and solid regions. Therefore, a thin first cell layer is needed in the solid to correctly predict the surface temperature, and since the thermal gradient in the solid and thermal response reduce with distance from the wall, a gradual increase in cell size is appropriate.

The benefit of using a prismatic layer can be easily visualised by solving a simple plate conduction thermal transient (Figure 3.3). A thick (L = 2 cm) stainless steel plate is initially at 600 K with a convection thermal boundary condition applied (HTC = 1000 W/m^2 K, T_f = 620 K). The time-varying surface temperature and heat flux for an inflation layer mesh and simple coarse mesh (Figure 3.3c) show that the surface temperature is initially 3 K too high for the coarse mesh, which reduces the heat flux into the plate. The inaccuracy of the surface temperature and through-thickness temperature profile (Figure 3.3d) for the coarse mesh reduces with time as the transient progresses. This highlights the importance of appropriately resolving the mesh in solids for unsteady CHT analysis or accurate surface temperature predictions. This is particularly relevant to applications that involve rapid fluctuations in the fluid temperature, such as thermal striping phenomena, PTS or ECCS injection.

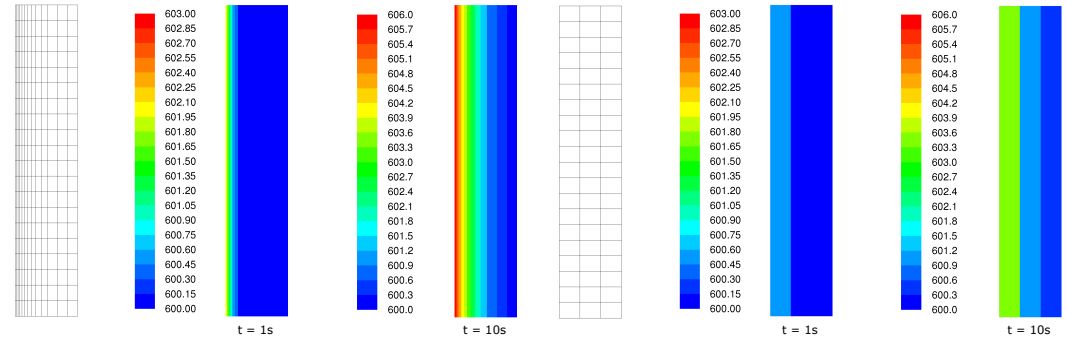

a: Cell temperature (K) contours: Inflation layer mesh

b: Cell temperature (K) contours: Coarse mesh

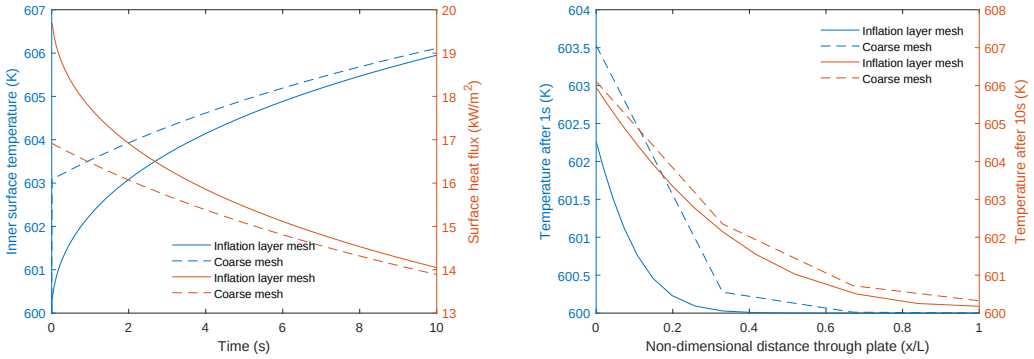

c: Inner surface temperature and heat flux variation

d: Node temperatures through plate

Figure 3.3: Impact of mesh density on transient temperatures in solid.

3.4.2.4 Meshing Fluid Volumes: LES

In LES, the filtering (between what turbulence is resolved and what is modelled) is usually related to the mesh resolution. Meshes for LES must therefore be sufficiently fine to enable appropriate resolution of turbulence length scales in three dimensions. It is important to ensure that a wide enough range of turbulence length scales is resolved, otherwise the assumptions LES is based on may not be valid. This range is generally considered to be that at least 80% of the turbulent kinetic energy in the flow is resolved and the remainder is accounted for by the SGS model (Pope, 2000 and Wagner *et al.*, 2007).

LES calculations are inherently transient, so a time step is required by the solver. It is important to note that this time step must be appropriate for the flow field, and also consistent with the mesh size (Volume 3, Section 3.2.5). Higher *Re* or *Gr* flows often need a finer mesh and therefore generally use smaller time steps. Since the appropriate mesh size to use depends on the flow field, it is normal to start LES work by performing an initial RANS calculation. This gives an initial solution and develops understanding of the flow under study. It also enables the required LES mesh dimensions to be estimated based on the RANS turbulence model predictions by calculating the integral length scale and Taylor microscale values, together with a representative cell length. Software-specific guidance should be checked because definitions may vary (particularly for k-ω

models), but equations normally have a form similar to:

$$\text{Integral length scale (m): } l_0 = \frac{k^{3/2}}{\varepsilon} = \frac{k^{1/2}}{C_\mu \omega}, \text{ where } C_\mu = 0.09 \text{ (Menter, 2015)}$$

$$\text{Taylor microscale (m): } \lambda \approx \sqrt{10\nu\frac{k}{\varepsilon}}, \text{ where } \nu \text{ is the kinematic viscosity}$$

$$\text{Cell length (m): } \Delta = V_{cell}^{1/3} \text{ for modest aspect ratios, where } V_{cell} \text{ is the cell volume}$$

Typically, 10 to 20 mesh cells are needed across l_0 to resolve 80% of the turbulent kinetic energy, so the suggested cell size is typically taken to be $\Delta = \max(\lambda, l_0/10)$ for full LES resolution (further detail is available in Addad *et al.*, 2008). This can be checked by plotting $l_0/\Delta < 10$ and $\lambda/\Delta < 1$ to identify areas that are under-resolved. Once the LES calculation is complete, its success in capturing the turbulence length scales can be checked by calculating the amount of turbulent kinetic energy that is resolved as a proportion of the total turbulent kinetic energy (Pope, 2000). The proportion of turbulent kinetic energy that is resolved in a LES solution can be estimated by:

$$\sigma = \frac{k_{res}}{k_{res} + k_{sgs}}$$

$$k_{res} = \frac{1}{2}\left(u_{rms}^2 + v_{rms}^2 + w_{rms}^2\right) \text{ and } k_{sgs} \approx \overline{\left(\frac{\mu_{sgs}}{\rho C \Delta}\right)^2}$$

Where k_{res} is the resolved turbulent kinetic energy, k_{sgs} is the time-averaged sub-grid scale (modelled) turbulent kinetic energy, u_{rms}, v_{rms} and w_{rms} are the Root Mean Square (RMS) fluctuations in the three components of velocity, μ_{sgs} is the sub-grid scale turbulent viscosity, ρ is the density, C is the Smagorinsky coefficient and Δ is the sub-grid scale filter length. A value of $\sigma > 0.8$ is considered to represent a good LES solution (Pope, 2000). It is worth noting that this definition of the proportion of turbulent kinetic energy resolved does not include the turbulent kinetic energy numerical discretisation error (k_{num}), which according to Celik *et al.* (2009) may be of similar magnitude to k_{sgs}. Further guidance on the methods used to assess the quality and reliability of LES models are detailed in Meyers *et al.* (2008).

LES is relatively intolerant to large cell aspect ratios and rapid changes in mesh size (because the turbulent viscosity is usually directly related to the local grid size). For boundary layer flows, a small near-wall mesh sizing ($y^+ < 1$) is required to model the small eddies in the inner-most part of the boundary layer (which are broadly comparable to wall distance in size). This therefore leads to similarly small mesh sizes in both streamwise and spanwise directions. An LES calculation that has properly resolved the near-wall scales is usually referred to as 'wall-resolved' LES. For most engineering flows, wall resolving leads to very onerous mesh requirements[1].

The near-wall region is often significant because the flow here directly affects heat transfer (Section 2.1.2). There have been attempts at developing wall functions for LES (see, for example, Piomelli, 2008), but these may be more restrictive than RANS counterparts since they need assumptions about how velocity fluctuations vary near the wall. However, in industrial cases it is common to use hybrid methods such as Wall Modeled Large Eddy Simulation (WMLES) to reduce

[1] For Reynolds number $Re > 10^5$, this becomes prohibitive quite quickly; Piomelli (2014) estimates that over 90% of the grid points may be needed to resolve less than 10% of the computational domain.

the expense of modelling near-wall flows (or high Re flows may be unresolved near walls).

It is noted that mesh sensitivity studies need care for LES, since finer meshes usually result in a greater proportion of the turbulent length scales being resolved (as opposed to being modelled) and the approach tends towards DNS. It is therefore not possible to achieve true 'mesh independence' in the flow fields in the same manner as is considered desirable for RANS approaches. Therefore, the quality of an LES simulation needs to be assessed based on cell aspect ratio and percentage of turbulent kinetic energy that is resolved, and potentially the convergence of time-averaged integral quantities (forces or heat fluxes on surfaces), or the frequency spectrum of fluctuating quantities of interest.

3.4.2.5 Meshing Fluid Volumes: RANS

For RANS models it is desirable to obtain mesh-independent solutions, so it is normal to use a mesh sensitivity study to understand the influence of the mesh on the solution. Ideally, at least three meshes of increasing resolution might be tested and compared using flow quantities of interest, ideally by doubling the mesh in all dimensions (increasing the mesh size by a factor of eight). However, due to computational expense, the impact of mesh resolution might be studied in key areas within the full computational domain, or a part of the computational domain might be meshed separately to study. This is discussed in more detail in Volume 4 (Confidence and Uncertainty). This section provides some guidance that may assist in developing a mesh-independent solution.

Near Walls: As introduced in Volume 1, a key aspect of RANS methods is the approach to modelling flow near walls. Methods introduced in Volume 1 include wall resolving (low-Re, fine mesh, small y^+), standard wall functions (high-Re, coarser mesh, larger y^+), enhanced wall functions (CFD code tailors approach to local y^+) and advanced wall functions (more complex models catering for non-equilibrium conditions), although the terms used and detailed implementations may vary between CFD software. Each approach has different requirements for the local mesh spacing near the wall, which is normally defined in meshing software before a flow solution is available. Software specific guidance should be consulted, but enhanced wall functions are often used for industrial flows, so that:

1. The CFD user decides where in the domain more detailed modelling of flows near walls is valuable (e.g. where there is significant surface heat transfer, or separating flows are expected) and designs the mesh in these areas to resolve the viscous sublayers of turbulent boundary layers (which occur between $0 \leq y^+ < 5$, Schlichting and Gersten, 2017, Chapter 17), consistent with a wall-resolving approach. To achieve this, the mesh is generally developed so that the nearest point to the wall at which the solver will compute flow variables is at $y^+ < 2$, ideally $y^+ \approx 1$. The mesh should then expand smoothly away from the wall.
2. In the other areas (where the CFD user considers detailed wall modelling less valuable, such as pipework or volumes where the details of the flow have less impact on the key results) the mesh is designed to only capture the fully turbulent region of boundary layers, consistent with a standard wall function approach. To achieve this, the mesh is generally developed so that the nearest point to the wall at which the solver will compute flow variables is at $y^+ \approx 30$ to 50 (the CFD solver can then apply scaled wall functions in these areas), but higher values of 100 of more may be permissible, depending on the situation.

Whatever approach is taken, the mesh often needs to be adjusted when an initial flow solution is available. If the mesh is poorly designed however, these initial flow solutions will be misleading, and more iterations will be needed to obtain an appropriate mesh. The following guidance may help reduce the amount of iteration needed. It may also be helpful to develop meshes using small test cases on parts of the geometry before completing the full mesh.

First Cell Height: To develop a near-wall mesh, the target y^+ value at a given point on a wall is turned into a distance between the wall and the nearest point to the wall at which the solver will compute flow variables (y). However, this can only be done with some understanding of the flow field, since the time-averaged wall shear stress ($\overline{\tau_w}$) is needed:

$$y = y^+_{target}\frac{\nu}{u_\tau} = y^+_{target}\frac{\nu}{\sqrt{\frac{\overline{\tau_w}}{\rho}}}$$

In practice, y is often set as a constant over a given surface (i.e. is not changed in response to the local flow field) and therefore:

$$y = y^+_{target}\frac{\nu}{\sqrt{\frac{C'_f\frac{1}{2}\rho U^2}{\rho}}} = y^+_{target}\frac{\mu}{\rho U\sqrt{\frac{C'_f}{2}}} = y^+_{target}\frac{1}{\left(\frac{Re}{L_{Re}}\right)\sqrt{\frac{C'_f}{2}}}$$

Re/L_{Re} is the Re per unit length, which can be assessed using estimated flow-field quantities (the lengths should cancel). ρU can be calculated from a mass flow rate where appropriate ($W = \rho A_{cs} U$). C'_f is the local skin (or 'Fanning') friction coefficient commonly used in external flow, which is related to the pipe (or 'Darcy', or 'Moody') friction coefficient (f) commonly used in internal flow as:

$$C'_f = \frac{f}{4} = \frac{\overline{\tau_w}}{\frac{1}{2}\rho U^2}$$

C'_f or f can be estimated using a resistance diagram (or 'Moody chart' for pipes) or a correlation (Schlichting and Gersten, 2017; Rohsenow *et al.*, 1998; Kakaç *et al.*, 1987; Miller, 2009; Idelčik and Ginevskiĭ, 2007). Example correlations for incompressible external flow over a smooth flat plate include:

$$C'_f = (2\log_{10}(Re_x) - 0.65)^{-2.3} \quad \text{for turbulent flow (after Schlichting)}$$

$$C'_f = 0.664(Re_x)^{-\frac{1}{2}} \quad \text{for laminar flow}$$

Where Re_x is based on the streamwise length x and free-stream velocity (laminar and turbulent flow are discussed in Volume 3, Section 2.2). Example correlations for fully developed flow through a straight rough pipe with circular cross-section include:

$$f = 0.25\left[\log_{10}\left(\frac{\epsilon}{3.7D} + \frac{5.74}{Re_D^{0.9}}\right)\right]^{-2} \quad \text{for turbulent flow (Swamee-Jain equation)}$$

$$f = \frac{64}{Re_D} \quad \text{for laminar flow}$$

Where Re_D is based on the pipe diameter and superficial velocity (Section 2.1.2.3) and ϵ is the surface roughness. The Swamee-Jain equation is one approximation of the implicit Colebrook-White equation (a number of other similar approximations are available).

As these diagrams and correlations are generally for simple geometry like flat plates or straight pipes, the predicted C_f' or f values will need to be increased to account for local acceleration of the flow over other geometries (which generally increase the wall shear stress). Engineering judgement is needed for this (as a rough starting point for external flow, a factor of 2 for streamlined shapes and 4 for shapes like cylinders may be useful).

Once y has been predicted, the height of the first cell away from the wall (the 'first cell height') can be specified in the meshing software. For vertex centred numerical schemes the First Cell Height (FCH) is normally equal to y, while for cell centred schemes it is normally equal to $2y$.

Near Wall Prismatic Mesh: As noted in Section 2.1.2, external flows often feature boundary layers near walls surrounded by a free-stream flow, while internal flows may feature significant gradients in flow variables across the domain. In either case however, the near-wall regions are likely to feature large gradients in flow variables normal to the wall, and smaller gradients along the wall. These areas are often meshed using a prismatic mesh (Volume 1, Section 4.5.2). As well as the FCH, the thickness of the prismatic mesh and the number and distribution of mesh cells across this thickness should be appropriate for the flow (Figure 3.4).

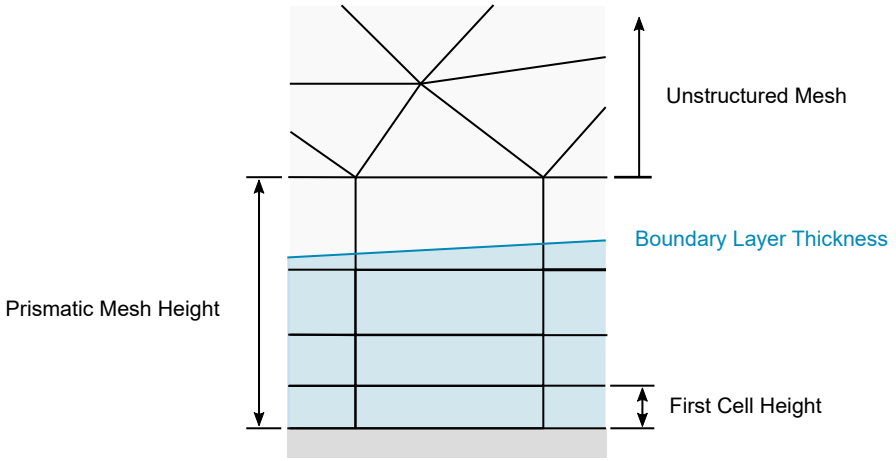

Figure 3.4: Illustration of FCH and near-wall prismatic mesh containing a boundary layer.

In general, the prismatic mesh should be designed so it is thick enough to accommodate the full thickness of the boundary layer. Boundary layer thickness (δ) for external flows can be predicted using a suitable correlation (Schlichting and Gersten, 2017). Example correlations for incompressible external flow over a flat plate include (Anderson, 2017):

$$\delta = \frac{0.37x}{Re_x^{1/5}} \quad \text{for turbulent flow}$$

$$\delta = \frac{5.0x}{Re_x^{1/2}} \quad \text{for laminar flow}$$

Where Re_x is evaluated at streamwise length x and free-stream velocity U_∞. As for the prediction of FCH, correlations are likely to be for simple geometry like flat plates, so predicted thicknesses will need to be increased to account for local deceleration of the flow (which generally increases boundary layer thickness). Similar factors to those used for estimating FCH above may provide

a rough starting point. For internal flows, the prismatic and adjoining mesh should be designed together to capture the expected flow gradients.

An appropriate number of cells should be placed across the boundary layer thickness, and these should be distributed correctly. The distribution is normally set using an expansion factor from the FCH out into the flow. Since the height of the boundary layer is likely to be growing within the prismatic mesh along the flow direction, either a) the number of cells across the height of the prismatic mesh should be larger than the number of cells required across the thickness of the boundary later, or b) the height of the prismatic mesh should be tailored to the thickness of boundary layer as it grows (by tailoring the expansion factor). The former approach is normally used in industrial cases, with the latter approach normally only applied for applications like aircraft wing or turbomachinery aerodynamics.

In practice, the prismatic mesh is normally defined using the FCH, a linear growth rate and the total number of cells. The prismatic mesh thickness is therefore not specified directly, and some iteration is needed to identify appropriate settings. Software specific guidance should be considered, but in general at least 10 to 20 mesh cells across the boundary layer thickness are often recommended, and 30 may be used in more detailed models (15 cells are often used as a minimum to reduce the risk of dropping below 10). However, this will depend on the wall treatment approach that is being used (i.e. wall-resolving or wall function method).

The thickness and number of cells across the prismatic mesh can be checked (using an initial flow solution) by visualising the turbulent viscosity across the boundary layer. This quantity should have a maximum in the middle of the boundary layer, so the thickness of the boundary layer can be estimated by doubling the distance between the wall and where this maximum occurs, and the number of cells across this distance can also be estimated. However, if the boundary layer grows out of the prismatic mesh and into a coarser or more dissipative region of adjacent mesh, the flow field may not develop properly and boundary layer thicknesses may be effectively limited. If this occurs, it may be difficult to know how thick the boundary layer mesh should have been and hence what expansion ratios should have been used making it difficult to know what adjustments to make to the mesh to predict the flow correctly. Allowing a greater thickness of prismatic mesh and reducing it later if needed may be helpful. It may not be practical or possible to create a prismatic boundary layer mesh that is large enough in all situations; in these cases (and in general) the size and quality of cells (which may be unstructured) immediately outside of the prism layer that transition to the wider mesh require care and attention, particularly to avoid large jumps in cell size and wall-normal resolution. The field values for the solution in these areas should be scrutinised.

Since temperature gradients are important for heat transfer, thermal boundary layers also need to be considered. This is important regardless of the wall boundary condition (adiabatic, specified temperature, specified heat flux, specified heat transfer coefficient etc). If Pr is close to unity, the Reynolds analogy can be used because the momentum and thermal boundary layers are likely to be similar (i.e. $C_f'/2 \approx St$). However, if Pr is not close to unity, the thermal and momentum boundary layers can be quite different; more detail is available in Volume 5.

Away From Walls: While the focus of this volume is on heat transfer to surfaces, it is also important that gradients in the wider flow field are appropriately resolved (especially for internal flows). As for boundary layers, enough mesh should be provided across areas of sheared flow (10 to 20 mesh cells across a shear flow are often used, but software specific guidance should be checked). It is also important to control the aspect ratio of cells near shearing flows. This is particularly true for natural convection cases, so these aspects are discussed further in Volume 3 (Section 3.2.3).

3.4.3 Case Definition

Once a computational mesh has been developed, the CFD case can be configured by defining physical information and solver settings. Setting fluid boundary conditions, fluid material properties and spatial and temporal discretisation are considered in Volume 3 (Section 3.2.4) as these are especially relevant to natural convection.

This section discusses additional aspects relevant to CHT analysis, considering boundary conditions, thermal radiation, the use of porous zones, and aspects associated with fluid to solid interfaces.

3.4.3.1 Boundary Conditions

Boundary conditions define the problem being solved, so if they contain inaccurate information or are applied incorrectly, it is likely the results will also be inaccurate. The application of boundary conditions in CFD tools varies, so software specific documentation should be consulted. For CHT analysis, the below aspects are particularly significant:

- Inflow and outflow boundary conditions should ideally be placed sufficiently far from areas of interest to avoid unwanted interactions. If an inflow is fully developed, suitable profiles for flow variables could be applied from literature sources, or created (e.g. by using a sub-model or extending the domain). The turbulence and temperature conditions for backflow at outlets may need to be carefully chosen, or backflow prevented by solver settings. Inlets and outlets also can have radiation settings applied so that the interior of the domain can ‘see’ a specified external temperature.
- Wall boundary conditions are important because they affect the pressure drop and heat transfer in the fluid domain. For CHT analysis, the surface roughness and thickness of deposits can have a significant impact on the shear stress, and hence heat transfer into the fluid (Section 2.2). The surface roughness should be estimated based on the best available knowledge, and potentially reviewed as part of a sensitivity assessment if through life considerations are important. Different CFD tools have different approaches and requirements for the relative size of the first cell height and the applied surface roughness; the treatment of roughness impacts the accuracy of the near-wall models and type of near-wall modelling approach that can be used.
- External heat transfer is often a key requirement in CHT analysis and is applied to the external solid surface of the model. This needs to be considered in the context of the analysis to assess whether the temperatures or thermal gradients are conservative, because there is often a lot of uncertainty and variation in the external conditions. The following methods are commonly used, and the values should be potentially reviewed as part of a sensitivity

assessment:

  - **Adiabatic:** A zero heat flux boundary condition is often used for surfaces that are covered by thermal insulation or to maximise temperature predictions when the external heat loss is considered insignificant.
  - **Constant heat flux:** This applies a constant heat flux (W/m^2) to the surface that is independent of the bulk temperature and flow conditions, such as electric heating elements or heat released as a result of radioactive decay or the fission process.
  - **Constant temperature:** This fixes the temperature of a surface to a specified value and can be used to represent high external heat transfer conditions, such as pump driven water cooling, or boiling at a known saturation temperature.
  - **Applied HTC and ambient temperature:** This is the most flexible and generic approach to applying external thermal boundary conditions, and involves specifying convection (HTC and bulk temperature) and thermal radiation (far-field temperature and emissivity) conditions. Therefore, the external heat transfer can vary and depends on the local wall temperature, which enables a more realistic representation of the external heat loss. For example, this can be used for forced or natural convection to air by using empirical correlations for HTC, such as a vertical or horizontal heated plate (Incropera *et al.*, 2011), although the limitations and uncertainty associated with empirical correlations should be borne in mind (Section 2.1.2.3).

- For thin-walls or shells (Section 3.3.3), the thickness and solid material properties need to be specified to enable the thermal gradient and thermal mass associated with the solid to be included in the model. This includes contact thermal resistance between two solid materials (Section 2.1.1.1), if this is considered significant.
- When porous zones are included (Section 3.3.4), the porosity (open volume fraction), pressure loss and effective material properties need to be defined (Section 3.4.3.3). In addition, the impact on turbulence generation and appropriate representation of the porous region to the physical geometry needs to be considered.
- For uncoupled or coupled partitioned models (Section 3.3), the interfaces between the CFD and FEA models need to be carefully defined and appropriate boundary conditions used to enforce continuity of temperature and heat flux across the two regions. This will depend on the purpose of the analysis and software-specific recommended approach.
- For coupled monolithic models (Section 3.3.2), the coupling between the fluid and solid regions is usually simple, as it is addressed within a single code. For non-conformal interfaces, it is important to ensure that heat transfer across the interface is enabled and large variations in the mesh resolution across the interface do not impact the accuracy of the temperature predictions.

3.4.3.2 Thermal Radiation

Radiative heat transfer is complex (Section 2.1.3), and it is generally only applied in a simplified and approximate manner in NTH analyses. The need to model thermal radiation depends on the properties of the fluid:

- Water and liquid metal: Radiative heat transfer is not important because thermal radiation does not penetrate any appreciable distance before it is absorbed.
- Air and most simple gases (e.g. helium and argon): Radiative heat transfer occurs between surfaces and they are considered non-participating media (neither absorb, emit or scatter thermal radiation at the IR wavelengths of interest), and variations of surface properties with temperature and wavelength are usually ignored.
- Water vapour, CO_2 and soot: For large volumes and significant concentrations, they emit, absorb and scatter thermal radiation, and so may need to be considered as a participating medium.
- Molten salts: These are semi-transparent media that absorb the different wavelengths emitted from a hot surface to different degrees according to its absorption spectrum and salt composition. This is discussed in detail in Volume 6.

Thermal radiation becomes significant when the radiant heat flux, $q_{rad} = \epsilon\sigma(T^4_{max} - T^4_{min})$, is large compared to the heat flux due to conduction or convection, which typically occurs at high temperatures.

However, radiative heat transfer can significantly impact the overall flow and thermal solution, and so should only be neglected after careful consideration. For example, Martyushev *et al.* (2014) investigated the unsteady regimes of convective-radiative heat transfer in a cubic enclosure with finitely thick heat-conducting walls in the presence of a constant-temperature energy source. The dominant mechanism of transfer of energy in this system is natural convection, but neglecting the radiative component can lead to considerable variations in integral characteristics and in the structure of the velocity and temperature fields.

There are a number of standard thermal radiation models available in most CFD software with different levels of complexity and medium participation. The most common models include:

P_1: The Radiative Transfer Equation (RTE) is simplified by the P_1 model to an approximate form that is fast to solve. It is mostly recommended for 'optically thick' (participating medium) applications, and does not include significant detail on directionality, so is not recommended for complex geometry or transparent media. The P_1 model can include the effect of absorption and particulates within the medium with properties that can vary with radiation wavelength i.e. non-gray and gray radiation. It assumes that the reflection of incident radiation at a surface is isotropic (diffuse).

Rosseland: When a medium is highly absorbing or scattering, then the Rosseland diffusion equation can be used as an approximation for radiation transport. The diffusion approximation does not retain any directionality in radiation and heat transfer appears as an additional radiative conductivity (that depends on T^3) added into the energy equation, so no additional radiation transport equations are solved. Because the diffusion approximation is not valid

near to a surface, 'temperature jump' (discontinuous) boundary conditions are needed when using this model.

Surface-to-Surface (S2S): The S2S radiation model is useful for modelling radiative heat transfer within an enclosure with non-participating media. It calculates the view factor (Section 2.1.3.3) for each face or cluster of faces to determine the energy transfer between two surfaces based on their size, separation distance and orientation (and does not consider the medium between them). The view factor calculation is usually undertaken as a pre-processing step, making the model faster to solve. The S2S model usually assumes gray radiation and that all surfaces are diffuse.

Discrete Ordinates (DO): The DO model has the capability to solve radiative heat transfer for participating and non-participating media, including semi-transparent walls (Murthy and Mathur, 1998). Therefore, it can include the effect of absorption, scattering and particulates within the medium for gray and non-gray radiation. It solves the RTE as a transport equation for radiation intensity for a finite number of discrete solid angles, and so the accuracy of the solution depends on the angular discretization. If the discretization is too coarse, it can lead to physically unrealistic 'bumps' and artfeacts in the incident radiation field. The main disadvantage of the DO model is that it can be computationally expensive, and so increases the solution time.

Monte Carlo (MC): The MC model simulates radiative heat transfer by tracking ('ray-tracing') a large number of representative photon bundles (histories) through the domain. It is a general-purpose method and also allows absorption, scattering and particulates within the medium for gray and non-gray radiation. MC simulations are also a balance between accuracy and computational costs, where improved accuracy is possible by increasing the number of photon histories tracked, making the simulation computationally more expensive. Some MC implementations have an S2S option for non-participating media, where the photons are tracked from wall to wall without interacting with the medium they are passing through.

For non-participating media, the key parameter is the emissivity of the surfaces in contact with the radiative heat transfer enclosure (Section 2.1.3.2). For participating media, it is also necessary to specify the absorption coefficient, scattering coefficient and refractive index for the fluid within the enclosure.

3.4.3.3 Porous Zones

As discussed in Section 3.3.4, porous zones can be used in CFD models to represent solid and fluid regions that are too complex to model explicitly, such as packed beds, perforated plates, filters and tube banks. Porous media models use an empirically calculated flow resistance that is applied to the porous zone. This is usually based on the superficial velocity (the velocity that the fluid would have through the zone without the solid component being present) and depends on the physical structure/arrangement of the porous medium and porosity (proportion of fluid by volume, ϕ).

The use of a superficial velocity enables the bulk pressure loss through the porous zone to be calculated, but it does not resolve the increased physical velocities that occur, which limits the accuracy of the model. More advanced porous media models based on the physical velocity do exist, but their assumptions and appropriateness for each application needs to be carefully considered.

The pressure drop in porous zones is usually represented by a viscous loss (laminar flow) and an inertial loss (turbulent flow). In laminar flow through porous media (e.g. packed beds), the pressure drop is typically proportional to the velocity and tends towards Darcy's Law, which depends on the permeability of the medium, k (m^2).

$$\text{Laminar flow, } \Delta P = \frac{\mu}{k} U L$$

In turbulent flow through porous media (e.g. tube banks or perforated sheets), the pressure drop is typically proportional to the dynamic pressure and depends on the loss coefficient per metre, K/L ($1/m$). Typical values of loss coefficients for standard geometrical arrangements are provided in Miller (2009), and are discussed in Volume 3 (Section 2.2.2). In some cases, it may be appropriate to use anisotropic values of pressure loss based on the geometry (such as a rod bundle where losses in cross-flow are different to those in the axial direction).

$$\text{Turbulent flow, } \Delta P = \frac{K}{L} \frac{1}{2} \rho U^2 L$$

The expression for the momentum sink that is added to the Navier-Stokes equations in CFD codes that contains both laminar and turbulent parts is known as the Darcy-Forchheimer equation, or sometimes the Darcy equation with the Forchheimer (turbulent) correction.

By default, most porous media models neglect the presence of the solid for turbulence generation or dissipation, which limits the accuracy of the model, although some modifications to the k-ε equations have been proposed to account for the effects of porosity on turbulence (Al-Aabidy *et al.*, 2020). For porous beds, turbulence will be reduced by the medium, while for cross-flow in tube banks turbulence is likely to be increased. Better understanding and accuracy of the porous media model could be achieved by using a CFD model to explicitly resolve the fluid and solid components in order to determine more accurate correlations for pressure drop and turbulence generation.

Examples of the derivation and application of porous models are shown in Study B: Fuel Assembly CFD and UQ for a Molten Salt Reactor and Study C: Reactor Scale CFD for Decay Heat Removal in a Lead-cooled Fast Reactor.

Effective Material Properties: For porous zones, it is necessary to calculate the effective material properties of the combined fluid and solid components. The effective properties are often automatically calculated in analysis software based on the porosity, but the method should be checked to confirm that it is appropriate for each application.

The effective volumetric heat capacity (ρc_p), or thermal mass, of a porous region is usually calculated based on the overall porosity, as follows:

$$\rho_{eff} = (1-\phi)\rho_s + \phi\rho_f \text{ and } c_{p,eff} = (1-\phi)\frac{\rho_s}{\rho_{eff}} c_{p,s} + \phi \frac{\rho_f}{\rho_{eff}} c_{p,f}$$

$$\therefore (\rho c_p)_{eff} = (1-\phi)(\rho c_p)_s + \phi(\rho c_p)_f$$

However, thermal conductivity is harder to calculate as it depends on the structure/composition of the porous media. The effective thermal conductivity (k_{eff}) is defined as the thermal conductivity of the medium with no fluid motion. For general porous structures, the true value will lie somewhere in between the idealised series and parallel values (Figure 3.5). More detailed correlations have

been developed for some porous structures (Rohsenow *et al.*, 1998), alternatively this could be calculated directly using CFD software if the geometry is explicitly known to validate the porous zone properties.

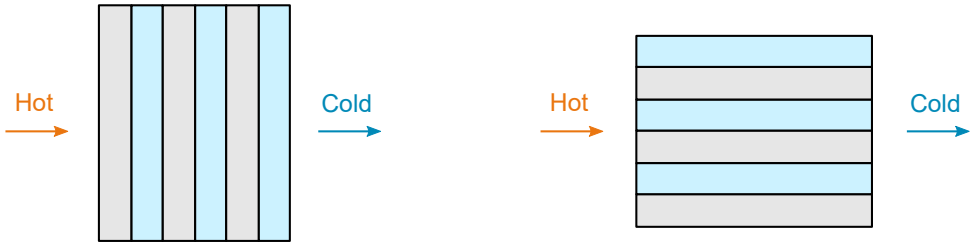

(a) Series (Perpendicular)

$$k_{eff} = \frac{1}{(1-\phi)/k_s + \phi/k_f}$$

(b) Parallel (Aligned)

$$k_{eff} = (1-\phi)k_s + \phi k_f$$

Figure 3.5: Bounding values for effective thermal conductivity.

In some cases, it may be more appropriate to use anisotropic values of thermal conductivity based on the geometry (e.g. rod bundle). For simple aligned solids, the thermal conductivity can be estimated using the series/parallel values (i.e. perpendicular to and aligned with the rod bundle respectively).

Depending on the porous structure (proportion of solid, open grid or random structure), radiative heat transfer is likely to be absorbed by a porous medium. Therefore, in most cases, the porous zone can be considered as a solid region that absorbs and emits thermal radiation.

For thermal radiation within the porous zone, the decomposition $(T_1^4 - T_2^4) = (T_1 - T_2)(T_1 + T_2)(T_1^2 + T_2^2)$ may be useful for creating equivalent thermal conductivity models in regions modelled with a porous representation where thermal radiation transport occurs, because if the approximation can be made that $T_1 \approx T_2 = \overline{T}$, then

$$T_1^4 - T_2^4 \approx 4\overline{T}^3(T_1 - T_2)$$

This allows an equivalent conductivity model to be created that depends on local temperature to the third power to represent the contribution of thermal radiation, without modelling thermal radiation explicitly.

3.4.4 LES Aspects

LES is introduced in Section 3.4.1 and meshing aspects are considered in Section 3.4.2.4. This section presents some advice for conducting LES work for CHT analysis with further details on the general application of LES modelling provided in Volume 3 (Section 3.2.5). Despite computational costs (discussed below) the application of LES to NTH is steadily increasing.

Unsteady CHT occurs due to the fluctuating heat loads generated by the turbulent flow. Simulations of turbulent flows using LES may capture the flow unsteadiness and associated variable heat loads on structures. Some industrial examples of LES with CHT include:

- Thermal fatigue and striping in T-junctions (Kuhn *et al.*, 2010, Ferrara and Di Marco, 2017);

- Round jet impinging on a flat plate (Hadžiabdić and Hanjalić, 2008);
- Fuel cladding temperatures in wire-wrapped fuel assembly (Doolaard *et al.*, 2015);
- Thermal mixing in annulus of control-rod guide tube (Bergagio *et al.*, 2020).

Computational Cost: As noted in Volume 3, the computational cost of LES is less than DNS but significantly higher than RANS. This is particularly so for high Re or Gr boundary layer flows, and because near-wall turbulence levels are coupled to surface heat transfer, the computational cost also increases as Ra increases. For CHT analysis, the thermal mass associated with the solid (Section 2.1.1.2) means that the temperature in the solid can take a long time to stabilise.

Because of the inherent computational cost associated with this method, the simulated physical time with such approaches is limited (typically several seconds up to one minute in most engineering applications, Koren *et al.*, 2017). Therefore, simulating low-cycle variations and long transients using LES is unlikely to be feasible currently.

Time Step: LES calculations are transient, so a time step is required by the solver. This is determined by the time step required for the flow field, as discussed in Volume 3 (Section 3.2.5), because the timescales associated with the flow are generally significantly smaller than any temperature variations within the solid.

Some solvers or coupling approaches allow different time steps to be used in the fluid and solid regions. This has the potential to significantly reduce the computational time required, for example by solving the solid domain every 50 iterations of the fluid domain. However, since the wall heat flux and temperature depends on the size of the coupling time step, a large value might impact the accuracy of an LES prediction as the unsteady phenomena may be under-resolved at the fluid-solid interface.

3.4.5 RANS Aspects

RANS is introduced in Section 3.4.1 and meshing aspects are considered in Section 3.4.2.5. This section presents some advice for conducting RANS work for CHT analysis with further details on the general application of RANS modelling provided in Volume 3 (Section 3.2.6).

Steady and Unsteady RANS: One of the key aspects of RANS is the ability to run models as either steady-state (RANS) or unsteady (URANS). While turbulent flows are, strictly, always unsteady (due to turbulent fluctuations in flow quantities), large-scale unsteady motion can also arise from non-turbulence phenomena or be imposed externally by time-varying boundary conditions. This large-scale 'coherent' unsteadiness can be considered distinct from the unsteady small-scale 'incoherent' unsteadiness typically associated with turbulence. URANS methods exploit this distinction by solving a form of the RANS equations which retain the time-derivative term.

Steady-state calculations account for the majority of engineering analysis, but the turbulence models used in RANS generally cannot account for large-scale flow motion. Therefore, *a steady RANS solution may not give the same results as a long-term time-averaged URANS solution with the same steady boundary conditions*.

As noted in Volume 1, for many decades URANS is likely to be the only practical CFD method for predicting long duration problems such as long reactor shut-down transients. This is particularly

true for CHT analyses as the timescales associated with low-cycle variations and long thermal transients are significant and can occur over several hours.

For flows whose stability is not certain, CHT should be carefully considered. Since the thermal properties of the solid have the potential to be substantially different from the fluid, it is worth understanding whether any large-scale flow motion has any impact on the solid temperatures and so whether a URANS analysis is necessary. In addition, due to the slow thermal response associated with solids it is often important to start any URANS analysis from a properly converged steady RANS solution where the solid temperature field has also reached steady-state. This may not be the appropriate choice in some cases; if modelling a relatively sudden change in plant conditions is the purpose of the simulation, then large thermal mass objects that are not in thermal equilibrium with either the initial or subsequent flow can significantly affect the response.

Time Step: If transient data is required from a URANS solution, a time step is normally specified. The choice of time step will depend on the timescales present in the flow, and can have a significant impact on the results. Estimating a time step based on the flow field is discussed in Volume 3 (Section 3.2.6).

As for LES, the timescales associated with the fluid motion are likely to be significantly smaller than the timescales associated with the solid. However, this means that the timescales required for the solid to reach a statistically steady value will be significantly higher, and so the model may need to run for a long time especially if simulating a long thermal transient. Depending on the coupling approach, it may be possible to use different time steps in the fluid and solid regions to reduce the overall computational time.

For coupled monolithic solvers, to minimise the time taken to solve each iteration the fluid and solid regions should be decomposed for parallel solution so that the computational effort is balanced, although CFD codes should be able implement this themselves without user intervention.

Turbulence and Near-Wall Modelling: RANS turbulence models and near-wall modelling approaches are considered in Volume 3 (Sections 2.2.4 and 3.2.6) as they are key aspects for buoyancy affected flows. Since the presence of a solid region does not fundamentally change the NTH phenomena being modelled, the most appropriate turbulence model should be selected based on the flow field, although some RANS models are being developed for CHT. For example, Craft *et al.* (2010) describe that predicting the correct details of the temperature response in a wall requires an accurate representation of the associated near-wall turbulence processes in the fluid.

For CHT analysis, the heat transfer at the wall is extremely important, and so a wall resolving (low-Re, fine mesh, small y^+) near-wall modelling approach is recommended to ensure that the near-wall thermal boundary layer is properly resolved.

3.4.6 Extracting Heat Transfer Data

It is often necessary to extract heat transfer data from CFD simulations. This can be either as a heat flux, surface temperature or HTC with a local bulk fluid temperature, where:

$$q = h(T_b - T_w)$$

Heat flux and surface temperature are a direct output of solving the energy equation within a CFD analysis and so can be easily extracted and used to pass information in a coupled partitioned approach (Section 3.3.2). Therefore, this section considers the methods available to calculate HTCs from a CFD solution, which are used to:

- Understand, interpret and assess CFD predictions by comparison against empirical correlations and theory.
- Undertake an uncoupled CFD/FEA solution (Section 3.3.1) when the thermal environment is changing so slowly that the fluids and solids can be considered to be in a quasi-steady-state, or the HTC is effectively independent of the solid temperature (i.e. forced convection).

As discussed in Section 3.3.2, HTCs are a useful way of exchanging heat transfer information, but are dependent on the local bulk temperature which is often non-uniform and not easy to define. Therefore, a number of different methods have been developed to extract HTCs. The most appropriate approach will depend on the local flow field and objectives of the analysis.

It is worth noting that for all but the simplest scenarios, there is often uncertainty in the calculated value of HTC. This needs to be taken into account in any subsequent FEA models. It is also important to ensure that the solid geometry, HTCs and bulk temperatures are consistent between models to ensure that the calculated temperatures and heat fluxes are appropriate.

Reynolds analogy: Under specific conditions (no external pressure gradient, Pr = 1 and uniform wall temperature), the momentum flux and heat flux can be shown to be analogous, and the velocity and temperature profiles have the same shape. This analogy can be used to estimate an HTC as follows:

$$\frac{C_f}{2} = St = \frac{h}{\rho_\infty U_\infty c_p}\ ,\ \therefore h = \frac{c_p \tau_w}{U_\infty}$$

Where C_f is the skin friction coefficient and U_∞ is the free-stream velocity. Chilton-Colburn developed an empirical correlation based on experimental data for a flat plate and fully developed pipe flow (Chilton and Colburn, 1934), which is often called the modified Reynolds analogy[2]:

$$\frac{C_f}{2} = StPr^{2/3}\ ,\ \therefore h = \frac{c_p \tau_w}{U_\infty Pr^{2/3}} \text{ for } 0.6 < Pr < 60$$

This analogy is not appropriate for liquid metal heat transfer due to the low Prandtl number as discussed in Volume 5.

[2] The term $StPr^{2/3} = Nu/(RePr^{1/3})$ is known as a *j-factor*; the Chilton-Colburn analogy is also applied to mass transfer, where Pr and Nu are replaced by Schmidt and Sherwood numbers respectively (Incropera *et al.*, 2011, Bird *et al.*, 2007, Chapter 22).

Bulk temperature: For forced convection in a pipe or mixed convection within an enclosed cavity, it is often convenient to calculate a 'bulk' or 'mean' static temperature ($\overline{T_s}$) based on an appropriate region (Section 2.1.2):

- If the fluid near a surface is well mixed, a single constant value of bulk temperature may be appropriate.
- For the flow along a pipe/duct, an offset line along the pipe axis should be used with the bulk temperature calculated based on the local average fluid temperature.
- An offset surface may also be used to determine a local fluid temperature and calculate a local HTC. The offset distance should be set so that it is at the edge of the thermal boundary layer and is only valid when thermal gradients in the free-stream are small. Since this does not take into account any variation in boundary layer thickness, a more general approach based on the y^+ at the edge of the boundary layer is discussed below.

This is a simplistic approach that needs to be used carefully as it can generate unrealistic or negative values of HTC when the local wall temperature equals the bulk temperature. Therefore, it is often appropriate to calculate an average value of HTC based on the average bulk temperature. This can provide a more representative estimate of the HTC on a surface.

Diabatic Y-plus Field (DYF): The local fluid temperature for the DYF is defined as the fluid temperature at the edge of the thermal boundary layer, where the thermal gradient is zero. This can be extracted from a CFD solution by creating a surface in the CFD model that is offset a fixed dimensionless distance from the wall i.e. y^+ of 60 to 250 (Łuczyński *et al.*, 2019). A local HTC can then be determined using the local fluid and wall temperature values.

This method is appropriate for forced convection flows, when the flow is clearly defined with no separation or stagnation, so that the edge of the thermal boundary layer can be identified. However, if there are large thermal gradients in the flow due to mixed convection or local forced convection effects, then it can lead to unrealistic or negative HTC values.

Thermal superposition: If the energy equation near the wall is linear with temperature, which is generally true if buoyancy effects and static temperature changes are small, superposition of solutions may be used to show that if the wall temperature is changed from T_1 to T_2 (Verdicchio, 2001), then HTC can be calculated explicitly as small changes in local wall temperature have a negligible effect on the local HTC and local fluid temperature:

$$q_1 = h(T_1 - T_b) \text{ and } q_2 = h(T_2 - T_b)\ ,\ \therefore h = \frac{q_1 - q_2}{T_1 - T_2}$$

This means that an estimate of HTC, and hence local fluid temperature, can be obtained from two CFD solutions with different wall temperatures. In practice, this can be achieved by calculating a baseline or adiabatic surface temperature in a CFD solution, extracting the temperature profile on a small zone or surface and applying a small fixed temperature change to it (e.g. 10 °C to 50 °C) and then re-solving the CFD solution with a fixed temperature boundary condition.

Since this method uses two solutions to derive the HTC, it can be applied when the local fluid temperature cannot be clearly defined or there is a complex free-stream flow field. This has been

successfully validated for a gas turbine compressor drum (Lewis and Provins, 2004) to extract HTCs from a CFD solution and apply them to an FEA model.

3.5 Experimental Methods

The role of experimental methods in NTH analysis and the value of experimental and modelling teams working together closely is introduced in Volume 1 (Section 4.6). This section builds on this, discussing the different techniques that might be used to measure temperature, and some of the challenges associated with them, while pressure, velocity and flow visualisation measurement techniques are discussed in Volume 3 (Natural Convection and Passive Cooling).

3.5.1 Temperature Measurement

A wide range of different temperature measurement techniques are available, with different levels of accuracy, response times and accessibility requirements.

Thermocouple: Thermocouples are based on the principle that a temperature-dependent voltage is produced when dissimilar metals are connected together. The five standard base metal thermocouples are chromel-constantan (Type E), iron-constantan (Type J), chromel-alumel (Type K), nicrosil-nisil (Type N) and copper-constantan (Type T). These are all relatively cheap to manufacture, but some can become inaccurate over time (Morris and Langari, 2020). This drift in calibration over time is less of a problem in experiments than in actual reactors, where thermocouples are expected to provide readings for decades. In addition, noble metal thermocouples have been developed that have high stability and long life even at high temperatures, but they are expensive and cannot be used in reducing atmospheres. In most cases, base metal thermocouples are used, which have a typical accuracy of $\pm 0.5\,\%$ to $\pm 0.75\,\%$, and the most appropriate type will depend on the environment, stability, operating life and accuracy requirement.

It is often impractical to connect a voltage-measuring instrument in close proximity to the point at which temperature is being measured, and so extension leads up to several meters long are required. This modifies the electrical circuit, and so care must be taken regarding the materials used in the extension leads and calibration of the thermocouple. If transient measurements are required the tip should be left exposed to maximise the speed of response, although they are delicate devices that must be treated carefully. Thermocouples can be protected using an insulated sheath (often called a probe), although this increases the time taken for the thermocouple to respond (e.g. $\approx 0.15\,\text{s}$ time constant for 1 mm diameter sheath).

Thermocouples respond quickly to changes in temperature, and are a simple, cheap and widely used method for measuring fluid and solid surface temperature.

Resistance Thermometer: Resistance thermometers or Resistance Temperature Devices (RTDs) are based on the principle that the resistance of a metal varies with temperature. Platinum has a good linear resistance/temperature characteristic and it also has good chemical inertness (Morris and Langari, 2020). In the case of non-corrosive and non-conducting environments, RTDs are used without protection. In all other applications, they are protected inside a sheath, which reduces the speed of response to changes in temperature.

RTDs are commonly used up to 650 °C with a measurement inaccuracy of ±0.5 %. They are generally more stable than thermocouples and can measure small temperature differences.

Distributed Temperature Sensor: Distributed Temperature Sensors (DTSs) use fibre optic cables to measure the temperature profile along the sensor cable because changes in temperature along the length of the cable alter the amount of light that is transmitted. Analysis of the backscattered radiation then enables temperature versus distance to be determined (Morris and Langari, 2020). High resolution DTSs have a high measurement accuracy, and have been used to measure temperature distributions near the core of a research reactor and in corrosive liquid-sodium environments (Gerardi *et al.*, 2017).

Thermography: Thermography, or thermal imaging, involves scanning an IR radiation detector across an object. This is a non-invasive technique used to provide temperature measurements at a single point or on a surface area (Kim *et al.*, 2016). The IR detector uses the principle that all objects emit electromagnetic radiation as a function of temperature. The temperature at the point that the instrument is focused on is inferred from a measurement of the incoming infrared radiation.

Measurement resolution can be high, with temperature differences as small as 0.1 °C being detectable (Morris and Langari, 2020). However, the thermal radiation from a body is very sensitive to the composition and surface condition of the body (i.e. its emissivity). Therefore, all IR detectors have to be carefully calibrated for each particular body or by applying patches of known emissivity. In addition, IR thermography requires line of sight with the emitting body and the results can be affected by absorption and scattering between the emitting body and the detector (e.g. dust and water droplets).

IR thermography has high sensitivity and fast response time, and can therefore be exploited to effectively measure convective heat fluxes with steady or transient techniques, or to perform detailed thermal surface flow visualisation (Astarita and Carlomagno, 2013). IR thermography can also be used in situations where contact measurements would be hazardous or impossible (e.g. at temperatures exceeding 1300 °C, Kim *et al.*, 2016). However, the method is relatively expensive and can only be used to measure the temperature on a solid surface with gas present between the surface and infrared detector.

Temperature Sensitive Paint: Temperature Sensitive Paint (TSP) is a method for measuring surface temperature, usually in aerodynamic settings (Liu, 2011). TSP is a paint-like coating that fluoresces under a specific illumination wavelength in differing intensities depending on the surface temperature due to thermal quenching that reduces the luminescent intensity. TSP is able to provide non-contact, high resolution, quantitative mapping of surface temperature on complex surfaces at low cost. A generic TSP measurement system is composed of paint, illumination light, photodetector and data acquisition/processing unit, with each pixel of the imaging camera acting like an individual thermocouple.

Time-resolved TSP applications involve pulsed excitation, and so depends on the ability to effectively detect the emission from TSP in short exposures. One can thus determine surface temperature variation as a function of time. In this case, the imaging devices must be synchronized to the excitation with multi-channel digital delay/pulse generators providing that synchronization. This

technique is used in both aerodynamic and turbomachinery applications, and can be used to identify the transition from laminar to turbulent flow due to the abrupt change from low to high heat transfer.

Since TSP uses imaging cameras, the test fluid and test section walls must be optically transparent, which makes it difficult to use at reactor pressures and temperatures.

3.5.2 Measurement Challenges

Use of test rigs to measure temperature and CHT effects at a system and component level can be challenging, as the material properties of the structure around the test section is a fundamental part of the test requirement. This limits the accessibility and visibility of the flow within the test section, making detailed concurrent flow and thermal measurements difficult.

If the transient response of the solid is important (high frequency fluctuations or long fault scenario), then the scaling of the rig is further complicated by the need to match the solid thermal mass as well as the flow phenomena. Other factors include understanding and minimising the impact of the external ambient conditions (e.g. heat loss), measurement accuracy and ensuring that the instrumentation does not impact the test results.

Thermocouples are often used within test rigs as they are simple to use and provide point transient temperature measurements of the fluid and solid, but care needs to be taken when installing and calibrating the instrumentation to ensure that:

- The thermocouple is in good contact with the surface, otherwise it can be influenced or offset by the fluid temperature. Surface measurements can be particularly difficult as they can be affected by the local flow and small gaps can form over time.
- The thermocouple does not influence the flow/temperature as they are about 1 mm diameter and attached to a cable.
- The responsiveness (time constant) of the thermocouple is appropriate for the timescales of temperature fluctuations being measured.
- The thermocouples are calibrated and the uncertainty is quantified, as this can be significant compared to the temperature changes being measured (approx. 2 °C).
- The location of the thermocouples is optimised to identify and measure the expected features of interest in the test.

As discussed in Volume 1, the most important aspect of a test rig designed for model validation is to ensure that the experimentalists and model developers work closely together throughout the design process to ensure that the rig meets the model validation requirements and that uncertainties are quantified and documented.

4 Future Developments

To conclude the present volume, this section considers how the aspects presented on the preceding pages may change in the future.

It is expected that the ongoing exponential increase in computational power and CFD software development will enable more accurate CFD predictions of convection, thermal radiation and conjugate heat transfer. As a result, there will be increased use of CFD methods to reduce cost, increase performance and improve the safety of advanced reactor designs. This is likely to include:

- Larger (amount of plant modelled) and longer (length of transient) RANS/URANS simulations.
- More widespread use of LES and hybrid methods, including to generate high-fidelity results and benchmark solutions for RANS/URANS model development and validation (Volume 3, Section 4).
- Automatic geometry and mesh generation for complex geometries to reduce the cost and timescales associated with CFD methods.
- Improved fluid-solid coupling to make it easier to include solid geometry and solve long thermal transients.

However, NPPs are complex, integrated systems involving a wide range of different physics, timescales and fault scenarios that need to be designed and assessed at a system level. Although CFD methods offer significant benefit in terms of accuracy and confidence, they are unlikely to be able to routinely simulate all of the details of a whole primary circuit in the near future. Therefore, the integrated digital design process and coarse grid CFD should be points of focus for future research intended to support the design of advanced reactors.

4.1 Integrated Digital Design Process

As discussed in Section 3.1, multiscale NTH analysis and multiphysics models that include thermal hydraulics are being increasingly developed and used as part of an integrated framework for reactor design. This has the potential to simulate the whole primary circuit with CFD resolution in local areas, and include coupled neutronics, structure and chemistry (CRUD, corrosion) calculations. Integrated frameworks that are currently being developed include:

MOOSE: Multiphysics Object-Oriented Simulation Environment (MOOSE)[1] is a multiphysics framework that has been developed by Idaho National Laboratory (INL) to provide a high-level interface for computational analysis. It provides a fully-coupled, fully-implicit solver that allows

[1] moose.inl.gov/SitePages/Home.aspx

independent codes to be coupled and exchange information, and has the capability to solve problems involving solid mechanics, phase field modelling, heat conduction and fluid flow.

It includes a number of thermal hydraulic analysis software, such as RELAP-7, SAM, TRACE and Nek5000, which are described in Volume 1 to enable multiscale analyses. In addition, the United States Nuclear Regulatory Commission (US NRC) has proposed a code suite for non-LWR systems safety analysis (US NRC, 2020), called the Comprehensive Reactor Analysis Bundle (CRAB), which is based around MOOSE. This documents the US NRC's vision and strategy for safety analysis and licensing of Advanced Nuclear Technologies (ANTs).

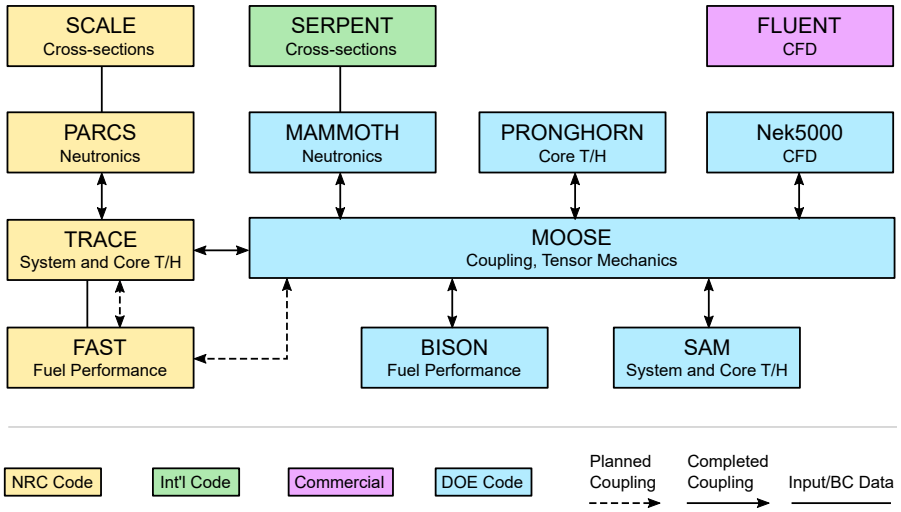

Figure 4.1: US NRC Comprehensive Reactor Analysis Bundle (CRAB) (US NRC, 2020). This image is reproduced courtesy of US NRC, and is not covered by the creative commons license defined in the legal statement for the present document.

NURESAFE: NUclear REactor SAFEty simulation platform (NURESAFE) was a European Commission (EC) funded collaborative research project that was completed in 2015 and involved 22 organisations (Chanaron, 2016). This built on previous EC Framework Programs (NURESIM and NURISP) and was intended to enhance the prediction capability for the design and safety assessment of LWR NPPs through the dynamic 3D coupling of multiphysics codes into a common simulation scheme.

The NURESIM platform, at the end of the NURESAFE project, includes neutronics, core simulators and fuel thermo-mechanics, as well as system (CATHARE, ATHLET), subchannel (CTF, SUBCHANFLOW) and CFD (NEPTUNE_CFD, TRIO_U) codes. This is based on the open source simulation platform SALOME[2] with uncertainty quantification analysis (URANIE) and includes a generic coupling interface called ICOCO (Interface for Code Coupling). Although this project was specifically focused on simulating normal operation and design basis accidents for LWRs, many of the codes within the platform are being developed and validated for ANTs.

ONCORE: The International Atomic Energy Agency (IAEA) Open-source Nuclear Codes for Reactor Analysis (ONCORE)[3] initiative is an international collaboration framework for the develop-

[2] www.salome-platform.org
[3] nucleus.iaea.org/sites/oncore/SitePages/Home.aspx

ment and application of open source multiphysics simulation tools. This includes neutronics, structural mechanics, fuel behaviour and thermal hydraulics analysis tools. ONCORE offers access to knowledge and tools that otherwise may not easily be available, and promotes collaboration and sharing of resources.

The objective is to develop a consistent open source platform with verification through standard problems and code-to-code comparison and documentation. It includes application frameworks for integrating multiple codes and a number of the codes are based on the OpenFOAM software package.

Further integration and cost benefit could be achieved in the future through an Integrated Nuclear Digital Environment (INDE) that covers the whole life-cycle of the reactor from prototype design through operations and decommissioning to storage and waste disposal (Patterson *et al.*, 2016). This would enable the model fidelity to increase as the reactor design develops and track the evolution of the geometry. In addition, multiscale and multiphysics models could be linked to real-world data from validation of prototypes, in-service monitoring and plant inspections to produce a digital twin of the reactor.

For example, the Nuclear Virtual Engineering Capability (NVEC)[4] project funded by the UK Government Department for Business, Energy and Industrial Strategy (BEIS) Nuclear Innovation Programme (NIP) (Volume 1, Appendix A) is using real project applications to demonstrate improved efficiency and position the UK as a leader in digital twin and virtual engineering.

4.2 Coarse Grid CFD

It is currently not feasible to use CFD to perform core-level design calculations due to its prohibitively high computational cost. Therefore, various solutions have been proposed, among which the low resolution approaches show great potential, because they not only retain the flexibility and 3D advantages of conventional CFD, but also balance the simulation accuracy and computing cost. These low resolution approaches can be roughly divided into two categories:

Porous media method: This uses porous media with uniform or non-uniform porosity to model the fluid and solid domain as a whole without representing the detailed geometry. The in-bundle friction, spacer induced mixing, and fluid-solid heat transfer are all modelled using empirical correlations. Under certain situations, this method can be seen as a flexible sub-channel approach implemented on the CFD framework (Gerschenfeld *et al.*, 2019, Yoon *et al.*, 2018).

Reduced resolution CFD: The fuel assembly geometry is resolved using a coarse body-fitted grid. To overcome the shortcomings of the coarse grid in capturing the near-wall effects, appropriate modelling strategies, empirical near-wall closure methods or other special treatments are usually required. The method proposed by Glass *et al.* (2011), referred to as Coarse-Grid CFD (CG-CFD) uses as few as 5 cells per sub-channel cross-section. Instead of solving the Navier-stokes governing equation, they solve an Euler equation with a volumetric force term implemented to mimic the effects of friction and turbulence. However, the derivation of this volume force relies on a large number of pre-performed resolved CFD

[4] n-vec.co.uk

simulations on the same geometry (or a representative geometry) and a subsequent parameterisation process of the flow conditions. Hanna *et al.* (2020) introduced an advanced machine learning approach to predict CG-CFD simulation errors, though work is at an initial stage and a long way from industry application.

An alternative approach to reduced resolution CFD is to use a novel CFD-based subchannel framework (Liu *et al.*, 2019). This combines the advantages of modern CFD and traditional subchannel codes, and has been developed as part of the BEIS thermal hydraulics NIP (Volume 1, Appendix A)[5]. This method includes the capability to embed resolved CFD models when local refinement is required, but is implemented in a single code to simplify the spatial and temporal data transfer.

Since this method uses a very coarse mesh, compared to traditional CFD approaches, large reactor components or even the whole reactor core can potentially be modelled. The wall modelling closure in Subchannel CFD (or 'SubChCFD') is achieved using well validated industry standard correlations, similar to those used in subchannel codes, to improve the reliability of the prediction without using a fine near-wall mesh. SubChCFD uses a two-level mesh system (Figure 4.2):

1. The filtering mesh, which is equivalent to the mesh of a traditional subchannel code, enabling the use of existing engineering correlations to account for the integral wall shear and heat transfer effects.
2. The computing mesh, on which a typical CFD solver can be used to resolve the inviscid flow with corrections for diffusion using a simple mixing length turbulence model, which can be calibrated for specific applications.

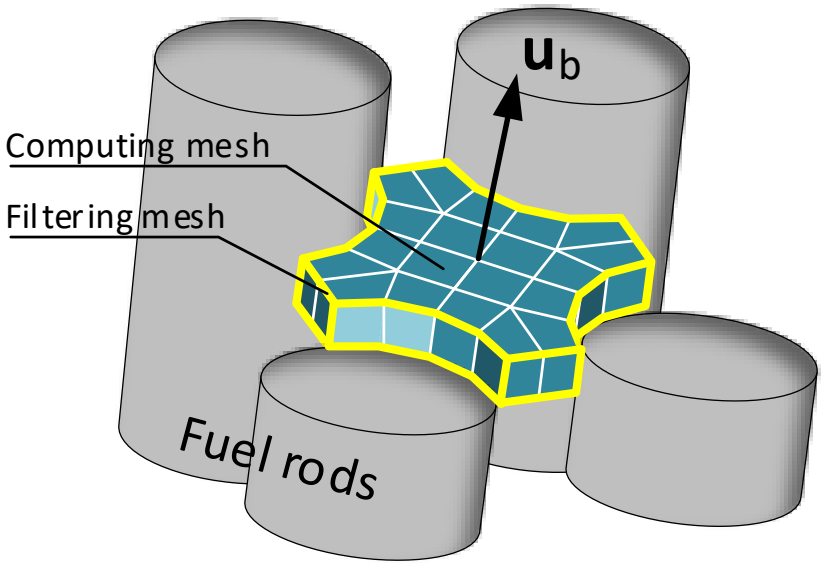

Figure 4.2: Mesh system in SubChCFD.

SubChCFD has been implemented in the Code_Saturne open source CFD code (but could be implemented as an add-on module in any CFD tool) and validated against a number of fuel bundle test cases. It is able to predict both the velocity and temperature fields for both standard and blocked fuel assemblies (Liu, 2019). The ability to include embedded resolved CFD models and

[5] www.innovationfornuclear.co.uk/nuclearthermalhydraulics.html

porous media has recently been implemented and validated to locally improve the simulation resolution where the flow and heat transfer exhibit complex features (Liu, 2021). This method is showing significant promise, and in the future could provide a more efficient and accurate way to model the reactor core and large reactor systems within a unified CFD framework.

5 References

Addad Y, Gaitonde U, Laurence D, Rolfo S (2008) Optimal Unstructured Meshing for Large Eddy Simulations. In *Quality and Reliability of Large-Eddy Simulations*, Ercoftac Series, pp. 93–103, Springer, Dordrecht, dx.doi.org/10.1007/978-1-4020-8578-9_8.

AFCEN (2018a) RCC-M: Design and Construction Rules for Mechanical Components of PWR Nuclear Islands. Association Française pour les règles de Conception, de Construction et de surveillance en Exploitation des chaudières électroNucléaires.

AFCEN (2018b) RSE-M: In-Service Inspection, Intallation and Maintenance Rules for Mechanical Components of PWR. Association Française pour les règles de Conception, de Construction et de surveillance en Exploitation des chaudières électroNucléaires.

Al-Aabidy Q, Craft T J, Iacovides H (2020) Improved Eddy-Viscosity Modelling of Turbulent Flow around Porous–Fluid Interface Regions. *Transport in Porous Media*, 131(2), 569–594, dx.doi.org/10.1007/s11242-019-01357-0.

Anderson J D (2017) Fundamentals of Aerodynamics. McGraw-Hill Series in Aeronautical and Aerospace Engineering, sixth edition, McGraw Hill Education.

Anderson N, Hassan Y, Schultz R (2008) Analysis of the Hot Gas Flow in the Outlet Plenum of the Very High Temperature Reactor Using Coupled RELAP5-3D System Code and a CFD Code. *Nuclear Engineering and Design*, 238(1), 274–279, dx.doi.org/10.1016/j.nucengdes.2007.06.008.

ASME (2019a) Boiler and Pressure Vessel Code (BPVC) Section II, Materials, Part D, Properties. BPVC-IID, American Society of Mechanical Engineers.

ASME (2019b) Boiler and Pressure Vessel Code (BPVC) Section III Rules for Construction of Nuclear Facility Components, Division 1, Subsection NE, Class MC Components. BPVC-III NE, American Society of Mechanical Engineers.

Astarita T, Carlomagno G M (2013) Infrared Thermography for Thermo-Fluid-Dynamics. Experimental Fluid Mechanics, Springer.

Aumiller D L, Bettis B (2000) The Effect of Nodalization on the Accuracy of the Finite- Difference Solution of the Transient Conduction Equation. In *2000 RELAP5 International Users Seminar*.

Avramova M, Cuervo D (2013) Assessment of CTF Boiling Transition and Critical Heat Flux Modeling Capabilities Using the OECD/NRC BFBT and PSBT Benchmark Databases. *Science and Technology of Nuclear Installations*, 2013, 1–12, dx.doi.org/10.1155/2013/508485.

Bergagio M, Fan W, Thiele R, Anglart H (2020) Large Eddy Simulation of Thermal Mixing with Conjugate Heat Transfer at BWR Operating Conditions. *Nuclear Engineering and Design*, 356, 110361, dx.doi.org/10.1016/j.nucengdes.2019.110361.

Bird R B, Stewart W E, Lightfoot E N (2007) Transport Phenomena. Second revised edition, Wiley.

References

BSI (2014) Unfired Pressure Vessels. BS EN 13445, British Standards Institution, dx.doi.org/10.3403/BSEN13445.

BSI (2017) Metallic Industrial Piping. British Standards Institution, dx.doi.org/10.3403/BSEN13480.

Celik I, Klein M, Janicka J (2009) Assessment Measures for Engineering LES Applications. *Journal of Fluids Engineering*, 131(3), 031102, dx.doi.org/10.1115/1.3059703.

Chanaron B (2016) NURESAFE Project Final Report.

Chilton T H, Colburn A P (1934) Mass Transfer (Absorption) Coefficients Prediction from Data on Heat Transfer and Fluid Friction. *Industrial & Engineering Chemistry*, 26(11), 1183–1187, dx.doi.org/10.1021/ie50299a012.

Choi T S, No H C (2010) Improvement of the Reflood Model of RELAP5/MOD3.3 Based on the Assessments against FLECHT-SEASET Tests. *Nuclear Engineering and Design*, 240(4), 832–841, dx.doi.org/10.1016/j.nucengdes.2009.11.043.

Collins B, Okhuysen B, Salko R, Andersson D, Stimpson S, Lange T, Elliott A, Wysocki A, et al. (2018) CASL Research and Development Activities and Results for the CRUD Induced Power Shift (CIPS) Challenge Problem. CASL-U-2018-1703-000, Oak Ridge National Laboratory.

Craft T J, Iacovides H, Uapipatanakul S (2010) Towards the Development of RANS Models for Conjugate Heat Transfer. *Journal of Turbulence*, 11, N26, dx.doi.org/10.1080/14685248.2010.494608.

CSNI (2011) Report of the OECD/NEA - Vattenfall T-Junction Benchmark Exercise. NEA/CSNI/R(2011)5, OECD NEA Committee on the Safety of Nuclear Installations.

CSNI (2015a) Assessment of CFD Codes for Nuclear Reactor Safety Problems - Revision 2. NEA/CSNI/R(2014)12, OECD NEA Committee on the Safety of Nuclear Installations.

CSNI (2015b) Best Practice Guidelines for the Use of CFD in Nuclear Reactor Safety Applications - Revision. NEA/CSNI/R(2014)11, OECD NEA Committee on the Safety of Nuclear Installations.

Cumpsty N A, Horlock J H (2005) Averaging Nonuniform Flow for a Purpose. *Journal of Turbomachinery*, 128(1), 120–129, dx.doi.org/10.1115/1.2098807.

D'Auria F (2017) Thermal-Hydraulics of Water Cooled Nuclear Reactors. Woodhead.

Davis J R (editor) (1998) Metals Handbook Desk Edition. Second edition, ASM International.

Deloffre P, Terlain A, Barbier F (2002) Corrosion and Deposition of Ferrous Alloys in Molten Lead–Bismuth. *Journal of Nuclear Materials*, 301(1), 35–39, dx.doi.org/10.1016/S0022-3115(01)00724-3.

Doolaard H, Shams A, Roelofs F, Van Tichelen K, Keijers S, De Ridder J, Degroote J, Vierendeels J, et al. (2015) CFD Benchmark for a Heavy Liquid Metal Fuel Assembly. In *NURETH-16*.

El Khoury R R, Errera M, El Khoury K, Nemer M (2017) Efficiency of Coupling Schemes for the Treatment of Steady State Fluid-Structure Thermal Interactions. *International Journal of Thermal Sciences*, 115, 225–235, dx.doi.org/10.1016/j.ijthermalsci.2017.02.001.

References

EPRI (2004) PWR Axial Offset Anomaly (AOA) Guidelines. 1008102 Revision 1, Electric Power Research Institute.

EPRI (2011) Simulated Fuel Crud Thermal Conductivity Measurements under Pressurized Water Reactor Conditions. 1022896, Electric Power Research Institute.

EPRI (2014) Fuel Reliability Guidelines: PWR Fuel Cladding Corrosion and Crud, Revision 1, Volumes 1 and 2. 3002002795, Electric Power Research Institute.

EPRI (2020) Boron-Induced Offset Anomaly (BOA) Risk Assessment Tool Version 4.0: Validation and Verification. 3002016027, Electric Power Research Institute.

ERCOFTAC (2000) Industrial Computational Fluid Dynamics of Single-Phase Flows ERCOFTAC Best Practice Guidelines. Version 1, Turbulence and Combustion European Research Community on Flow.

Errera M P, Moretti R, Salem R, Bachelier Y, Arrivé T, Nguyen M (2019) A Single Stable Scheme for Steady Conjugate Heat Transfer Problems. *Journal of Computational Physics*, 394, 491–502, dx.doi.org/10.1016/j.jcp.2019.05.036.

Féron D (editor) (2012) Nuclear Corrosion Science and Engineering. Woodhead.

Ferrara P, Di Marco P (2017) CFD Analysis of Turbulent Heat Transfer and Thermal Striping Phenomena in T-Junctions with Liquid Sodium. *Journal of Physics: Conference Series*, 796, 012009, dx.doi.org/10.1088/1742-6596/796/1/012009.

Gebhart B, Jaluria Y, Mahajan R L, Sammakia B G (1988) Buoyancy-Induced Flows and Transport. Hemisphere.

Gerardi C, Bremer N, Lisowski D, Lomperski S (2017) Distributed Temperature Sensor Testing in Liquid Sodium. *Nuclear Engineering and Design*, 312, 59–65, dx.doi.org/10.1016/j.nucengdes.2016.06.017.

Gerschenfeld A (2019) Multiscale and Multiphysics Simulation of Sodium Fast Reactors: From Model Development to Safety Demonstration. In *Proceedings of 18th International Topical Meeting on Nuclear Reactor Thermal Hydraulics (NURETH-18)*.

Gerschenfeld A, Gorsse Y, Fauchet G (2019) Development of a Polyhedral Staggered Mesh Scheme Application to Subchannel and CFD SFR Thermal-Hydraulics. In *Proceedings of 18th International Topical Meeting on Nuclear Reactor Thermal Hydraulics (NURETH-18)*.

Giles M B (1997) Stability Analysis of Numerical Interface Conditions in Fluid–Structure Thermal Analysis. *International Journal for Numerical Methods in Fluids*, 25(4), 421–436, dx.doi.org/10.1002/(SICI)1097-0363(19970830)25:4<421::AID-FLD557>3.0.CO;2-J.

Glass A, Viellieber M, Batta A (2011) Coarse-Grid-CFD for Pressure Loss Evaluation in Rod Bundles. In *Proceedings of ICAPP 2011*, p. 2851.

Hadžiabdić M, Hanjalić K (2008) Vortical Structures and Heat Transfer in a Round Impinging Jet. *Journal of Fluid Mechanics*, 596, 221–260, dx.doi.org/10.1017/S002211200700955X.

Hanna B N, Dinh N T, Youngblood R W, Bolotnov I A (2020) Machine-Learning Based Error Pre-

diction Approach for Coarse-Grid Computational Fluid Dynamics (CG-CFD). *Progress in Nuclear Energy*, 118, 103140, dx.doi.org/10.1016/j.pnucene.2019.103140.

Henshaw J, McGurk J C, Sims H E, Tuson A, Dickinson S, Deshon J (2006) A Model of Chemistry and Thermal Hydraulics in PWR Fuel Crud Deposits. *Journal of Nuclear Materials*, 353(1-2), 1–11, dx.doi.org/10.1016/j.jnucmat.2005.01.028.

Howell J R, Mengüç M P, Siegel R (2016) Thermal Radiation Heat Transfer. Sixth edition, CRC Press.

IAEA (2006) Thermophysical Properties Database of Materials for Light Water Reactors and Heavy Water Reactors. IAEA-TECDOC-1496, International Atomic Energy Agency.

IAEA (2008) Computational Analysis of the Behaviour of Nuclear Fuel under Steady State, Transient and Accident Conditions. IAEA-TECDOC-1578, International Atomic Energy Agency.

IAEA (2009) Thermophysical Properties of Materials for Nuclear Engineering: A Tutorial and Collection of Data. IAEA-THPH, International Atomic Energy Agency.

IAEA (2010) Pressurized Thermal Shock in Nuclear Power Plants: Good Practices for Assessment. IAEA-TECDOC-1627, International Atomic Energy Agency.

Idelčik I E, Ginevskiĭ A S (2007) Handbook of Hydraulic Resistance. Fourth edition, Begell House.

Incropera F P, DeWitt D P, Bergman T L, Lavine A S (2011) Fundamentals of Heat and Mass Transfer. Seventh edition, John Wiley & Sons.

Jo J C, Choi Y H, Choi S K (2003) Numerical Analysis of Unsteady Conjugate Heat Transfer and Thermal Stress for a Curved Piping System Subjected to Thermal Stratification. *Journal of Pressure Vessel Technology*, 125(4), 467–474, dx.doi.org/10.1115/1.1613947.

Kakaç S, Shah R K, Aung W (1987) Handbook of Single-Phase Convective Heat Transfer. Wiley.

Kaneko S, Nakamura T, Fumio Inada, Kato M, Ishihara K, Nishihara T, Langthjem M A (2014) Flow-Induced Vibrations. Elsevier, dx.doi.org/10.1016/C2011-0-07518-X.

Kendrick B K, Petrov V, Walter D, Manera A, Collins B, Downar T, Secker J, Belcourt K (2013) CASL Multiphysics Modeling of Crud Deposition in PWRs. In *Top Fuel 2013 ANS Fuel Performance*, p. 5.

Kim J, Roidt R, Deardorff A (1993) Thermal Stratification and Reactor Piping Integrity. *Nuclear Engineering and Design*, 139(1), 83–95, dx.doi.org/10.1016/0029-5493(93)90263-9.

Kim T, Lu T J, Seung Jin Song (2016) Application of Thermo-Fluidic Measurement Techniques: An Introduction. Elsevier, dx.doi.org/10.1016/C2015-0-01881-0.

Koren C, Vicquelin R, Gicquel O (2017) Self-Adaptive Coupling Frequency for Unsteady Coupled Conjugate Heat Transfer Simulations. *International Journal of Thermal Sciences*, 118, 340–354, dx.doi.org/10.1016/j.ijthermalsci.2017.04.023.

Kuhn S, Braillard O, Ničeno B, Prasser H M (2010) Computational Study of Conjugate Heat Transfer in T-Junctions. *Nuclear Engineering and Design*, 240(6), 1548–1557, dx.doi.org/10.1016/j.nucengdes.2010.02.022.

References

Lewis L V, Provins J I (2004) A Non-Coupled CFD-FE Procedure to Evaluate Windage and Heat Transfer in Rotor-Stator Cavities. In *Volume 4: Turbo Expo 2004*, pp. 321–329, ASMEDC, dx.doi.org/10.1115/GT2004-53246.

Li D, Liu X, Yang Y (2016) Improvement of Reflood Model in RELAP5 Code Based on Sensitivity Analysis. *Nuclear Engineering and Design*, 303, 163–172, dx.doi.org/10.1016/j.nucengdes.2016.04.014.

Lienhard J H IV, Lienhard J H V (2020) A Heat Transfer Textbook. Fifth edition, Phlogiston Press.

Liu B (2019) Smart Component Models for Nuclear Reactors. FNC 53798/48650R, Frazer-Nash Consultancy.

Liu B (2021) Project FORTE - Nuclear Thermal Hydraulics Research & Development: Sub-Channel CFD for Nuclear Reactors: Phase 2 Developments. FNC 60148/51218R, Frazer-Nash Consultancy.

Liu B, He S, Moulinec C, Uribe J (2019) Sub-Channel CFD for Nuclear Fuel Bundles. *Nuclear Engineering and Design*, 355, 110318, dx.doi.org/10.1016/j.nucengdes.2019.110318.

Liu T (2011) Pressure- and Temperature-Sensitive Paints. In **Blockley R, Shyy W** (editors) *Encyclopedia of Aerospace Engineering*, p. eae076, John Wiley & Sons, Ltd, dx.doi.org/10.1002/9780470686652.eae076.

Łuczyński P, Giesen M, Gier T S, Wirsum M (2019) Uncoupled CFD-FEA Methods for the Thermo-Structural Analysis of Turbochargers. *International Journal of Turbomachinery, Propulsion and Power*, 4(4), 39, dx.doi.org/10.3390/ijtpp4040039.

Martyushev S G, Miroshnichenko I V, Sheremet M A (2014) Numerical Analysis of Spatial Unsteady Regimes of Conjugate Convective-Radiative Heat Transfer in a Closed Volume with an Energy Source. *Journal of Engineering Physics and Thermophysics*, 87(1), 124–134, dx.doi.org/10.1007/s10891-014-0992-6.

Menter F R (2015) Best Practice: Scale-Resolving Simulations in ANSYS CFD. Version 2.0, ANSYS Germany.

Merzari E, Fischer P, Yuan H, Van Tichelen K, Keijers S, De Ridder J, Degroote J, Vierendeels J, et al. (2016) Benchmark Exercise for Fluid Flow Simulations in a Liquid Metal Fast Reactor Fuel Assembly. *Nuclear Engineering and Design*, 298, 218–228, dx.doi.org/10.1016/j.nucengdes.2015.11.002.

Meyers J, Geurts B, Sagaut P (editors) (2008) Quality and Reliability of Large-Eddy Simulations. ERCOFTAC Series, Springer Netherlands.

Miller D S (2009) Internal Flow Systems. Second edition, Mentor Graphics.

Modest M F (2013) Radiative Heat Transfer. Third edition, Academic Press.

Moorthi A, Kumar Sharma A, Velusamy K (2018) A Review of Sub-Channel Thermal Hydraulic Codes for Nuclear Reactor Core and Future Directions. *Nuclear Engineering and Design*, 332, 329–344, dx.doi.org/10.1016/j.nucengdes.2018.03.012.

Morris A, Langari R (2020) Measurement and Instrumentation. Third edition, Elsevier, Inc.

References

Mowforth C, Hinds K, Smith N (2015) Control of Carbon Deposition within the Primary Circuit of Advanced Gas-Cooled Reactors. Chemistry in Energy Conference, Edinburgh.

Murthy J Y, Mathur S R (1998) Finite Volume Method for Radiative Heat Transfer Using Unstructured Meshes. *Journal of Thermophysics and Heat Transfer*, 12(3), 313–321, dx.doi.org/10.2514/2.6363.

NAFEMS (2019) General Guidelines for Good Convergence in Computational Fluid Dynamics. https://www.nafems.org/publications/guidelines-for-good-convergence-in-cfd/.

NSC (2015) Handbook on Lead-Bismuth Eutectic Alloy and Lead Properties, Materials Compatibility, Thermal-Hydraulics and Technologies. 7268, OECD NEA Nuclear Science Committee.

ONR (2019) Chemistry of Operating Civil Nuclear Reactors. NS-TAST-GD-088 Revision 3, Office for Nuclear Regulation.

ORNL (2006) The Effect of Elevated Temperature on Concrete Materials and Structures - a Literature Review. NUREG/CR-6900 ORNL/TM-2005/553, Oak Ridge National Laboratory, dx.doi.org/10.2172/974590.

Osakabe M, Sudo Y (1983) Heat Transfer Calculation of Simulated Heater Rods throughout Reflood Phase in Postulated PWR-LOCA Experiments. *Journal of Nuclear Science and Technology*, 20(7), 559–570, dx.doi.org/10.1080/18811248.1983.9733433.

Papukchiev A, Geffray C, Grishchenko D, Kudinov P (2019) Validation of the System Thermal-Hydraulics Code ATHLET for the Simulation of Transient Lead-Bismuth Eutectic Flows. In *Proceedings of 18th International Topical Meeting on Nuclear Reactor Thermal Hydraulics (NURETH-18)*.

Patankar S V (1980) Numerical Heat Transfer and Fluid Flow. Series in Computational Methods in Mechanics and Thermal Sciences, Hemisphere.

Patterson E A, Taylor R J, Bankhead M (2016) A Framework for an Integrated Nuclear Digital Environment. *Progress in Nuclear Energy*, 87, 97–103, dx.doi.org/10.1016/j.pnucene.2015.11.009.

Peng W, Zhang T, Sun X, Yu S (2016) Thermophoretic and Turbulent Deposition of Graphite Dust in HTGR Steam Generators. *Nuclear Engineering and Design*, 300, 610–619, dx.doi.org/10.1016/j.nucengdes.2016.02.006.

Piomelli U (2008) Wall-Layer Models for Large-Eddy Simulations. *Progress in Aerospace Sciences*, 44(6), 437–446, dx.doi.org/10.1016/j.paerosci.2008.06.001.

Piomelli U (2014) Large Eddy Simulations in 2030 and Beyond. *Philosophical transactions. Series A, Mathematical, physical, and engineering sciences*, 372(2022), dx.doi.org/10.1098/rsta.2013.0320.

Pioro I L (editor) (2016) Handbook of Generation IV Nuclear Reactors. Number Number 103 in Woodhead Publishing Series in Energy, Woodhead.

Platt P, Allen V, Fenwick M, Gass M, Preuss M (2015) Observation of the Effect of Surface Roughness on the Oxidation of Zircaloy-4. *Corrosion Science*, 98, 1–5, dx.doi.org/10.1016/j.corsci.2015.05.013.

References

Pope S B (2000) Turbulent Flows. Cambridge University Press.

Rogers G F C, Mayhew Y (1992) Engineering Thermodynamics: Work and Heat Transfer. Fourth edition, Prentice Hall.

Rohsenow W M, Hartnett J P, Cho Y I (1998) Handbook of Heat Transfer. Third edition, McGraw-Hill.

Rupp I, Christophe P, Tommy M M (2009) Large Scale Finite Element Thermal Analysis of the Bolts of a French PWR Core Internal Baffle Structure. *Nuclear Engineering and Technology*, 41(9), 1171–1180.

Saha S K, Tiwari M, Sundén B, Wu Z (2016) Advances in Heat Transfer Enhancement. Springer International Publishing, dx.doi.org/10.1007/978-3-319-29480-3.

Salko R K, Pointer W D, Delchini M O, Gurecky W L, Clarno K T, Salttery S R, Petrov V, Manera A (2019) Implementation of a Spacer Grid Rod Thermal-Hydraulic Reconstruction (ROTHCON) Capability into the Thermal-Hydraulic Subchannel Code CTF. *Nuclear Technology*, 205(12), 1697–1706, dx.doi.org/10.1080/00295450.2019.1585734.

Schlichting H, Gersten K (2017) Boundary-Layer Theory. Ninth edition, Springer, dx.doi.org/10.1007/978-3-662-52919-5.

Selvam P K, Kulenovic R, Laurien E (2015) Large Eddy Simulation on Thermal Mixing of Fluids in a T-Junction with Conjugate Heat Transfer. *Nuclear Engineering and Design*, 284, 238–246, dx.doi.org/10.1016/j.nucengdes.2014.12.025.

Sugimoto J, Muraov Y (1984) Effect of Grid Spacers on Reflood Heat Transfer in PWR-LOCA. *Journal of Nuclear Science and Technology*, 21(2), 103–114, dx.doi.org/10.1080/18811248.1984.9731021.

Terrani K A (2018) Accident Tolerant Fuel Cladding Development: Promise, Status, and Challenges. *Journal of Nuclear Materials*, 501, 13–30, dx.doi.org/10.1016/j.jnucmat.2017.12.043.

Tiselj I, Flageul C, Oder J (2020) Direct Numerical Simulation and Wall-Resolved Large Eddy Simulation in Nuclear Thermal Hydraulics. *Nuclear Technology*, 206(2), 164–178, dx.doi.org/10.1080/00295450.2019.1614381.

Tunstall R, Laurence D, Prosser R, Skillen A (2016) Large Eddy Simulation of a T-Junction with Upstream Elbow: The Role of Dean Vortices in Thermal Fatigue. *Applied Thermal Engineering*, 107, 672–680, dx.doi.org/10.1016/j.applthermaleng.2016.07.011.

US NRC (2020) NRC Non-Light Water Reactor (Non-LWR) Vision and Strategy, Volume 1 – Computer Code Suite for Non-LWR Design Basis Event Analysis. Revision 1, U.S. Nuclear Regulatory Commission.

Verdicchio J A (2001) The Validation and Coupling of Computational Fluid Dynamics and Finite Element Codes for Solving Industrial Problems. Ph.D. thesis, University of Sussex.

Versteeg H K, Malalasekera W (2007) An Introduction to Computational Fluid Dynamics: The Finite Volume Method. Second edition, Pearson Education.

References

Wagner C, Hüttl T, Sagaut P (editors) (2007) Large-Eddy Simulation for Acoustics. Cambridge University Press, dx.doi.org/10.1017/CBO9780511546143.

Wu Z, Laurence D, Iacovides H, Afgan I (2017) Direct Simulation of Conjugate Heat Transfer of Jet in Channel Crossflow. *International Journal of Heat and Mass Transfer*, 110, 193–208, dx.doi.org/10.1016/j.ijheatmasstransfer.2017.03.027.

Yoon S J, Kim S B, Park G C, Yoon H Y, Cho H K (2018) Application of CUPID for Subchannel-Scale Thermal–Hydraulic Analysis of Pressurized Water Reactor Core under Single-Phase Conditions. *Nuclear Engineering and Technology*, 50(1), 54–67, dx.doi.org/10.1016/j.net.2017.09.008.

Zhang J (2009) A Review of Steel Corrosion by Liquid Lead and Lead–Bismuth. *Corrosion Science*, 51(6), 1207–1227, dx.doi.org/10.1016/j.corsci.2009.03.013.

Zhang K (2020) The Multiscale Thermal-hydraulic Simulation for Nuclear Reactors: A Classification of the Coupling Approaches and a Review of the Coupled Codes. *International Journal of Energy Research*, 44(5), 3295–3315, dx.doi.org/10.1002/er.5111.

Zheng G, Sridharan K (2018) Corrosion of Structural Alloys in High-Temperature Molten Fluoride Salts for Applications in Molten Salt Reactors. *JOM*, 70(8), 1535–1541, dx.doi.org/10.1007/s11837-018-2981-2.

6 Nomenclature

Latin Symbols

A	Area, m^2
At	Atwood number ($At = (\rho_1 - \rho_2)/(\rho_1 + \rho_2)$)
Bi	Biot number ($Bi = hL/k_s$)
c_p, c_v	Specific heat at constant pressure or volume, $J\,kg^{-1}\,K^{-1}$
d or D	Diameter ($D_h = 4A_{cs}/p_{cs}$ for hydraulic diameter), m
f	Darcy-Weisbach friction factor
Fo	Fourier number ($Fo = \alpha_s t/L^2$)
Gr	Grashof number ($Gr = gL^3\Delta\rho/\nu^2\rho = gL^3\beta\Delta T/\nu^2$, using the Boussinesq approximation $\Delta\rho/\rho \approx -\beta\Delta T$, where ΔT is often taken as $T_w - T_{s,\infty}$)
g	Acceleration due to gravity, $m\,s^{-2}$
h	Specific enthalpy, $J\,kg^{-1}$, Heat Transfer Coefficient (HTC), $W\,m^{-2}\,K^{-1}$ or height, m
I	Radiative intensity, $W\,m^{-2}\,sr^{-1}$ or $W\,m^{-2}\,sr^{-1}\,\mu m^{-1}$ for a spectral density, where sr (steradian) is solid angle
J	Radiosity, $W\,m^{-2}$
k	Thermal conductivity, $W\,m^{-1}\,K^{-1}$
L	Length or wall thickness, m
M	Molar mass of a species, $kg\,kmol^{-1}$
Ma	Mach number ($Ma = U/a$, where a is the speed of sound)
n	Refractive index
Nu	Nusselt Number ($Nu = hL/k_f$)
p	Perimeter, m
P	Pressure (P_s = static pressure, P_T = total pressure), $N\,m^{-2}$ or Pa
Pe	Péclet number ($Pe = RePr$)
Pr	Prandtl number ($Pr = c_p\mu/k_f$)
q	Heat flux (rate of heat transfer per unit area, $q = Q/A$), $W\,m^{-2}$
Q	Rate of heat transfer, W
r	Radius, m
R	Gas constant (for a particular gas, $R = \tilde{R}/M$), $J\,kg^{-1}\,K^{-1}$
$\tilde{R}$	Universal gas constant, $8314.5\,J\,kmol^{-1}\,K^{-1}$
R_{th}	Thermal resistance, $K\,W^{-1}$
Ra	Rayleigh number ($Ra = GrPr$)
Re	Reynolds number ($Re = \rho UL/\mu$, or for an internal flow $Re = WD_h/A_{cs}\mu$)
Ri	Richardson number ($Ri = Gr/Re^2$)
Sr	Strouhal number ($Sr = fL/U$, where f is frequency)

St	Stanton number ($St = Nu/RePr$)
t	Time, s
T	Temperature (T_s = static temperature, T_T = total temperature), K
u_τ	Wall friction velocity ($u_\tau = \sqrt{\overline{\tau_w}/\rho}$), $\mathrm{m\,s^{-1}}$
U	Velocity, $\mathrm{m\,s^{-1}}$ or thermal transmittance, $\mathrm{W\,m^{-2}\,K^{-1}}$
v	Specific volume, $\mathrm{m^3\,kg^{-1}}$
V	Volume, $\mathrm{m^3}$
W	Mass flow rate, $\mathrm{kg\,s^{-1}}$
y	Wall distance, m
y^+	Non-dimensional wall distance ($y^+ = y u_\tau/\nu$)

Greek Symbols

α	Thermal diffusivity ($\alpha = k/\rho c_p$), $\mathrm{m^2\,s^{-1}}$
β	Volumetric thermal expansion coefficient ($\beta = -(1/\rho)(\partial\rho/\partial T)$), $\mathrm{K^{-1}}$
γ	Ratio of specific heats ($\gamma = c_p/c_v$)
ϵ	Emissivity or surface roughness height, m
κ	Absorption coefficient, $\mathrm{m^{-1}}$
λ	Wavelength, m
μ	Viscosity, $\mathrm{kg\,m^{-1}\,s^{-1}}$
ν	Kinematic viscosity and momentum diffusivity ($\nu = \mu/\rho$), $\mathrm{m^2\,s^{-1}}$
ρ	Density, $\mathrm{kg\,m^{-3}}$
σ	Stefan Boltzmann constant, $5.67 \times 10^{-8}\,\mathrm{W\,m^{-2}\,K^{-4}}$
τ	Shear stress, $\mathrm{N\,m^{-2}}$
ϕ	Porosity or void fraction

Subscripts and Modifications

b	Bulk (mass-averaged) quantity
cs	Cross-sectional quantity
f	Quantity relating to a fluid
i	Quantity relating to a particular species
T	Total (stagnation) quantity
t	Turbulent quantity
s	Static quantity or quantity relating to a solid
w	Quantity relating to a wall or surface
∞	Quantity far from a wall or in free-stream
$\overline{\square}$	Average quantity
$\tilde{\square}$	Molar quantity
$\square'$	Varying quantity

7 Abbreviations

AGR	Advanced Gas-cooled Reactor
ANT	Advanced Nuclear Technology
AOA	Axial Off-set Anomaly
BEIS	Department for Business, Energy and Industrial Strategy
BWR	Boiling Water Reactor
CAD	Computer Aided Design
CASL	Consortium for Advanced Simulation of Light Water Reactors
CCFL	Counter-Current Flow Limitation
CFD	Computational Fluid Dynamics
CG-CFD	Coarse-Grid CFD
CHT	Conjugate Heat Transfer
CIPS	CRUD Induced Power Shift
CRAB	Comprehensive Reactor Analysis Bundle
CRUD	Chalk River Unidentified Deposits
CSNI	Committee on the Safety of Nuclear Installations
DNS	Direct Numerical Simulation
DO	Discrete Ordinates
DTS	Distributed Temperature Sensor
DYF	Diabatic Y-plus Field
EC	European Commission
ECCS	Emergency Core Cooling System
FAC	Flow-Accelerated Corrosion
FCH	First Cell Height
FEA	Finite Element Analysis
FIV	Flow Induced Vibration
FSI	Fluid-Structure Interaction
HTC	Heat Transfer Coefficient
IAEA	International Atomic Energy Agency
IET	Integral Effect Test
INDE	Integrated Nuclear Digital Environment
INL	Idaho National Laboratory
IR	Infrared
ISO	International Organization for Standardization
LBE	Lead-Bismuth Eutectic
LES	Large Eddy Simulation
LMFR	Liquid Metal-cooled Fast Reactor
LOCA	Loss-Of-Coolant Accident
LWR	Light Water Reactor
MC	Monte Carlo
MOOSE	Multiphysics Object-Oriented Simulation Environment

Abbreviations

MSR	Molten Salt Reactor
NDT	Non-Destructive Testing
NIP	Nuclear Innovation Programme
NPP	Nuclear Power Plant
NTH	Nuclear Thermal Hydraulics
NURESAFE	NUclear REactor SAFEty simulation platform
NVEC	Nuclear Virtual Engineering Capability
ONCORE	Open-source Nuclear Codes for Reactor Analysis
PCT	Peak Cladding Temperature
PHRS	Passive Decay Heat Removal System
PTS	Pressurised Thermal Shock
PWR	Pressurised Water Reactor
RANS	Reynolds-Averaged Navier-Stokes
RMI	Reflective Metallic Insulation
RMS	Root Mean Square
ROM	Reduced Order Model
RPV	Reactor Pressure Vessel
RTD	Resistance Temperature Device
RTE	Radiative Transfer Equation
S2S	Surface-to-Surface
SFR	Sodium-cooled Fast Reactor
SGS	Sub-Grid-Scale
SSC	Structure, System and Component
TSP	Temperature Sensitive Paint
URANS	Unsteady Reynolds-Averaged Navier-Stokes
US NRC	United States Nuclear Regulatory Commission
V&V	Verification and Validation
VERA	Virtual Environment for Reactor Applications
WALT	Westinghouse Advanced Loop Tester
WMLES	Wall Modeled Large Eddy Simulation

Volume 2